TRIBLOCK TERPOLYMER DERIVED ISOPOROUS ULTRAFILTRATION MEMBRANES

A Dissertation

Presented to the Faculty of the Graduate School

of Cornell University

In Partial Fulfillment of the Requirements for the Degree of

Doctor of Philosophy

by

Yuk Mun Li

May 2018

TRIBLOCK TERPOLYMER DERIVED ISOPOROUS ULTRAFILTRATION MEMBRANES

Yuk Mun Li, Ph.D.

Cornell University 2018

Block copolymer derived nanostructured materials provide a unique platform for the development of nanotechnological applications ranging from the microelectronics industry all the way to separation. A particularly interesting approach that has received increasing attention in the last couple of years is the formation of isoporous ultrafiltration membranes via the combination of block copolymer self-assembly (SA) with industrially proven non-solvent induced phase separation (NIPS), a process now referred to as SNIPS. Triblock terpolymer based NIPS membranes have been investigated as a result of their improved mechanical toughness over the corresponding diblock copolymer derived membranes.

To expand our understanding of this new area of block copolymer science and engineering, in this thesis SNIPS derived membranes were investigated based on triblock terpolymer poly(isoprene-*b*-styrene-*b*-4-vinylpyridine) (ISV). In a first effort, the effects of different casting parameters on membrane substructure morphology were studied. Experimental results elucidated a substructure morphology transition from finger-like to sponge-like through increasing dope concentration, evaporation time, and varying solvent compositions. Membranes with finger-like and sponge-like substructures were integrated with nylon supports to enhance mechanical stability for testing and handling and were evaluated for their hydraulic permeabilities.

The effects of an important but often overlooked environmental casting parameter, relative humidity, were subsequently assessed on ISV membranes with a focus on membrane surface pore structure. Membranes cast at an optimized relative humidity of 40% were characterized by a high density of square packed surface pores. Additionally, precise control over the rate of permeation of a small molar mass solute was realized through variation in triblock terpolymer molar mass.

After investigation of the SNIPS process and the associated molecular engineering of membrane properties via variation of process parameters and molecular architecture, new insights into the fabrication of asymmetric membranes were obtained from employing two chemically distinct triblock terpolymers in the dope used during the SNIPS process. Initial proof-of-principle experiments with mixtures of ISV and poly(isoprene-*b*-styrene-*b*-(dimethylamino)ethylmethacrylate) (ISA) demonstrated that the use of mixtures of chemically distinct triblock terpolymers enables the tailoring of membrane pore surface chemistries. This approach was subsequently used to improve membrane fouling properties by working with mixtures from ISV and terpolymer poly(isoprene-*b*-styrene-*b*-ethylene oxide) (ISO) which on its own is difficult to process into useful SNIPS membranes. Experimental results established that blended triblock terpolymer membranes exhibited a combination of properties intrinsic to the two specific block copolymers utilized. This opens access to designer membranes with desired pore surface chemical properties via a facile “mix and match” approach. The results of this thesis taken together highlight the tremendous potential of SNIPS derived membranes to become the basis for next generation ultrafiltration technologies for applications in areas as diverse as biopharmaceutical separations, virus filtration, and drug delivery.

BIOGRAPHICAL SKETCH

Yuk Mun Li, the youngest of three daughters, was born and raised in New York City to immigrant parents; Chi Leung and Lin Tai Li. Much of her accomplishments and successes are a testament to her parent's sacrifices. During a time of chaos in China's Cultural Revolution, her parents risked their lives by swimming six hours from Mainland China to Hong Kong to escape labor camps. Searching for the American Dream, they immigrated to the United States in 1977 to build a better life for themselves and their future family. Because of their denied formal education, higher education became an important aspect in her family.

Living in NYC, Yuk Mun grew up in a melting pot, exposed to a variety of cultures and foods. With this appreciation of cultural diversity, she caught the travel bug. In her first year of high school, she participated in an exchange program to Italy, fostering her wanderlust. Yuk Mun attended Brooklyn Technical High School, one of the top three specialized NYC high schools at the time, majoring in chemistry. Here, she got her first taste of real chemistry in a Quantitative Forensic Analysis class, awaking her natural curiosity in how things work and accelerating her towards engineering.

Naturally, Yuk Mun started studying chemical engineering at Syracuse University in 2008. She was an active member in the engineering community as a mentor and facilitator for the Pathfinders and Academic Excellence Workshop programs. In the summer of her sophomore year, she participated in a Research Experience for Undergraduates at Cornell University in Professor Uli Wiesner's group working on block copolymer membranes for water applications. The following summer, she joined Professor Jason Burdick's group at the University of Pennsylvania developing hyaluronic

acid based 2D hydrogels for hMSCs attachment. Yuk Mun graduated summa cum laude from Syracuse University with a B.S. in chemical engineering.

Yuk Mun spent a gap year traveling before beginning her PhD in chemical engineering in the Robert Frederick Smith School of Chemical and Biomolecular Engineering at Cornell University. In the fall of 2013, due to her enriching summer experience, she rejoined Prof. Uli Wiesner's research group in the Department of Materials Science and Engineering. As part of an industry collaboration, Yuk Mun was able to continue researching the structure and function of hierarchically porous triblock terpolymer membranes as dynamic multifunctional materials for a second skin. This collaboration and truly intriguing project allowed her to be at the forefront of cutting edge science, technology, and innovation.

DEDICATED TO MY FAMILY AND FRIENDS.

ACKNOWLEDGEMENTS

Firstly, I would like to express my sincere gratitude to my advisor Prof. Uli Wiesner for sharing his expertise, valuable insights, and endless enthusiasm. His ability to convey research as an adventure with an immense excitement for teaching is truly inspirational. Without his guidance and dedicated involvement in every step of the process, the successful completion of this dissertation would not be possible. My time at Cornell University was a rewarding experience that has allowed me to grow as a research scientist propelling me to new heights.

Additionally, I would like to thank the rest of my thesis committee: Prof. Lara Estroff and Prof. Yong Joo. During our discussions, they raised many interesting questions and perspectives and I hope I managed to address them here.

It was a great pleasure to be a part of the Wiesner group. For the many memories and conversations in and out of the laboratory, I must thank each and every group member. I am very thankful to have had the opportunity to learn from and work with Dr. Rachel M. Dorin and, particularly, Dr. Yibei Gu, who jump started my training by teaching me synthesis, instrumentation, characterization, and analysis. It was a great honor to have mentored Parth Vaidya and Lilly Tsaur. I would like to acknowledge my undergraduate students who worked with me: Divya Srinivasan, Juan R. Álvarez-Palacio, and Rebecca Mort. Additionally, I would like to thank Qi Zhang, for our close collaborations and endless hours bonding in our office, and Teresa Kao, for personal and professional support as well as our shared interest in “great” shows. I sincerely appreciate their friendships as it reminded me that I wasn’t alone in this journey.

I wish to express my thanks to the following university staff and facility managers: Dolores Dewbury, Michele Conrad, Shelby Clark, Johanna Tuttle, Phillip Carubia, Don Werder, Anthony Condo, Detlef Smilgies, and Teresa Porri.

Finally, I am forever grateful to my family, particularly my parents, for their sacrifices in order to give me the opportunities they were denied. To my sisters, I am thankful for their encouragement, moral and emotional support and the occasional care package. I am also grateful to my dog, Tiger, for her constant companionship.

Lastly, I would like to thank my partner for his unconditional love and endless support throughout my dissertation.

TABLE OF CONTENTS

LIST OF FIGURES

LIST OF TABLES

CHAPTER 1

INTRODUCTION

Rise in global water scarcity, stricter government regulations, and the need to reduce operational expenditures (operations and maintenance costs) have contributed to the rising market and demand for membrane technologies. In particular, the global market for wastewater treatment technologies is expected to reach $12.1 billion by 2020.[1] Additionally, consumers' needs for product differentiation or customized membrane technologies will also drive industry growth.

Membrane technologies provide separations based on the use of a physical barrier. This physical barrier, a semi permeable membrane, allows certain substances to pass through while others are retained. The advantages associated with membrane technologies are their low operating pressures resulting in low energy consumption, high flux, and wide range of application.[2] The separation process is pressure-driven and utilizes membranes varying in pore sizes. Membrane filtration can be split into microfiltration, ultrafiltration (UF), nanofiltration, and reverse osmosis.

With pore sizes between 10 and 100 nm, the main application of UF membranes is to remove high molecular weight substances, viruses, bacteria, and suspended solids as seen in Figure 1.1.[3] UF membranes are widely utilized across research activities in pharmaceuticals, water purification, the life science, and the food industry.

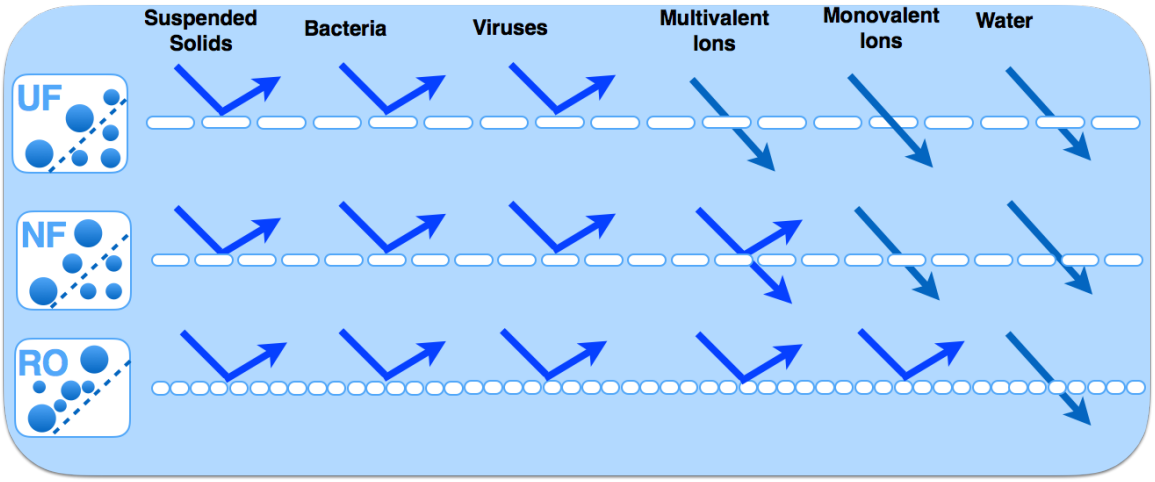

Figure 1.1. Diagram comparing the effective removal of certain components in wastewater treatment by ultrafiltration, nanofiltration, and reverse osmosis membranes[3]

There are several membrane preparation techniques such as sintering, track-etching, phase inversion, and dip-coating.[4] Phase inversion membranes formed by non-solvent induced phase separation (NIPS) are commonly and widely reported and used in chemical and biotechnology industries.[5] The NIPS process was one of the first to be industrialized about seventy years ago and since then has been studied extensively. In this process, shown in the schematic in Figure 1.2,[6] a polymer dope solution is coated onto a membrane backing layer by blade casting. It is then submerged into a coagulation bath containing a non-solvent (usually water). Due to the solvent and non-solvent exchange, precipitation takes place to produce the phase inversion membrane. Phase inversion membranes are usually derived from homopolymers and are characterized by low resolution yet high fluxes.

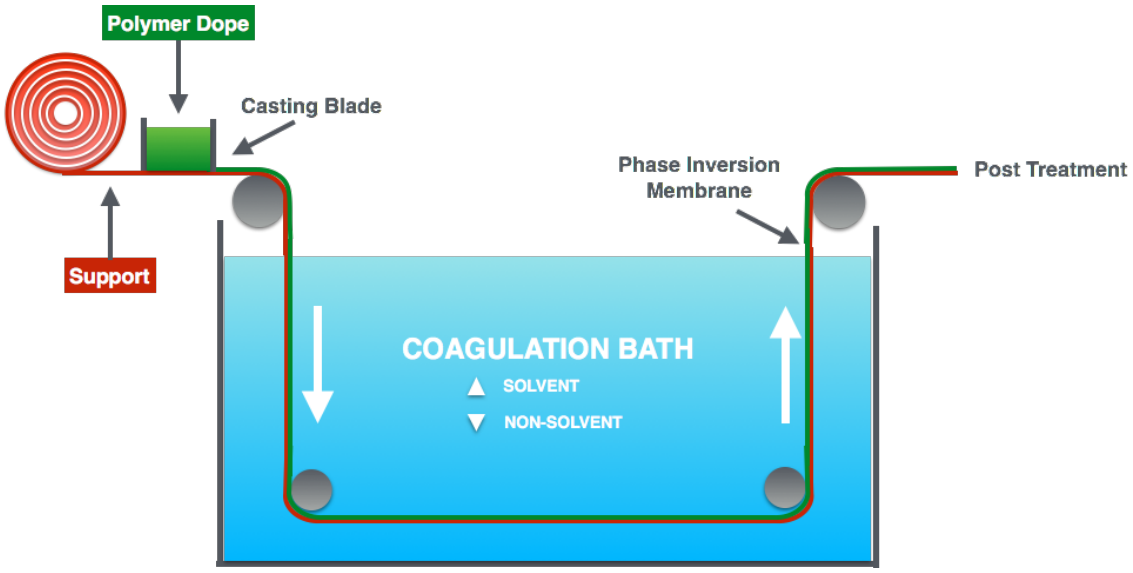

Figure 1.2. Schematic of the phase inversion technique[6]

Moving away from homopolymers, materials derived from block copolymers by phase inversion provide a unique platform for novel asymmetric membranes used for ultrafiltration. These membranes exhibit a regularly structured top separation layer with high pore density derived from block copolymer self-assembly on top of an asymmetric substructure common for phase inverted membranes. Block copolymers are an attractive materials class due to their ability to self-assemble into different morphologies ideal for the fabrication of thin top surface layers with structural length scales of ~5 to 50 nm. Under equilibrium conditions, AB diblock copolymers microphase separate and form multiple well-ordered structures (spherical, cylindrical, gyroidal, and lamellar) as a function of block volume fraction, f_A, shown in Figure 1.3.[7] This self-assembly behavior allows for membranes with high porosities and narrow pore size distributions. The self-assembly process is the product of the balance of repulsive interactions and conformational entropy loss between chemically distinct segments.[8]

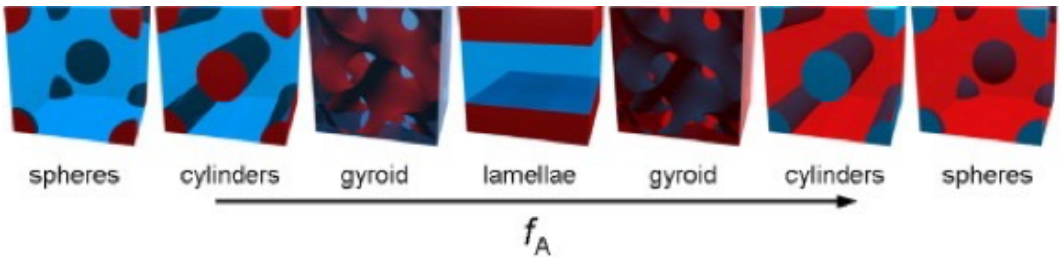

Figure 1.3. Schematic of diblock copolymer phase separated morphologies with increasing volume fraction of red block A.[7]

Peinemann *et al.*[9] pioneered the use of diblock copolymer self-assembly with non-solvent induced phase separation to fabricate isoporous membranes. The first poly(styrene-*b*-4-vinylpyridine) (PS-P4VP) diblock copolymer derived asymmetric membranes were characterized by a selective hexagonally ordered skin layer atop an asymmetric support layer. Since then, other diblock copolymer systems have been explored.[10-12]

Moving from diblock copolymers to triblock terpolymers, Phillip *et al.*[13] extended the SNIPS process to poly(isoprene-*b*-styrene-*b*-4-vinylpyridine) (PI-PS-P4VP or ISV), leading to superior mechanical membrane toughness associated with the addition of a rubbery PI block. Asymmetric triblock terpolymer membranes were synthesized by employing the SNIPS technique as depicted in Figure 1.4.

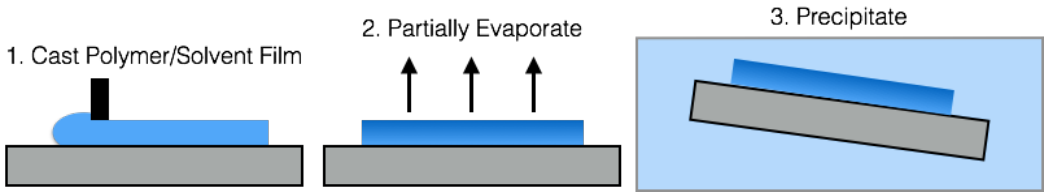

Figure 1.4. Schematic depicting the SNIPS process used to fabricate membranes

Thin films were blade cast and allowed to evaporate for a predetermined amount of time before plunging into a non-solvent bath where the non-solvent exchanges with the solvent mixture to induce precipitation of the polymer and kinetically trap the structure in a non-equilibrium state. Membranes fabricated from this triblock terpolymer had triple the toughness compared to a diblock copolymer reference while maintaining tunable pore sizes, pH-responsive permeability due to the P4VP block,[14] and permeability levels superior to commercial ultrafiltration membranes. These advanced membrane materials combine the narrow pore size distribution from track-etched membranes with the high flux associated with phase inverted membranes thereby accessing a performance regime hitherto unknown for ultrafiltration membranes.

Few studies are available elucidating details of the formation mechanisms of block copolymer derived UF membranes.[15,16] The Wiesner group has made progress in this area through application of small angle x-ray scattering (SAXS)[17] to the casting dope solution as well as through use of *in-situ* grazing incidence SAXS (GISAXS)[18] to probe the top surface structure evolution during the evaporation process. Fabrication of membranes with block copolymers can be a time consuming trial and error process. However, insights provided by these techniques have accelerated screening typical optimization parameters including dope solution concentration and evaporation time for membrane fabrication thereby facilitating access to advanced UF membranes with improved property characteristics.

Thesis outline

The leverage of nanotechnology is the key to securing block copolymer membranes as next generation ultrafiltration technology widely utilized in industry. In

order to advance block copolymer membranes as competitive alternatives in the market, further studies on structure-property relationships and tunability over structural components are essential.

Chapter 1 describes work on systematically varying membrane casting parameters to tune membrane substructure while retaining an ordered surface structure. Elucidating pathways to two different substructures with either sponge-like or finger-like morphology, these membranes were subsequently cast on nylon supports to enhance their mechanical stability. Performance tests were conducted to evaluate the effect of the nylon support on pH-dependent permeability.

In chapter 2, the effect of an environmental casting parameter (relative humidity) on membrane surface structure is investigated. Subsequently, the influence of relative humidity dependent structural changes is described on small molar mass solute permeation. Additionally, ISV membranes varying in molar mass were investigated as chemical valves with permeability changes as a function of pH.

Designer membranes or product differentiation will drive technological advancements in the field of membrane technologies. A “one size fits all” type membrane will be replaced by the need for customized membranes for specialized separations in *e.g.* the biopharmaceutical industry. To that end chapter 3 describes the fabrication of SNIPS membranes from a mixture of two chemically distinct triblock terpolymers in the dope solution. Results demonstrate that this simple “mix and match” approach opens a pathway to next generation block copolymer derived UF membranes with the ability to precisely tailor membrane pore surface chemistries and associated functionalities for complex separation applications. Chapter 4 finally expands the “mix and match”

approach to an alternative blend of triblock terpolymers in the dope used for the generation of SNIPS membranes addressing the problem of membrane fouling.

The thesis concludes with perspectives on future research directions on hierarchically porous asymmetric membranes derived from triblock terpolymers as a basis for advanced membrane technologies for a number of applications in a range of fields including, but not limited to, filtration and separation.

REFERENCES

[1] Frost & Sullivan, "Augmentation of Membrane Filtration Technology." *ww2.frost.com*. 2018. Web 7 Jan. 2018.

[2] Lenntech, "Membrane Technology." *www.lenntech.com.* 2018. Web 6 Jan. 2018.

[3] Koch Membrane System, "Membrane Technologies." *Kochmembrane.com.* 2018. Web. 6 Jan. 2018.

[4] Mulder, M., *Basic Principles of Membrane Technology* Kluwer Academic Publishers: Dordrecht, The Netherlands, 2003.

[5] Guillen, G.R., Pan, Y., Li, M., & Hoek, E.M.V., "Preparation and Characterization of Membranes Formed by Nonsolvent Induced Phase Separation: A Review" *Industrial & Engineering Chemistry Research* **50**, 3798-3817 (2011).

[6] Adapted from Mulder (1984, 1997)

[7] Darling, S.B., "Directing the self-assembly of block copolymers" *Progress in Polymer Science* **32**, 1152-1204 (2007).

[8] Abetz, V., & Simon, P.F.W., "Phase behavior and morphologies of block copolymers", *Advances in Polymer Science* **189**, 125-212 (2005).

[9] Peinemann, K.V., Abetz, V., & Simon, P.F.W., "Asymmetric superstructure formed in a block copolymer via phase separation", *Nature Materials* **6**, 992-996 (2007).

[10] Phillip, W.A., Hillmyer, M.A., & Cussler, E.L., "Cylinder Orientation Mechanism in Block Copolymer Thin Films Upon Solvent Evaporation", *Macromolecules* **43**, 7763-7770 (2010).

[11] Shevate, R.; Karunakaran, M.; Kumar, M.; Peinemann, K.-V. Polyanionic pH-responsive polystyrene-b-poly (4-vinyl pyridine-N-oxide) isoporous membranes. *J. Membr. Sci.* **2016**, 501, 161–168.

[12] Hahn, J., Filiz, V., Rangou, S., Clodt, J., Jung, A., Buhr, K., Abetz, C. and Abetz, V., (2013). Structure formation of integral‐asymmetric membranes of polystyrene‐block‐Poly (ethylene oxide). *Journal of Polymer Science Part B: Polymer Physics*, *51*(4), 281-290.

[13] Phillip, W.A., Dorin, R.M., Werner, J., Hoek, E.M.V., Wiesner, U., & Elimelech, M., "Tuning Structure and Properties of Graded Triblock Terpolymer-Based Mesoporous and Hybrid Films", *Nano Letters* **11**, 2892-2900 (2011).

[14] Nunes, S.P., Behzad, A.R., Hooghan, B., Sougrat, R., Karunakaran, M., Pradeep, N., Vainio, U., & Peinemann, K.V., "Switchable pH-Responsive Polymeric Membranes Prepared *via* Block Copolymer Micelle Assembly", *ACS Nano* **5**, 3516-3522 (2011).

[15] Marques, D.S., Vainio, U., Chaparro, N.M., Calo, V.M., Bezahd, A.R., Pitera, J.W., Peinemann, K.V. and Nunes, S.P., (2013). Self-assembly in casting solutions of block copolymer membranes. *Soft Matter*, *9*(23), 5557-5564.

[16] Stegelmeier, C., Exner, A., Hauschild, S., Filiz, V., Perlich, J., Roth, S.V., Abetz, V. and Förster, S.,(2015). Evaporation-induced block copolymer self-assembly into membranes studied by in situ synchrotron SAXS. *Macromolecules*, *48*(5), 1524-1530.

[17] Dorin, R. M., Marques, D. S., Sai, H., Vainio, U., Phillip, W. A., Peinemann, K. V., Nunes, S.P., & Wiesner, U. (2012). Solution small-angle X-ray scattering as a

screening and predictive tool in the fabrication of asymmetric block copolymer membranes. *ACS Macro Letters*, *1*(5), 614-617.

[18] Gu, Y., Dorin, R. M., Tan, K. W., Smilgies, D. M., & Wiesner, U. (2016). In situ study of evaporation-induced surface structure evolution in asymmetric triblock terpolymer membranes. *Macromolecules*, *49*(11), 4195-4201.

CHAPTER 2

TUNING SUBSTRUCTURE AND PROPERTIES OF SUPPORTED ASYMMETRIC TRIBLOCK TERPOLYMER MEMBRANES

Abstract

Asymmetric poly(isoprene-*b*-styrene-*b*-4-vinylpyridine) (ISV) block copolymer membranes fabricated via self-assembly and non-solvent induced phase separation (SNIPS) process have drawn significant attention due to the simple processing method and the generation of high-quality isoporous ultrafiltration membranes. With the present study on SNIPS membrane substructure, we systematically varied membrane casting parameters to tune the cross-sectional morphologies of SNIPS membranes. Parameters such as polymer concentration, evaporation time, solvent ratio, and coagulation bath temperature were investigated to control transformation of commonly produced sponge-like cross-sectional morphologies into more open and permeable finger-like substructures. Membranes with sponge-like and finger-like substructures were then integrated onto nylon supports for enhanced mechanical properties. Hydraulic permeability tests at various pH conditions gave distinct open-state flux values for SNIPS membranes with different sublayer morphologies, while maintaining pH responsive functionality resulting from the poly(4-vinylpyridine) block.

Adapted with permission from Q. Zhang, Y.M. Li, Y. Gu, R.M. Dorin, U. Wiesner, Tuning Substructure and properties of supported asymmetric triblock terpolymer membranes, *Polymer* **107**, 398-405 (2016).

Introduction

Polymeric membranes have widely been used in filtration fields because of their plentiful materials choices, robust mechanical properties, and compatibility with various fabrication techniques such as track-etching, lithography, and solvent based methods.[1]

Among these methods, membranes generated through non-solvent induced phase separation (NIPS) attract great interest due to the simple fabrication procedure and accessibility to a range of pore sizes under various casting conditions. The polymer, commonly a homopolymer (e.g. polysulfone[2]), is dissolved into a good solvent, casted on a substrate and immersed into a coagulation bath. As phase inversion occurs with the exchange of solvent and non-solvent (coagulant), membranes are formed by precipitation of the polymer. One of the most useful properties of NIPS membranes is the ability to tailor pore size with casting solution compositions and membrane casting conditions.[3] There are generally two types of cross-sectional membrane morphologies obtained through varying system conditions: 1) dense, sponge-like and 2) open, finger-like structures. Sponge-like and finger-like membranes are used as reverse osmosis and ultrafiltration membranes, respectively, due to their pore size distribution. Although widely used in industry, NIPS membranes are limited due to the trade-off between selectivity and permeability[4]. Membranes with a sponge-like cross section usually have low permeability due to their dense structure. On the other hand, finger-like membranes have high permeability yet low selectivity with respect to solute rejection due to a wide pore size distribution.

Advancing the field from conventional NIPS membranes, Peinemann *et al.*[5] first reported and demonstrated the fabrication of poly(styrene-*b*-4-vinylpyridine) (PS-*b*-P4VP

or SV) diblock copolymer derived asymmetric membranes. Block copolymers are an attractive material for the fabrication of membranes due to their ability to self-assemble into well-ordered structures. PS-*b*-P4VP derived membranes were generated through a hybrid process of block copolymer self-assembly and NIPS (SNIPS)[6]. Membranes were prepared by 1) dissolving the polymer into an appropriate solvent system, 2) casting a thin film with a doctor blade, 3) solvent evaporation for a specified amount of time to allow block copolymer self assembly, and 4) immersion into a non-solvent (water) bath to induce precipitation of the polymer and kinetically trap the structure in a thermally non-equilibrium state. The resultant membranes were characterized by a disordered graded macroporous substructure beneath an ordered selective skin layer. Since then, Phillip *et al.*[7] applied the hybrid SNIPS process to a triblock terpolymer, poly(isoprene-*b*-styrene-*b*-4-vinylpyridine) (PI-*b*-PS-*b*-P4VP or ISV) because of the inherent mechanical stability associated with the addition of the rubbery PI block. Membranes made from this triblock terpolymer had triple the toughness compared to its diblock counterpart.

The asymmetry of the SNIPS membranes eliminates the trade-off of permselectivity by enabling selectivity, attributed to the isoporous skin layer, and permeability, associated with the macroporous substructure. Numerous studies have been reported on the tunability of the isoporous self-assembled selective layer. Nunes *et al*. studied the effect of different solvent system compositions[8], and metal-complexation[9,10] on their PS-*b*-P4VP system. Pendergast *et al.*[11] investigated various parameters including varying polymer concentration, compositions of volatile to less volatile solvent mixtures, and evaporation times on their ISV polymer system. Dorin *et al.* explored the effect of

block copolymer molar mass[12] and the use of small angle x-ray scattering (SAXS)[6] as a screening tool to predict the top surface structure.

In contrast to the past focus on the top separation layer, few studies report on the investigation of parameters controlling the substructure. Current literature details various block copolymer membrane systems with sponge-like[5,7,12-15], comblike[15] and fingerlike[15,16] morphologies. The current study focuses on the investigation of parameters affecting the substructure to enable its tunability which in turn controls membrane performance (i.e. permeability) without disrupting the self-assembly of the top surface selective layer.

To that end we systematically study several key factors in order to tune the substructure of ISV SNIPS membranes from sponge-like to finger-like. Parameters such as polymer concentration, evaporation time, solvent system, and coagulation bath temperature are shown to affect the substructure morphology. Tunability between sponge-like and finger-like substructures is achieved while preserving the isoporous skin layer responsible for membrane selectively, regardless of substructure morphology. Hydraulic permeability tests at various pH conditions demonstrate the substructure's influence on permeability while leaving pH responsive behavior, associated with the P4VP block[17,18], unperturbed. Additionally, ISV membranes with both types of substructures are integrated onto nylon supports to further improve mechanical stability.

Experimental

Polymer synthesis: Four triblock terpolymers, poly(isoprene-*b*-styrene-*b*-4-vinylpyridine) (PI-*b*-PS-*b*-P4VP, ISV) were synthesized via sequential anionic

polymerization as previously detailed by Phillip *et al.*[7]. ISV terpolymer characteristics were determined by a combination of gel permeation chromatography (GPC) and ^{1}H NMR. The experimentally determined molar mass (M_n), volume fractions of each block (*f)* and polydispersity index (PDI) of each triblock terpolymer are listed in Table 2.1.

Table 2.1. Summary of ISV terpolymer characteristics.

Polymer	M_n (kg/mol)	f_{PI}	f_{PS}	f_{P4VP}	PDI
ISV115	115	0.26	0.62	0.12	1.16
ISV117	117	0.29	0.59	0.12	1.13
ISV118	118	0.23	0.66	0.11	1.12
ISV139	139	0.26	0.61	0.13	1.16

*Number average molar mass (M_n), volume fraction (*f)* and polydispersity index (PDI).

Membrane Fabrication: ISV terpolymers were dissolved in a binary solvent system of 1,4-dioxane (DOX) and tetrahydrofuran (THF) in the appropriate ratios (by weight) and concentrations (see results and discussion section). Utilizing the SNIPS process to prepare membranes, the following steps were taken: 1) the casting solution was pipetted onto a substrate, 2) a thin film was casted with a doctor blade, 3) evaporation of the solvent system for a specified amount of time, and 4) immersion into a coagulation bath. The resultant membranes were dried at ambient conditions before further characterization.

Scanning Electron Microscopy (SEM): ISV membranes were sputter coated with gold-palladium for 6-7 s prior to SEM imaging using a Denton Vacuum Desk II. SEM micrographs were acquired using a Tescan Mira3 field emission scanning electron microscope (FE-SEM).

Membrane Performance Tests: For permeability tests and to evaluate the pH-responsive nature of the ISV membranes, neat and supported membrane films were evaluated in a stirred cell (Amicon 8010, Millipore, Co.) with a volume of 10 mL with an

applied pressure of N_2 gas at 1-2 psi. Three data points were averaged to estimate the permeability under varying pH conditions. pH buffers of sodium acetate and acetic acid were prepared for pH values ranging from 3 to 6. pH buffers of imidazole and hydrochloric acid were prepared for pH values ranging from 7 to 8. The buffer solutions were tested with a pH probe before conducting performance tests.

Viscosity Tests: The rheological properties of all solutions were measured by a Discovery Hybrid Rheometer (DHR-3) with a 40 mm 2.0° cone plate configuration at room temperature.

Solubility parameters calculation: Hansen solubility parameters (δ_d, δ_p, δ_h) of water, DOX and THF were obtained from literature[3]. Equation (1) was used to calculate solubility parameters (δ_d, δ_p, δ_h) of solvent mixtures:

$$\delta_{i,S} = \frac{\sum_j (X_j V_j \delta_{i,j})}{\sum_j (X_j V_j)} \quad (1)$$

where X_j, V_j and $\delta_{i,j}$ denote the mole fraction, molar volume and solubility parameter of a specific component j in the mixture, respectively.

The solubility parameter difference ($\delta_{S\text{-}NS}$) between solvent and non-solvent was calculated by

$$\delta_{S-NS} = \sqrt{[(\delta_{d,S} - \delta_{d,NS})^2 + (\delta_{p,S} - \delta_{p,NS})^2 + (\delta_{h,S} - \delta_{h,NS})^2]} \quad (2)$$

Both equations were obtained from the literature[19].

Results and Discussion

The formation mechanism of sponge-like and finger-like substructures in NIPS membranes has been extensively studied.[3,19] One dominating theory in the field attributes the different substructures to the demixing rate. In this theory, upon plunging the thin

film into a coagulation bath, the casting dope solution separates into two liquid phases, a polymer-rich phase and a polymer-poor phase, designated as liquid-liquid demixing. The substructure's pore sizes are largely determined by this demixing rate. If instantaneous demixing occurs, the polymer-rich phase precipitates quickly to form a solid membrane while the polymer-poor phase converts into large voids, resulting in an open, finger-like cross-sectional morphology. If demixing is delayed, polymer, solvent and non-solvent stay miscible in one phase before phase separation occurs causing a denser sponge-like structure in the final membrane. As the SNIPS process is a combination of self-assembly and NIPS, the formation mechanism of cross-sectional morphology deduced from NIPS membranes should be applicable to SNIPS membranes to tailor sublayer structure.

Among the many variables that influence the demixing rate, we investigated four parameters– casting solution concentration, evaporation time, solvent system, and coagulation bath temperature – to study their effects on the substructure of SNIPS membranes. These parameters are easily adjusted in the membrane fabrication process and include both kinetic and thermodynamic factors that influence the demixing rate.

Concentration and evaporation time dependence: ISV117 was dissolved in a solvent system of DOX/THF = 5/5 with varying polymer concentrations of 9 wt%, 10 wt% and 11 wt%. ISV117 membranes were prepared by the SNIPS process with evaporation times of 45 s and 60 s. SEM characterizations of ultrafiltration layers and cross sections are presented in Figure 2.1. With increasing solution concentration at a constant evaporation time (45 s), the membrane cross section transformed from a dominantly finger-like substructure to a half finger-like, half sponge-like substructure. By

increasing the evaporation time from 45 s to 60 s, membranes casted with varying concentrations all resulted in dense sponge-like substructures.

The transformation from finger-like to sponge-like morphology at higher concentrations, as well as longer evaporation times, as previously demonstrated, is due to delayed demixing.[20] With increasing concentration or evaporation time, the casting dope solution becomes more viscous before being plunged into the coagulation bath. This rheological hindrance reduces the solvent and non-solvent exchange rate, delaying liquid-liquid demixing, therefore resulting in denser sponge-like substructures.

In addition to the tunable sublayers, SEM images of the top surfaces of all six membranes showed similar mesopores with narrow pore size distributions (inset images in Figure 2.1). The ability to maintain the isoporous skin layer while changing the substructure promises high selectivity with tunable permeabilities but also distinguishes the ISV terpolymer system as a robust system for the fabrication of ultrafiltration membranes via SNIPS process.

Solvent system dependence: Typically in the SNIPS process, the solvent system used for the casting solution is a mixture of two or more solvent components. At least one solvent is volatile which aids in the formation of an isoporous skin layer derived from block copolymer self-assembly. Specifically for the ISV system, a mixture of DOX and THF are used. By adjusting the solvent ratio in the casting solutions, substructure morphologies can be tuned. ISV139 was dissolved in solvent systems of DOX/THF in ratios of 5/5, 6/4, and 7/3 at the same polymer concentration (9 wt%). Under the same casting conditions (45 s of evaporation), membranes' cross-sectional structures changed significantly. The membrane casted from DOX/THF=5/5 system exhibited a hierarchical

cross-sectional morphology (Figure 2.2a). Pore sizes gradually increase from the membrane's top to bottom surface. By increasing the DOX/THF ratio to 6/4, a half sponge-like and half-finger-like substructure appeared (Figure 2.2b). In the membrane casted from DOX/THF=7/3 system, the finger-like morphology ran through almost the entire substructure of the membrane as indicated in Figure 2.2c. The SEM characterization of the respective isoporous skin layers are shown in Figure A.1 again demonstrating excellent control over pore size distribution.

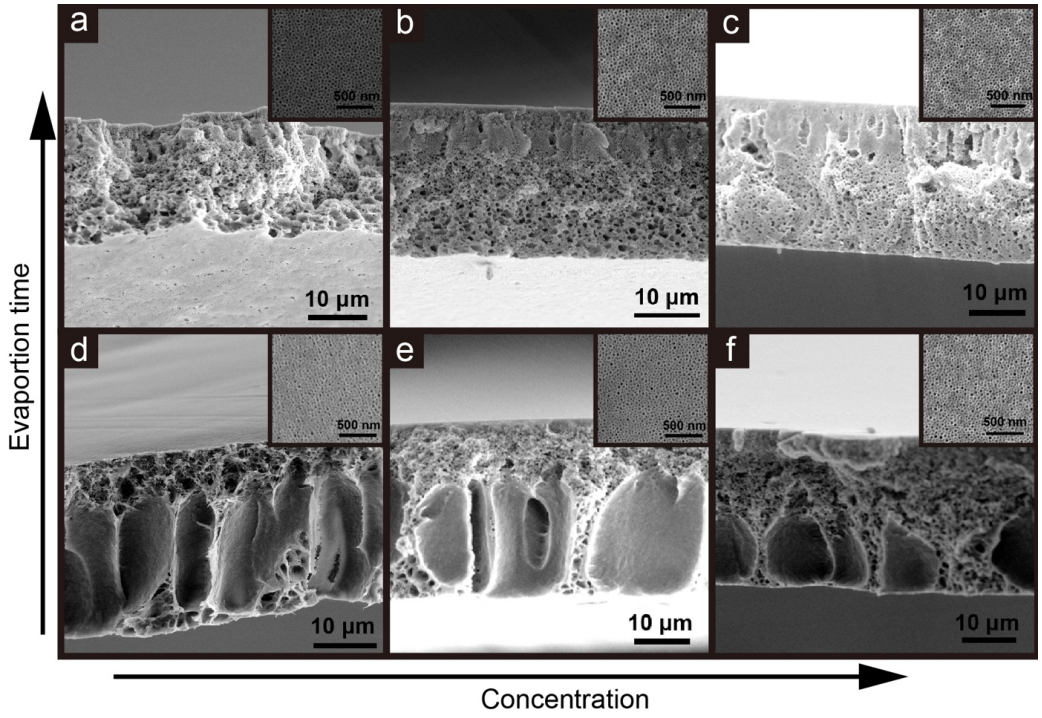

Figure 2.1. SEM images of cross sections and top surfaces (inset images) of SNIPS membranes cast from (a,d) 9 wt%, (b,e) 10 wt%, and (c,f) 11 wt% solutions at evaporation times of (a-c) 60 s and (d-f) 45 s.

To understand the cause of this trend, viscosities of the three casting solutions were analyzed with a rheometer under a series of shear rates. Viscosity data are shown in Figure 2.3. The casting solution containing DOX/THF=7/3 has the highest viscosity while the casting solution in DOX/THF=5/5 is the least viscous. As mentioned above,

more viscous solutions usually result in delayed demixing giving denser, sponge-like structures due to rheological hindrance. From the opposite trend seen here, viscosity is not the leading factor in determining substructure morphology in this case.

Solvent-Non-Solvent (S-NS) affinity is another important parameter that determines the demixing rate. Calculation of S-NS affinity is detailed in the Experimental Section. A low solubility parameter difference between S-NS ($\delta_{S\text{-}NS}$) indicates a high S-NS affinity, which favors instantaneous demixing because of the fast solvent - non-solvent exchange. Vandezande *et al.*[19] varied S-NS affinities by several approaches and observed cross section morphology changes. The variation of solvent mixture ratios could also result in different S-NS affinities. Therefore, we calculated $\delta_{S\text{-}NS}$ between water and various solvents including DOX, THF and their mixtures at ratios of 5/5, 6/4, and 7/3 (Table 2.1). The $\delta_{S\text{-}NS}$ values in Table 2.2 indicate that DOX has the highest affinity with water while THF has the lowest. In the mixture systems, $\delta_{S\text{-}NS}$ decreases with increasing DOX/THF ratio. Accordingly, the affinity between solvent and coagulant has the trend of 7/3 > 6/4 > 5/5. Therefore, DOX/THF = 7/3 system has the highest S-NS exchange rate (i.e. instantaneous demixing) resulting in a more finger-like structure.

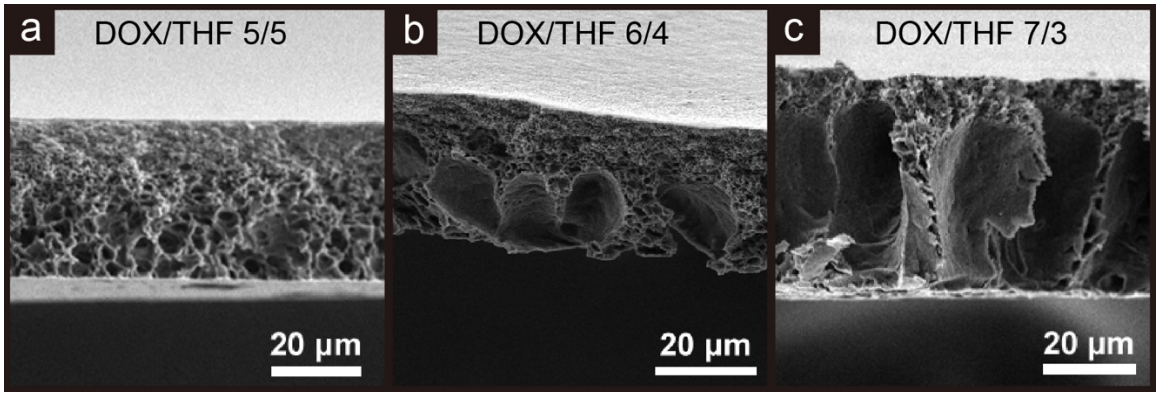

Figure 2.2. SEM images of cross sections of SNIPS membranes cast from solutions with (a) DOX/THF=5/5 (b) DOX/THF=6/4 and (c) DOX/THF=7/3 solvent systems.

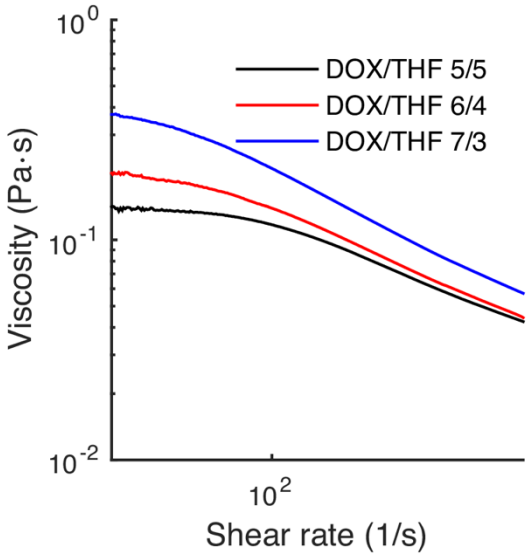

Figure 2.3. Viscosity of casting solutions with DOX/THF=5/5 (black) DOX/THF=6/4 (red) and DOX/THF=7/3 (blue) solvent systems.

Table 2.2. Hansen solubility parameters (δ_d, δ_p, δ_h) of solvents and non-solvents and solubility parameter differences ($\delta_{S\text{-}NS}$) between solvent and non-solvent

	δ_d ($MPa^{1/2}$)	δ_p ($MPa^{1/2}$)	δ_h ($MPa^{1/2}$)	$\delta_{S\text{-}NS}$ ($MPa^{1/2}$)
H_2O	15.5	16	42.3	0
DOX	16.8	5.7	8	35.8
THF	19	10.2	3.7	39.2
DOX/THF 7/3	17.5	7.2	6.6	36.9
DOX/THF 6/4	17.8	7.7	6.1	37.2
DOX/THF 5/5	18.0	8.1	5.7	37.5

Coagulation bath temperature dependence: In addition to changing the concentration and evaporation time, coagulation bath temperature can kinetically influence the demixing rate. In Figure 2.4, SNIPS membranes cast from the same solution (7 wt% ISV139, DOX/THF=5/5) and casting conditions (45 s) were plunged into coagulation baths at room temperature (~20 °C) and at 50 °C. SEM images show a clear transformation from predominant sponge-like to predominant finger-like substructures as

coagulation bath temperature increases. SEM characterization of the isoporous skin layers is shown in Figure A.2. Previously, this behavior was also reported and explained in NIPS membrane systems.[21] At high coagulation bath temperatures, the system kinetically favors instantaneous demixing which results in larger pore sizes and, in our case, the finger-like substructure.

Obvious transformations between sponge-like and finger-like substructures are only observed under certain casting conditions. Although, as shown in Figure A.3, cross-sectional morphologies transformed to larger pore sizes with increasing bath temperature, this temperature increase cannot completely overcome the rheological hindrance due to the high concentration (9 wt%) and long evaporation time (55 s), and as a result, did not fully convert the membrane to a finger-like substructure.

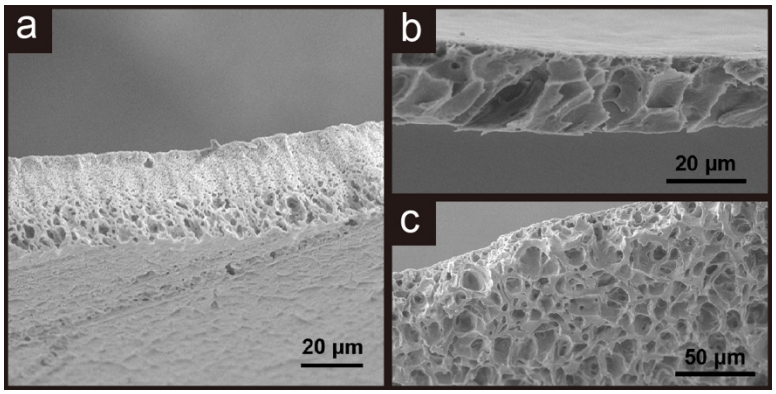

Figure 2.4. SEM images of cross sections and bottom layer of SNIPS membranes immersed in (a) room temperature and (b,c) 50°C coagulation baths.

Membranes atop nylon support: For final use of block copolymer derived SNIPS membranes it is desirable to cast the material on supports that provide additional mechanical stability during handling and use. In the last part of this study we therefore wanted to find out whether control over sponge-like and finger-like substructures could be preserved when casting was performed in the presence of a support structure and

finally how the support would influence permeability of the final assembly. To this end ISV115 and ISV118 polymer casting solutions were prepared by dissolving ISV terpolymer into a binary solvent system of DOX and THF in a 7/3 ratio (by weight). Neat and supported ISV115 membranes were cast from a 11 wt% polymer solution with an evaporation time of 30 s. Neat and supported ISV118 membranes were cast from a 11 wt% polymer solution with an evaporation time of 30s. A lower concentration neat ISV118 membrane was cast from a 9 wt% polymer solution and an evaporation time of 45s. Casting solutions were pipetted onto glass substrates to generate neat, unsupported membranes. For supported membranes, casting solutions were pipetted directly onto 0.1 or 0.2 μm nylon substrates (Sterlitech, Inc.) as it eliminates additional fabrication steps and is therefore preferred. The casting solutions were casted using a doctor blade with a height between 0.203 and 0.229 mm. The neat and supported thin films were allowed to evaporate for specified times before immersion into a coagulation bath.

The optimized casting conditions chosen for ISV115 and ISV118 membrane fabrication were based on polymer concentration, solvent ratio, and evaporation time parameters that yielded an ordered, uniform, and porous top surface above the desired sponge-like or finger-like macroporous substructure. An additional parameter, viscosity, was taken into consideration for the fabrication of supported ISV118 membranes as the increased viscosity of the casting solution impeded its infiltration through the nylon substrate while allowing the membrane to remain atop the nylon substrate.

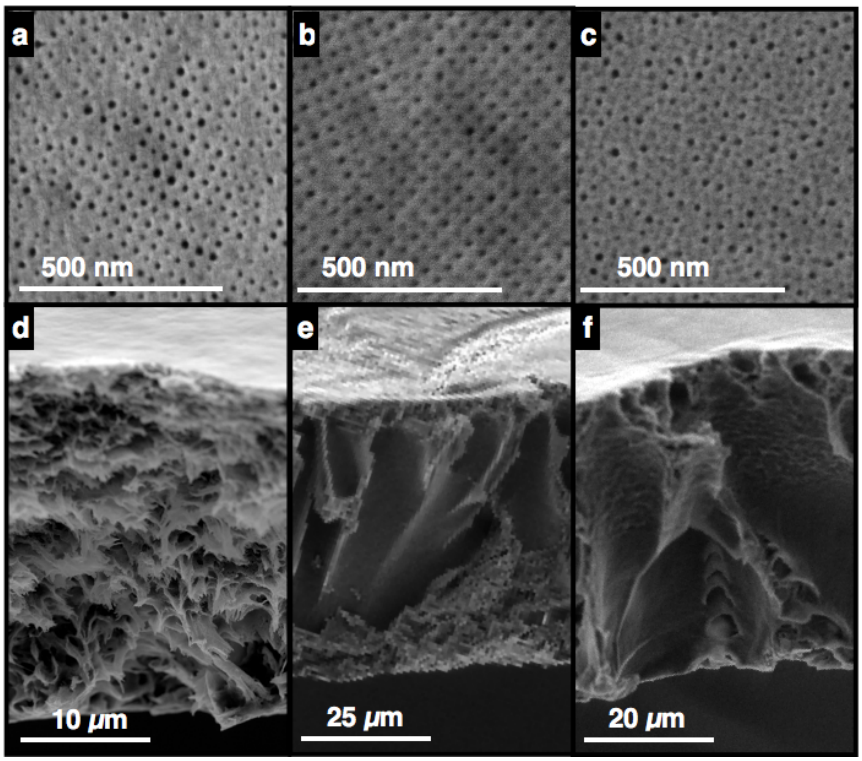

Figure 2.5. SEM micrographs of top surfaces (top row) and cross sections (bottom row) of SNIPS membranes cast from (a,d) 11 wt% ISV115, (b,e) 11 wt% ISV118, and (c,f) 9 wt% ISV118.

Casting under the aforementioned conditions for neat ISV115 and ISV118 resulted in ordered, isoporous membranes with a sponge-like and finger-like substructure, respectively, see SEM micrographs of top surfaces and cross sections depicted in Figure 2.5. Supported membranes were then fabricated by directly casting the ISV115 and ISV118 (both 11 wt%) thin films onto porous, nylon substrates. Figure 2.6a,d depicts the top surface and cross sectional image of a 0.2 μm nylon substrate with an internally inert polyester support. As demonstrated in Figure 2.6, the top surface, characterized by ordered and uniform pores, and the respective sponge-like or finger-like cross sections were retained atop the nylon substrates. This demonstrates that membranes characterized by sponge-like and finger-like substructures can both be integrated with a support layer.

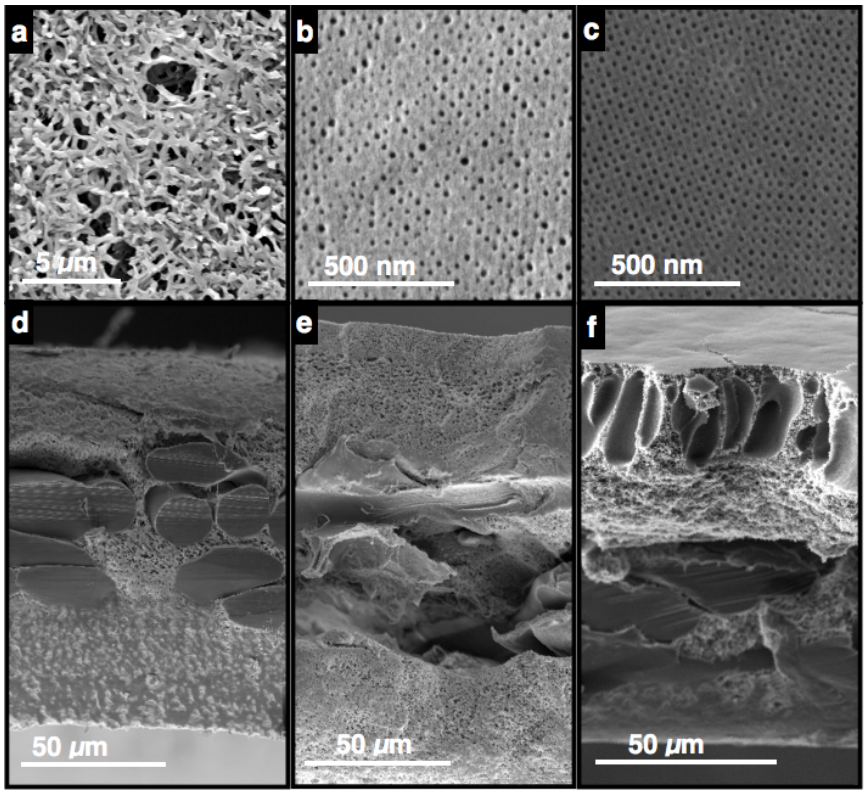

Figure 2.6. SEM micrographs of top surfaces (top row) and cross sections (bottom row) of (a,d) 0.2 um nylon support and SNIPS membranes cast from (b, e) 11 wt% ISV115 on 0.2 µm nylon and (c, f) 11 wt% ISV118 on 0.1 µm nylon. 0.1 and 0.2 µm nylon differ by average pore sizes (see supporting information, Figure A.4).

Due to the pH-responsive nature of the P4VP block membrane performance was characterized by measuring the permeability at varying pH conditions[7,9,10,14]. Permeability measurements were taken with a stirred cell on membranes with an active area of 4.1 cm^2. From the results shown in Figure 2.7, it can be concluded that the pH-responsive nature of the ISV membranes adhered to a nylon support was preserved.

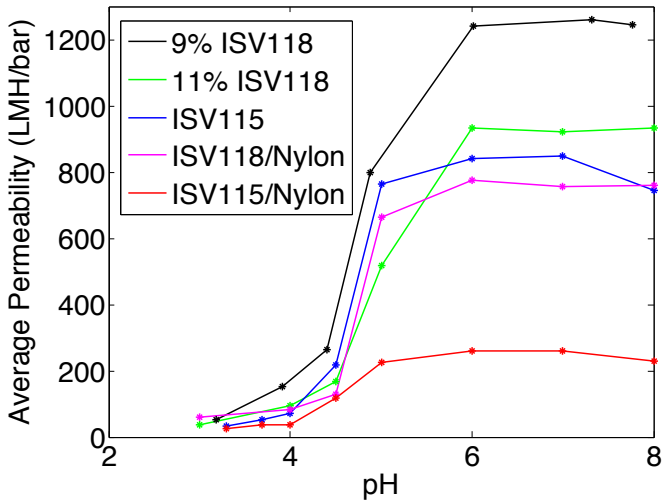

Figure 2.7. Performance of neat and supported ISV115 and ISV118 membranes under varying pH conditions.

As expected, in general membranes with a finger-like substructure have enhanced permeability as compared to membranes with sponge-like substructures. However, it is important to look at the structural details of block copolymer derived SNIPS membranes casted on supports in order to fully understand the observed behavior. For example, adhering a ISV115 membrane with a sponge-like substructure to a nylon support resulted in a permeability reduction by a factor of 3.3 at neutral pH conditions. When analyzing SEMs of the cross-sectional structure of this membrane we observed the formation of a dense layer at the interface of the membrane and nylon support (see supporting information, Figure A.5) not observed for the unsupported membrane and most likely responsible for this large permeability reduction. A smaller permeability reduction factor of 1.7 at similar pH conditions was found for supported finger-like ISV118 membranes. Despite the complexities of the SNIPS membrane system which are due to the multitude of parameters associated with the SNIPS process, these results suggest tunability of

membrane performance as a consequence of specifics of the substructure even in the case that membrane supports are used during membrane fabrication.

Conclusions

In this work, we systematically demonstrated methods to tune the substructure of SNIPS membranes between sponge-like and finger-like morphologies while simultaneously leaving the self-assembled and ordered top surface layer intact. The mechanism of substructure formation was shown to be determined by the demixing rate, which was influenced by kinetic parameters such as concentration, evaporation time, and coagulation bath temperature, as well as by thermodynamic parameters including solvent and non-solvent (S-NS) affinity. Asymmetric ISV membranes integrated with a porous nylon support for improved mechanical stability maintained isoporous ultrafiltration surface layers and simultaneously allowed control over sponge-like and finger-like substructures. Results suggest high tunability and robustness of asymmetric membrane structure for the ISV triblock terpolymer system which should enable fine tuning of structure to simultaneously maximize membrane selectivity and permeability.

Acknowledgments

The authors would like to acknowledge funding of this work by the Defense Threat Reduction Agency (DTRA) Contract No. HDTRA1-13-C0003. Y.G. was funded by the National Science Foundation (DMR-1409105). This work utilized the Cornell Center for Materials Research (CCMR) facilities supported by NSF MRSEC program (DMR-1120296).

APPENDIX A

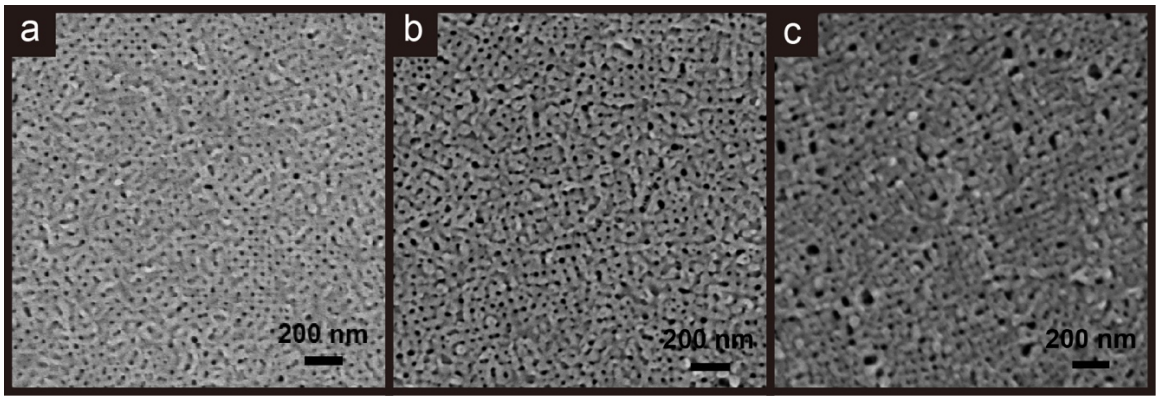

Figure A.1. SEM images of top surface of SNIPS membranes cast from solutions with (a) DOX/THF=5/5 (b) DOX/THF=6/4 and (c) DOX/THF=7/3 solvent systems.

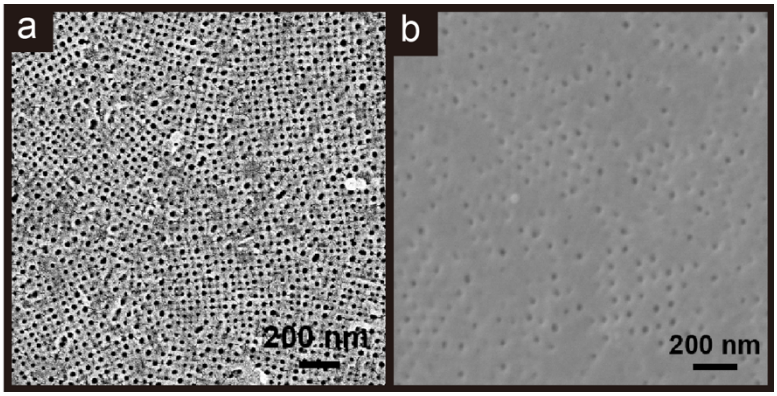

Figure A.2. SEM images of top surface of SNIPS membranes immersed in (a) room temperature and (b,c) 50°C coagulation baths.

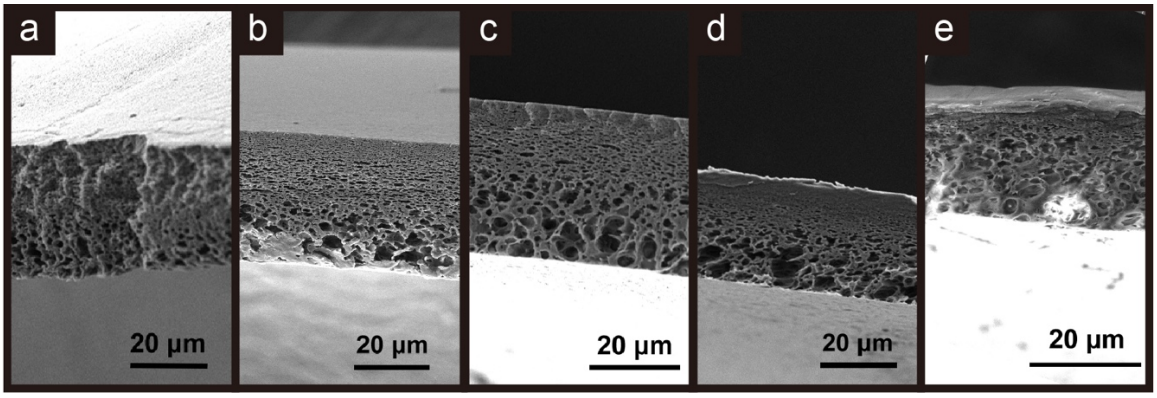

Figure A.3. SEM images of cross sections of SNIPS membranes cast from ISV139, DOX/THF=5/5, 9 wt% solution immersed in (a) 8 °C (b) 20 °C (c) 30 °C (d) 40 °C and (e) 50 °C coagulation baths.

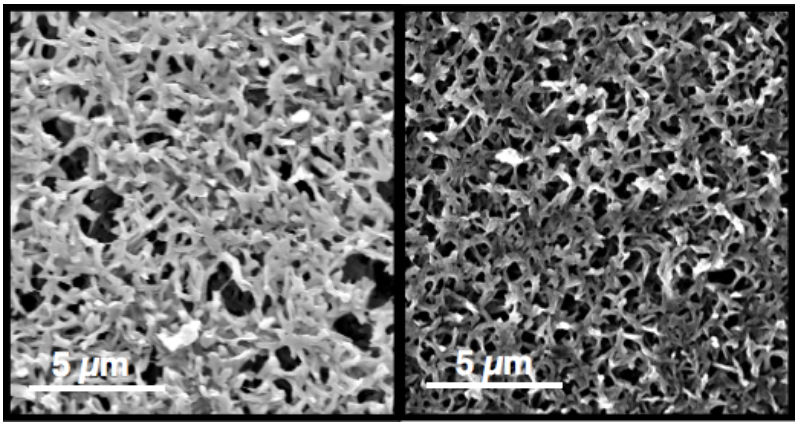

Figure A.4. The difference between 0.1 (right) and 0.2 (left) µm nylon substrates are their average pore sizes.

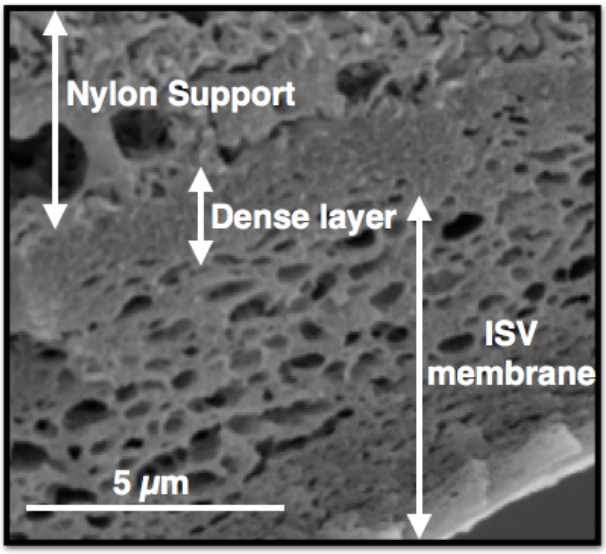

Figure A.5. Supported ISV115 membranes exhibit a reduction in permeability by a factor of 3.3 due to the formation of a dense layer at the interface of the membrane and the nylon support.

REFERENCES

[1] D. A. Bernards, T. A. Desai, Nanoscale porosity in polymer films: fabrication and therapeutic applications, Soft Matter 6 (2010) 1621-1631.

[2] Q. Z. Zheng, P. Wang, Y. N. Yang, Rheological and thermodynamic variation in polysulfone solution by PEG introduction and its effect on kinetics of membrane formation via phase-inversion process, J. Membr. Sci. 279 (2006) 230-237.

[3] G. R. Guillen, Y. Pan, M. Li, E. M. Hoek, Preparation and characterization of membranes formed by nonsolvent induced phase separation: a review, Ind. Eng. Chem. Res. 50 (2011) 3798-3817.

[4] J. R. Werber, C. O. Osuji, M. Elimelech, Materials for next-generation desalination and water purification membranes, Nat. Rev. Mater. (2016) 16018.

[5] K.V. Peinemann, V. Abetz, P.F.W. Simon, Asymmetric superstructure formed in a block copolymer via phase separation, Nat. Mater. 6 (2007) 992-996.

[6] R. M. Dorin, D. S. Marques, H. Sai, U. Vainio, W. A. Phillip, K. V. Peinemann, S.P. Nunes, U. Wiesner, Solution small-angle X-ray scattering as a screening and predictive tool in the fabrication of asymmetric block copolymer membranes, ACS Macro Lett. 1 (2012) 614-617.

[7] W.A. Phillip, R.M. Dorin, J. Werner, E.M.V. Hoek, U. Wiesner, M. Elimelech, Tuning Structure and Properties of Graded Triblock Terpolymer-Based Mesoporous and Hybrid Films, Nano Lett. 11 (2011) 2892-2900.

[8] S. P. Nunes, M. Karunakaran, N. Pradeep, A. R. Behzad, B. Hooghan, R. Sougrat, H. He, K. V. Peinemann, From micelle supramolecular assemblies in selective solvents to isoporous membranes, Langmuir 27 (2011) 10184-10190.

[9] S. P. Nunes, A. R. Behzad, B. Hooghan, R. Sougrat, M. Karunakaran, N. Pradeep, U. Vainio, K. V. Peinemann, Switchable pH-responsive polymeric membranes prepared via block copolymer micelle assembly, Acs Nano 5 (2011) 3516-3522.

[10] S. P. Nunes, R. Sougrat, B. Hooghan, D. H. Anjum, A. R. Behzad, L. Zhao, N. Pradeep, I. Pinnau, U. Vainio, K. V. Peinemann, Ultraporous films with uniform nanochannels by block copolymer micelles assembly, Macromolecules 43(2010) 8079-8085.

[11] M.M. Pendergast, R.M. Dorin, W.A. Phillip, U. Wiesner, E.M.V. Hoek, Understanding the structure and performance of self-assembled triblock terpolymer membranes, J. Membr. Sci. 444 (2013) 461-468.

[12] R.M. Dorin, W.A. Phillip, H. Sai, J. Werner, M. Elimelech, U. Wiesner, Designing block copolymer architectures for targeted membrane performance, Polymer 55 (2014) 347-353.

[13] J. Hahn, V. Filiz, S. Rangou, J. Clodt, A. Jung, K. Buhr, C. Abetz, V. Abetz, Structure formation of integral‐asymmetric membranes of polystyrene‐block‐Poly (ethylene oxide), J. Polym. Sci., Part B: Polym. Phys. 51 (2013) 281-290.

[14] Y. Gu, U.Wiesner, Tailoring Pore Size of Graded Mesoporous Block Copolymer Membranes: Moving from Ultrafiltration toward Nanofiltration, Macromolecules 48 (2015) 6153-6159.

[15] F. Schacher, T. Rudolph, F. Wieberger, M. Ulbricht, A. H. Muller, Double stimuli-responsive ultrafiltration membranes from polystyrene-block-poly (N, N-dimethylaminoethyl methacrylate) diblock copolymers, ACS Appl. Mater. Interfaces 1(2009) 1492-1503.

[16] Y. Gu, R. M. Dorin, U. Wiesner, Asymmetric organic–inorganic hybrid membrane formation via block copolymer–nanoparticle co-assembly, Nano lett. 13 (2013) 5323-5328.

[17] A. M. Mika, R. F. Childs, J. M. Dickson, Chemical valves based on poly (4-vinylpyridine)-filled microporous membranes, J. Membr. Sci. 153 (1999) 45-56.

[18] M. Tagliazucchi, O. Azzaroni, I. Szleifer, Responsive polymers end-tethered in solid-state nanochannels: when nanoconfinement really matters, J. Am. Chem. Soc. 132 (2010) 12404-12411.

[19] P. Vandezande, X. Li, L. E. Gevers, I. F. Vankelecom, High throughput study of phase inversion parameters for polyimide-based SRNF membranes, J. Membr. Sci. 330 (2009) 307-318.

[20] A. K. Hołda, B. Aernouts, W. Saeys, I. F. Vankelecom, Study of polymer concentration and evaporation time as phase inversion parameters for polysulfone-based SRNF membranes. J. Membr. Sci. 442 (2013) 196-205.

[21] Q. Z. Zheng, P. Wang, Y. N. Yang, D. J. Cui, The relationship between porosity and kinetics parameter of membrane formation in PSF ultrafiltration membrane, J. Membr. Sci. 286 (2006) 7-11.

CHAPTER 3

EFFECT OF HUMIDITY ON SURFACE STRUCTURE AND PERMEATION OF TRIBLOCK TERPOLYMER DERIVED SNIPS MEMBRANES

Abstract

Block copolymer (BCP) ultrafiltration (UF) membranes derived from a hybrid process of BCP self-assembly and non-solvent induced phase separation (SNIPS) exhibit an asymmetric structure consisting of ordered pores in a selective skin layer above a highly permeable substructure. In this work, we investigate relative humidity (RH) as a casting condition that influences poly(isoprene-*b*-styrene-*b*-4-vinylpyridine) (ISV) membrane surface structure in terms of order and uniformity. An optimum RH of 40-45% is determined to produce membranes characterized by a high density of square packed pores with a narrow pore size distribution. Membranes casted at lower and higher RH show a drop off in order and uniformity. The RH dependent structural changes correlate well with small molar mass dye solute (methyl orange; molar mass of 327 g/mol) diffusion rates: Membranes casted at 40% RH reveal higher diffusivity than when casted at 75% RH. The rate of permeation is further controlled via pH dependent pore closure as well as through ISV terpolymer molecular architecture with increasing solute diffusivity observed in membranes casted from increasing terpolymer molar mass. Experimental findings on small molar mass solute permeability can only be accounted for when compared with theoretical predictions from a hydrodynamic theory combined with the

effects of tortuosity when a simplified membrane structure is assumed. Results suggest that SNIPS derived BCP membranes may have potential for applications in drug delivery.

Introduction

Polymeric membranes fabricated via block copolymer (BCP) self-assembly plus non-solvent induced phase separation (SNIPS)[1] process rise as strong candidates for next generation asymmetric ultrafiltration (UF) membranes due to their advantageous combination of uniform pore size and high pore density. The highly ordered mesoporous surface with narrow pore size distribution promises high resolution while the high pore density together with the macroporous substructure gives rise to high permeability. Since the first publication on SNIPS membranes derived from BCP poly(styrene-*b*-4-vinylpyridine) (SV) in 2007,[2] the SNIPS process has been studied extensively for various BCPs over the past decade.

A primary focus in the emerging SNIPS derived BCP membrane field to date has been the exploration of membrane properties through molecular design. Functionalizing membranes through molecular architecture rather than process control is a paradigm shift in the membrane field and promises substantial expansion of membrane capabilities. For example, BCP membranes containing a poly(4-vinylpyridine) (P4VP) or poly(acrylic acid) (PAA) block are pH-responsive [2-4] resulting in changes in effective pore size upon pH variations. Mechanical properties like membrane toughness can be largely enhanced through the addition of a rubbery polyisoprene block to the high glass transition (T_g) matrix block of BCP UF membranes.[3] For foreign molecule attachment, membranes can be designed with covalent binding sites by e.g. adding a functional group at the hydrophilic chain end decorating the pore walls allowing for thiol-ene click chemistry based post-fabrication steps.[5] Lastly, the blending of two (or more) BCPs into the casting

dope enables a novel "mixing and matching" approach to e.g. tailoring of membrane surface chemistry from different polymers.[6]

Another main focus of SNIPS membrane studies has been the structure control of the selective top separation layer. Although first systematic studies regarding control of SNIPS membrane substructure are emerging,[7] the overwhelming majority of reports has the regularly patterned, self-assembled mesopores at the top surface at the center of attention. For a number of BCP systems casting conditions have been tested to achieve a regularly patterned surface structure including casting dope composition, evaporation time and coagulation bath conditions.[8-10] Other studies have focused on the tuning of pore size, by varying BCP molar mass or through the incorporation of additives.[9,11] Finally, several studies elucidate the formation mechanisms of these well-organized selective layers.[3,12-15] Most recently, *in-situ* grazing incidence small angle x-ray scattering (GISAXS) has been employed to better understand the structure evolution during organic solvent evaporation steps,[16-18] revealing structural phase transitions in the top separation layer.[17]

Despite numerous studies of parameters affecting SNIPS membrane structure and membrane formation mechanisms, systematic investigations of the relationship between surface structure and membrane performance as well as comparisons and benchmarking with existing UF membranes in terms of achievable resolution are still limited. In previous work, polyethylene oxide (PEO) or protein rejection and flux tests have been used to characterize membrane performance. Rejection tests have mainly been employed for pore size characterization via molecular weight cut off (MWCO) curves[3] while permeability has been assessed via flux tests. To move the use of SNIPS membranes

beyond conventional separation applications and towards protein or drug delivery vehicles, and inspired by studies of single file diffusion through nanochannels for protein delivery applications,[19] it is interesting to characterize the diffusion of small molar mass solutes through asymmetric SNIPS membranes as a function of membrane structure. To that end, in the present study we first investigated the effects of relative humidity (RH) on surface structure of SNIPS derived UF membranes from poly(isoprene-*b*-styrene-*b*-4-vinylpyridine) (PI-*b*-PS-*b*-P4VP, ISV) and subsequently correlated the observed structural changes with the permeation of a model dye solute through the BCP membranes thereby identifying parameters that tailor the rate of diffusion.

To the best of our knowledge, this is the first report on the influence of RH on the top surface structure of SNIPS derived UF membranes. Results demonstrate that ISV based membrane top surface structure is sensitive to RH and reaches an optimum at mid-range RH around 40-45%, while higher or lower humidity disturbs the surface structure. Interestingly, it is observed that higher casting solution concentrations render the membranes less sensitive to RH changes. Top surface structural changes directly correlate with model small molar mass dye solute permeation rates, with membranes casted at optimum mid-range RH possessing higher diffusivities. Additional control over the rate of small model solute diffusion is achieved through parent terpolymer molar mass as evidenced by membranes fabricated under RH conditions providing optimized surface structures. Finally, measured membrane permeability is compared to theoretical predictions to account for the experimental observations.

Experimental

Polymer synthesis: Three ISV triblock terpolymers were synthesized via sequential anionic polymerization as previously described.[8] The polymers were characterized by gel permeation chromatography (GPC) and ^{1}H NMR for molar mass (M_n), volume fractions of each block (f), and polydispersity index (PDI). A summary of characterization results for each ISV triblock terpolymer used in this study is provided in Table 3.1.

Table 3.1. Summary of ISV terpolymer characteristics.

Polymer	M_n (kg/mol)	f_{PI}	f_{PS}	f_{P4VP}	PDI
ISV43	43	0.24	0.56	0.20	1.02
ISV99	99	0.23	0.63	0.14	1.20
ISV119	119	0.19	0.65	0.16	1.17

*Number average molar mass (M_n), volume fraction (f), and polydispersity index (PDI).

Membrane fabrication: ISV terpolymers were dissolved in a binary solvent system of 1,4-dioxane (DOX) and tetrahydrofuran (THF) in a 7/3 weight ratio and appropriate concentrations (see results and discussion section). The SNIPS process was conducted inside a drybox following these steps: 1) the casting solution was pipetted onto a substrate (glass or nylon support); 2) a thin film was casted with a doctor blade at a gate height of 220 μm; 3) solvent evaporated for a specified amount of time, and 4) the film was immersed into a water coagulation bath. Levels of RH inside the drybox were controlled by either introducing a hot water bath or sparging with dry N_2 to increase or decrease RH, respectively. A humidity meter (Model: VWR-61161-378) was used to monitor RH during casting. Levels of RH were adjusted before casting. The stream of dry N_2 was stopped before the start of the casting process to prevent air disturbances during

the evaporation step. Humidity fluctuations during the evaporation step were within +/- 2% RH.

Scanning electron microscopy (SEM): Scanning electron microscopy (SEM) images of membranes were acquired on a Tescan LM Mira3 FE-SEM with an in-lens detector. Pore Size distributions and Fast Fourier transform (FFT) analyses of the top surfaces were performed via ImageJ with the Radial Profile Extended plugin (Philippe Carl). For comparison, the pore size data was fitted with both a normal Gaussian distribution and a log-normal distribution using Matlab's fitting tool with the bin width set to 1.

Membrane permeation studies: The permeation of a model dye solute, methyl orange, through the series of ISV based triblock terpolymer membranes was evaluated in a side-by-side diffusion cell (PermeGear). The setup (Figure 3.1) consisted of two chambers, the donor (right chamber) and receptor (left chamber) cell, with a volume of 3 mL each and containing a magnetic stirrer. The terpolymer membrane was placed between the two chambers with the selective surface layer facing the donor cell. The setup was sealed by clamping the cells tightly together and placed on a stir plate with a continuous stir rate of 200 rpm. The donor cell was filled with 3 mL of a methyl orange solution (1.0 mg methyl orange per mL buffer solution of the respective pH) while the receptor cell was filled with the same volume of the respective buffer solution. For membrane "closed state" studies, pH=4 buffer solutions were prepared with sodium acetate and acetic acid. For membrane "open state" studies, pH=7 buffer solutions were prepared with imidazole and hydrochloric acid. 0.1M buffer solutions were tested with a pH probe before conducting experiments. Receptor cell aliquots (300 μL) were taken

every 20 minutes for three hours for "open state" experiments and every 20 minutes for four hours for "closed state" experiments. Receptor cell aliquots were replaced with the same volume of the corresponding buffer solution.

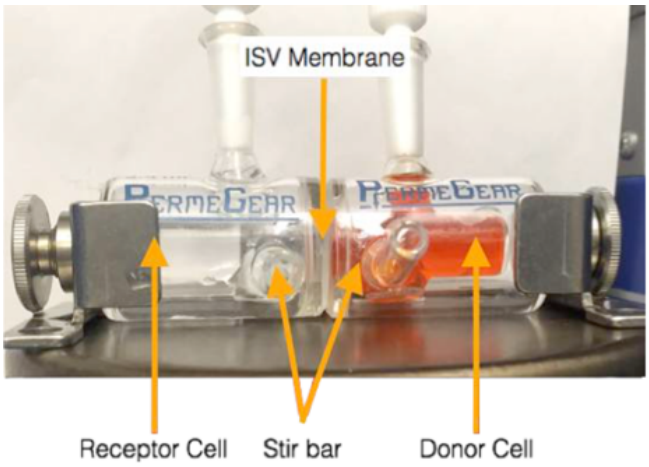

Figure 3.1. Experimental setup for membrane permeation studies: side-by-side stirred cell

The concentration of diffusant (methyl orange) was measured using a UV-VIS spectrophotometer (Varian Cary Model 5000) at a wavelength of 480 nm. Concentrations were determined based on standard curves of methyl orange. The diffusion constant of methyl orange can be determined from the cumulative mass $Q(t)$ of permeant passing through the membrane. The relevant relation is obtained by integration of the flux through the membrane (which is given by the well-known solution to Fick's second law for solute diffusion through pores) and reads as[20]

$$Q(t) = C(\varepsilon A)(\tau l)\left\{\frac{Dt}{(\tau l)^2} - \frac{1}{6} - \frac{2}{\pi^2}\sum_{n=1}^{\infty}\frac{(-1)^n}{n^2}e^{-n^2\pi^2\frac{Dt}{(\tau l)^2}}\right\} \quad (1)$$

Here, $Q(t)$ describes the cumulative mass of solute at time t. (eA) is the effective pore area of the membrane (e is the porosity of the membrane and, A = 1.54 cm^2), (tl) is the length of the tortuous path (with, t being the tortuosity). C is the concentration of solute

(methyl orange) in the donor cell (C = 1 mg/mL) and, D is the diffusion coefficient (in our results section also referred to as D(exp). In the limit of large time t (*i.e.,* in the case of the steady state) $Q(t)$ simplifies to,

$$Q(t) = C(\varepsilon A)\frac{D}{\tau l}\left\{t - \frac{(\tau l)^2}{6D}\right\} \tag{2}$$

Equation (2) has an intercept on the *t-axis*, referred to as the "time lag" [21,] or t_{lag}, that follows as,

$$t_{\text{lag}} = \frac{(\tau l)^2}{6D} \tag{3}$$

The steady state permeability, P (also referred to as P(exp) in our results section), for the transport of the permeant through the pores of the membrane can be evaluated by dividing Eqn. 2 by the concentration C and evaluating the time derivative to get,

$$P = \frac{1}{AC}\frac{dQ(t)}{dt} \equiv \frac{\varepsilon D}{\tau l} \tag{4}$$

Note that either Eqn. 3 or Eqn. 4 can be applied to get the diffusion constant of solutes from the cumulative mass measurements (i.e. D(exp) = $P\tau\, l/\varepsilon$). If a lag time can be obtained experimentally (*i.e.*, if t_{lag} is in the range of conveniently accessible timescales), then analysis of Eqn. 3 is generally the preferable approach since only knowledge of the tortuosity is required.

Since in the presence of nano-sized pores hydrodynamic effects on the mobility of the solute molecules cannot be excluded, the theoretical effective diffusion coefficient of methyl orange diffusing in the membranes, $D(\lambda)$, was determined using Renkin's hydrodynamic model (that describes the diffusion of a solid, spherical solute through an array of cylindrical pores with comparable size) valid for $0 \leq \lambda < 0.4$ [22]:

$$D(\lambda) = (1-\lambda)^2(1 - 2.104\lambda + 2.09\lambda^3 - 0.95\lambda^5)D_w \tag{5}$$

where λ is the solute-to-pore ratio (r_s/r_p) and D_w is the diffusivity of methyl orange dye in water. The first term in Eqn. 5, known as the 'steric factor', describes the restriction of the solute molecules entering into the pores (it is given by the ratio of the effective area $\pi(r_p\text{-}r_s)^2$ to the actual area πr_p^2). The second term describes the effect of the viscous drag due to the wall once the diffusant enters the pore. Membrane pore size was determined through image analysis of SEM micrographs using the ImageJ package. The solute size (in nm) was calculated by [23]:

$$\log_{10}(r_s) = -1.3363 + 0.395\log_{10}(M_w) \quad (6)$$

where M_w is the molar mass of methyl orange (327 g/mol).

Eqn. 6 yields a solute radius equal to 0.45 nm, in good agreement with the value, r_s = 0.47 nm, obtained from a geometrical approximation ($r_s = (3M_w / (4\pi\rho N_{Av}))^{1/3}$), where ρ = 1.28 g/ml denotes the density of methyl orange at T = 25°C and N_{Av} is the Avogadro number,[22] and an experimental value of r_s=0.40 nm in NaCl solution.[24]

The permeability coefficient, $P(\lambda)$, can be estimated theoretically as follows,

$$P(\lambda) = \frac{\varepsilon D(\lambda)}{\tau l} \quad (7)$$

Results and Discussion

Effect of relative humidity (RH) on membrane top surface structure: The quality of the top surface pore structure is a key factor with regards to the high-performance of SNIPS derived UF membranes. SNIPS membranes are of particular interest due to their highly ordered mesopores derived from BCP self-assembly leading to high pore densities and uniform pore size. The casting conditions to achieve membranes with an optimum surface structure, including solvent system, solution concentration,

evaporation time, etc., have been studied extensively. In this work, we evaluated another crucial, yet easy-to-ignore factor – relative humidity (RH).

ISV SNIPS membranes were casted inside a drybox as detailed in the experimental section. Inside the drybox, RH was controlled during the casting process by introducing water vapor or sparging with dry N_2. A humidity meter was used to determine RH during the evaporation process.

A membrane series from a solution of 9 wt% ISV119 in a 7/3 DOX/THF solvent mixture was produced by casting membranes at different RH employing an evaporation time of 200 s. Resultant membrane top surface structures as revealed by scanning electron microscopy (SEM) are shown in the top row of Figure 3.2. Associated FFT analyses of these SEM images are shown in Figure 3.3a.

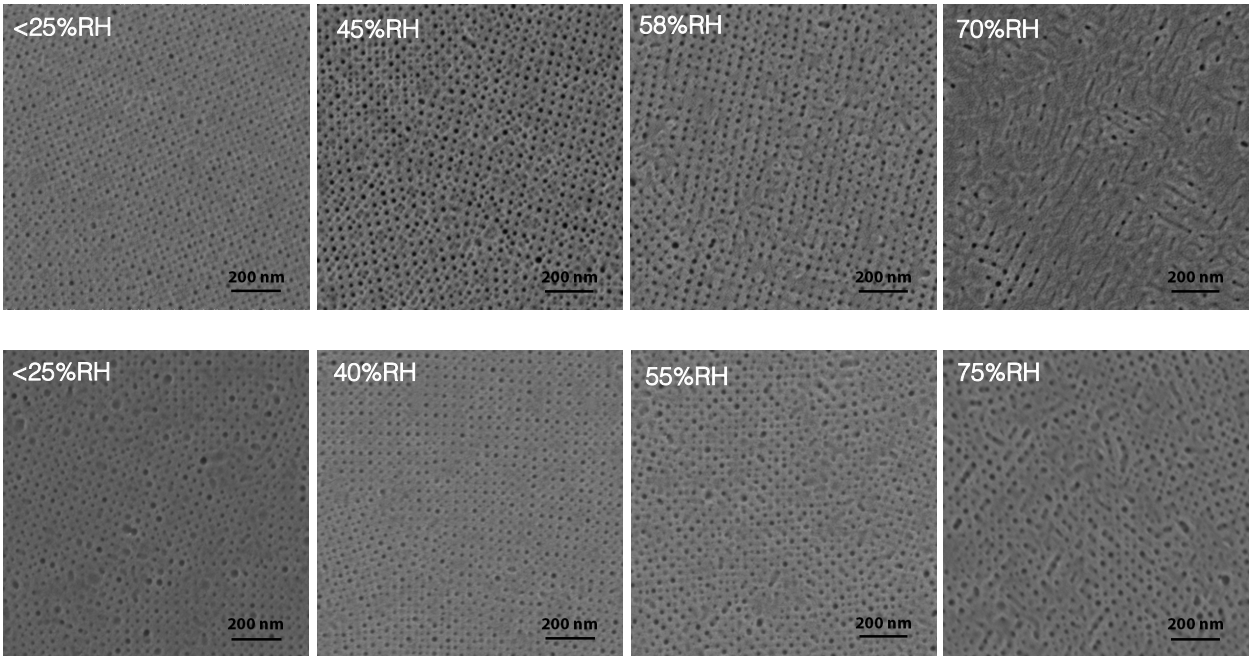

Figure 3.2. SEM micrographs of ISV119 membrane top surfaces casted at varying RH Membranes in the top row were obtained from a solution of 9 wt% ISV119 in a 7/3 DOX/THF solvent mixture and an evaporation time of 200 s. Membranes in the bottom row were fabricated from a solution of 11 wt% ISV119 in 7/3 DOX/THF solvent system casted onto 0.1 μm Nylon supports with an evaporation time of 100 s.

From the SEM images, top surfaces exhibited open and highly ordered pores with few defects when casted at 45% RH. FFT analysis confirmed pores packed in a 2D square lattice consistent with previous reports on ISV membranes.[3,25] At low humidity, (<25% RH), the top surface retained a well-ordered structure but with less open pores as compared to membranes casted at 45% RH. Increasing the humidity to 58% resulted in the presence of wormlike defects in the top surface. By further increasing the RH to 70%, top surface structure deteriorated substantially and assignment of a pore lattice from the associated FFT analysis is difficult. This series of membrane top surface structures suggested that the optimum RH value for casting ISV SNIPS membranes is at ~45%, with deterioration of the ordered pore surface structure when moving in particular to higher RH.

A second RH series was performed from a more concentrated ISV polymer solution. A solution of 11 wt% ISV119 in 7/3 DOX/THF solvent system was casted onto 0.1 μm Nylon supports with an evaporation time of 100 s. The corresponding membrane top surface SEM images are shown in the bottom row of Figure 3.2. From these SEM images, the optimum RH remained to be around 40%, while this time higher and lower RH lead to an increase in surface defects. Furthermore, when compared with results of the 9 wt% ISV series, the 11 wt% ISV image series does not present as much of a surface structure disruption as RH is increased to 70% or above. This is also reflected in the FFT analyses (Figure 3.3), exhibiting improved lattice formation for higher RH values when moving from 9 wt% to 11 wt% ISV solutions. At RH above 70%, it was not possible from the FFT analysis to assign a lattice of the membrane casted from 9 wt% solution,

while the counterpart from 11 wt% solution matched well with a square lattice. SEM top surface images were further analyzed for pore size distribution using ImageJ as shown in Figure 3.4. Results reveal that the membrane casted at 40% RH has the smallest average pore size when compared to membranes casted at <25%, 55%, and 75% RH. Furthermore, the membrane casted at 40% RH also exhibits a substantially narrower pore size distribution which is crucial for achieving high-resolution in separation processes. The coefficient of variation, σ/μ (ratio of standard deviation, σ, and mean, μ), is smallest in membranes casted at 40% RH (σ/μ= 0.36, 0.28, 0.36, and 0.38 for 25%, 40%, 55%, and 75% RH, respectively, for normal Gaussian fits and σ/μ= 0.14, 0.12, 0.14, and 0.15 for 25%, 40%, 55%, and 75% RH, respectively, for log-normal distributions[26]).

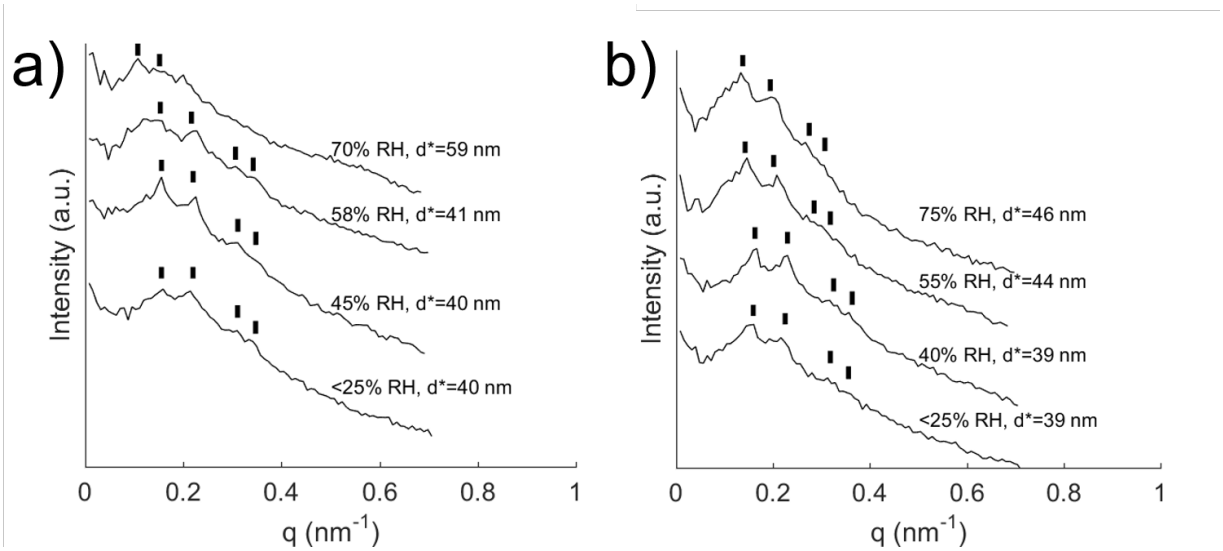

Figure 3.3. Radially integrated FFTs of SEM images of ISV119 membranes casted at varying RH from polymer casting solutions of a) 9 wt% and b) 11 wt%.

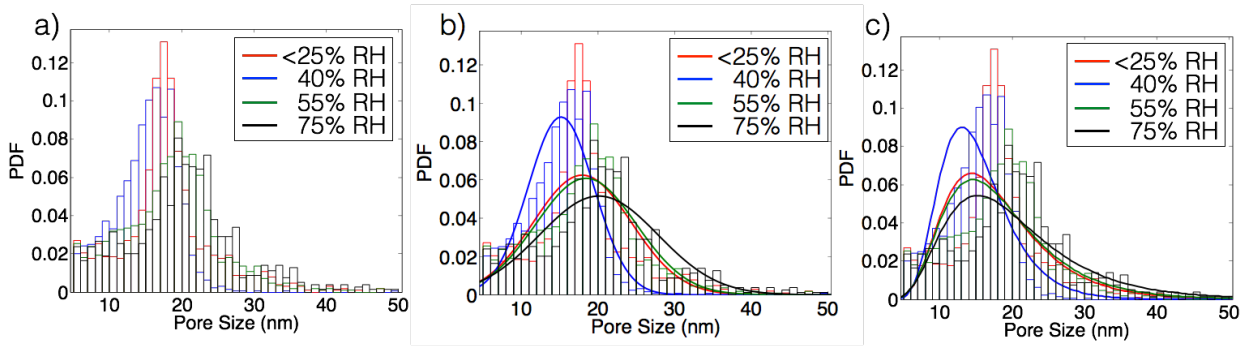

Figure 3.4. Pore size distribution analyses of ISV119 membranes casted at varying RH from polymer casting solutions of 11 wt%. a) pore size histograms; b) histograms with corresponding normal Gaussian fits (σ/μ= 0.36, 0.28, 0.36, and 0.38 for 25%, 40%, 55%, and 75% RH, respectively); c) histograms with corresponding log-normal fits (σ/μ= 0.14, 0.12, 0.14, and 0.15 for 25%, 40%, 55%, and 75% RH, respectively).

The FFT analyses of the top surface SEM images also allowed us to quantify the respective pore-to-pore distances, *d**. Comparing results in Figure 3.3a and b for both 9 wt% and 11 wt% ISV humidity series suggests that with increasing humidity, *d** increases. While values for *d** stay unchanged for low (<25%) and mid range (45% and 40%) RH, increasing RH further to first 58% or 55%, and then to 70% or 75%, increases *d** substantially. This increase in pore-to-pore distance results in a concomitant decrease in surface pore density, see results for the 11 wt% ISV series in Table 3.2. Therefore, when assuming a constant pore size and pore size distribution, membranes casted at RH around 45% not only have more well defined top surface layers with narrower pore-size distributions expected to provide higher resolution, they should also be more permeable as a result of higher pore densities.

Table 3.2. Pore density of humidity series casted from 11 wt% solution

Humidity	Pore density (x10^{14} pores/m^2)
<25%RH	6.8
40%RH	8.0
55%RH	6.7
75%RH	5.1

Permeation studies of small molar mass model solute

Influence of relative humidity on permeation

We investigated the effect of RH on solute transport properties of ISV119 membranes (11 wt%; 100s evaporation time) casted at 40% and 75% RH conditions. Figure 3.5 shows the cumulative amounts of methyl orange dye permeated through ISV119 membranes at neutral pH, i.e. at a pH where the poly(4-vinlypyridine) chains are un-protonated and the pores therefore open, as compared to pH=4, i.e. a pH at which protonation leads to chain stretching and therefore to closed pores (pK_a(P4VP)=4.6)[3]. The values of the diffusion coefficient, *D*(exp), calculated from the time-lag method (Eqn. 3), for the open states are listed in Table 3.3. A convexity or lag-time can be observed at short elapsed times before the system reaches a pseudo-steady state. The permeation rate of methyl orange is higher by almost a factor 4 in membranes casted at the optimized RH of 40% as compared to membranes cast at 75% RH. The higher permeation rate is consistent with the more highly ordered surface structure with fewer defects and resulting higher pore density of more narrowly size-distributed pores. On the time scale of the experiments, membranes in the closed state at pH=4 were not permeable at all to the small molar mass solute methyl orange.

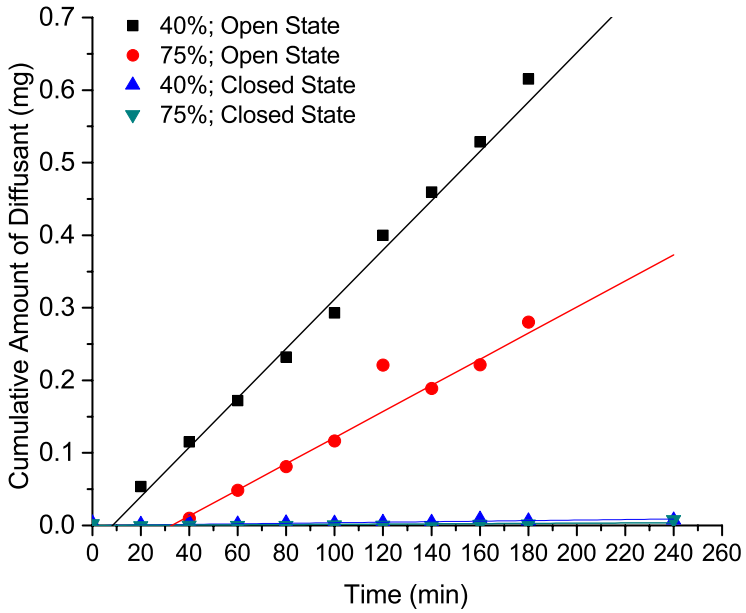

Figure 3.5. Cumulative amounts of methyl orange permeated through ISV119 membranes casted at 40% and 75% RH in open and closed states. Lag-times for ISV119 membranes in the open state are 8.3 min and 33 min for membranes casted at 40% and 75% RH, respectively (Table 3.3).

Table 3.3. Diffusion coefficient of methyl orange diffusing through ISV119 membranes casted from 40% and 75%RH together with membrane pore size analysis results.

Polymer	***D*(exp) (x10^{-8} cm^2/s)[a]**	***ε***	***r_p=μ***	***σ***
ISV119 40% RH	3.3 t_{lag}= 8.3 min	15.76%	7.9	2.5
ISV119 75% RH	0.8 t_{lag}= 33 min	18.34%	10.7	4.7

[a]As determined through the time-lag method (Eqn. 3).
Average pore size (r_p or μ) and porosity (ε) determined from ImageJ analysis and σ calculated from log normal fits (see text).

Influence of pore size on permeation

To gain a greater understanding of the relationship between BCP architecture, membrane structure, and performance, the permeation of the model dye methyl orange

was evaluated for a series of ISV membranes with varying molar mass. As previously reported by Dorin *et al.*[25], membranes fabricated from ISV terpolymers with similar volume fractions but increasing molar mass are characterized by increasing pore diameters. As a result, ISV membrane water and polymer solute rejection performance could be systematically tuned through tailoring of terpolymer molar mass. The present study was designed to assess small molar mass solute transport through ISV membranes as a function of molar mass.

Membranes fabricated from varying molar mass terpolymers were prepared by dissolving the triblock terpolymer into a binary solvent system of 7/3 DOX/THF by weight ratio. Supported membranes were cast from a 16 wt% ISV43, 12 wt% ISV99, and 11 wt% ISV119 polymer solution pipetted directly onto a 0.1 μm nylon support (Sterlitech Inc.) with an evaporation time of 100s and the optimized casting condition of 40% RH. SEM micrographs of the top surfaces are shown in Figure 3.6. All membrane top surfaces are characterized by highly ordered pores forming square lattices.

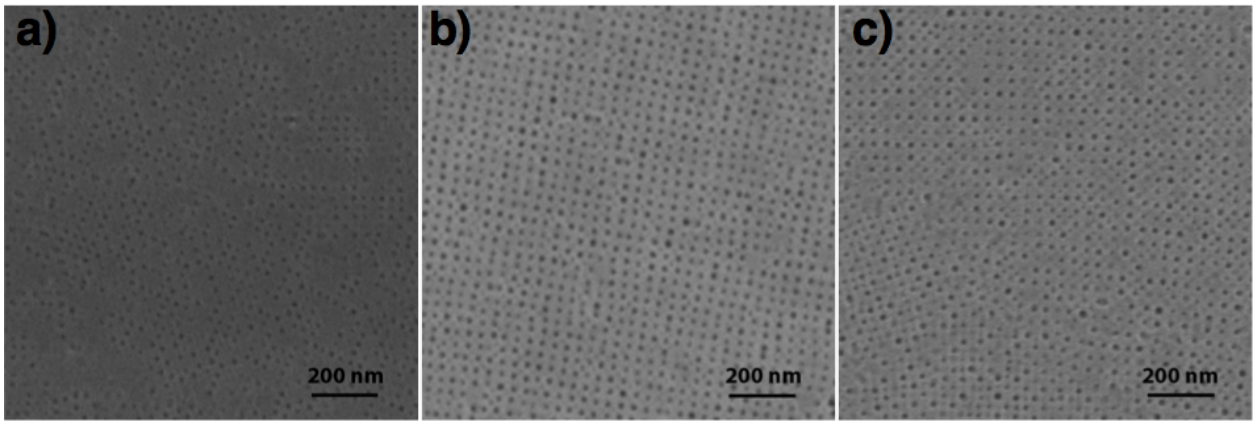

Figure 3.6. SEM characterization of top surfaces of ISV membranes from a) ISV43, b) ISV99, and c) ISV119, all cast at 40% RH. Supported membranes were cast from a 16 wt% ISV43, 12 wt% ISV99, and 11 wt% ISV119 polymer solution in 7/3 DOX/THF pipetted directly onto a 0.1 μm nylon support (Sterlitech Inc.) with an evaporation time of 100s.

The ISV43, ISV99, and ISV119 membranes were subjected to pH 7 ("open" state) and pH 4 ("closed" state) solutions of methyl orange as described above. The 0.1M buffer solutions used in the permeation experiments is expected to screen the electrostatics associated with the charged dye molecule. The cumulative amount of diffusant through the membranes in different states over time is shown in Figure 3.7 with corresponding calculated values of *D*(exp) listed in Table 3.4.

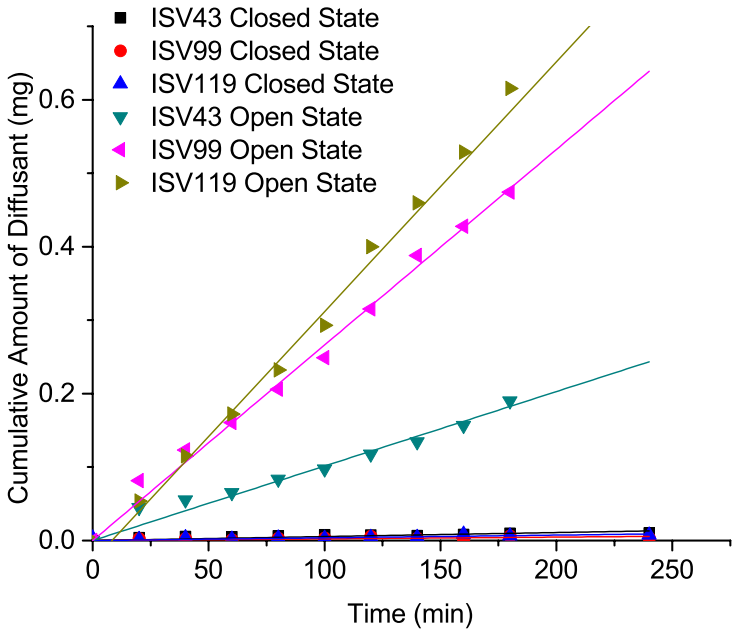

Figure 3.7. Cumulative amounts of methyl orange permeated through varying molar mass ISV triblock terpolymer membranes for open and closed states.

Table 3.4. Diffusion and permeability coefficients of methyl orange permeating through different ISV membranes for closed and open states together with membrane pore size analysis results.

	Closed State	Open State	Open State				
Polymer	***D*(exp)[a] (x10^{-8} cm^2/s)**	***D*(exp) (x10^{-8} cm^2/s)**	***P*(exp)* (x10^{-5} cm/s)**	**Pore density (x10^{14} pores/m^2)**	**ε**	**r_p=μ**	**σ**
ISV43	15.3	280[a]	1.1	4.6	3.86%	5.2	1.4
ISV99	1.4	160[a]	2.9	7.2	18.33%	9.0	2.0
ISV119	2.5	220[a]/3.3[b] t_{lag}=8.3 min	3.5	8.0	15.76%	7.9	2.5

* As determined from Eqn. 4 *i.e.*, *P*(exp)=slope/(*AC*)
[a] As determined through Eqn. 4.
[b] As determined through the time-lag method (Eqn. 3).
Average pore size (r_p or μ) and porosity (ε) determined from ImageJ analysis and σ calculated from log normal fits (see text).

Under neutral conditions ("open" state), the permeation rate of methyl orange increased with ISV terpolymer molar mass. While this is the expected behavior, closer inspection reveals that this trend is based on two different effects. Average pore size from image analysis (see Table 3.4) first increases from 10 nm for ISV43 to 18 nm for ISV99, but then decreases to 16 nm for ISV119. Therefore, pore size alone cannot explain the observed trend in *P*(exp) in Table 3.4.

Interestingly, for the molar mass series of terpolymer membranes studied here contrary to expected behavior the pore density increases with molar mass (Table 3.4, right side). So while moving from ISV99 to ISV119 average pore size decreases from 18 to 16 nm, pore density increases from 7.2 to 8.0x10^{14} pores/m^2. Together with differences in substructure not assessed here, this may account for the increased diffusion of the small molar mass model solute. The low pore density of ISV43 membranes may be due to closed pores, unrecognized by ImageJ during analysis, compare top surface SEM images in Figure 3.6.

As expected, under acidic conditions ("closed" state), the permeation rate again is reduced to a minimal amount for all membranes tested (compare Figures 3.5 and 3.7). In the "closed" state, pores are effectively closed preventing diffusion of methyl orange through the membranes. The lack of diffusion through the ISV membrane is likely a result of pore size changes and not primarily an effect of electrostatics. This is supported by the fact that the charge of the methyl orange dye in the 0.1M buffer solution is expected to be fully screened. The change in permeation rate from 220 x 10^{-8} cm^2/s ("open" state) to 2.5 x 10^{-8} cm^2/s ("closed" state) for ISV119 membranes can be regarded as an "on" and "off" switch brought on by pH changes.

In order to provide deeper insights into the effects of membrane structure on small molar mass solute transport, experimental results were compared to theoretical predictions. It is essential to characterize the entirety of the cross section of ISV membranes for permeation analysis. ISV membranes are characterized by a surface separation layer, which has a simple cubic structure[3,17] (~100-200 nm thick; described above) on top of a 3D interconnected macroporous sponge-like substructure. Furthermore, the relatively thick (~50-60 μm) and asymmetric sponge type substructure of these ISV membranes consists of macropore walls that themselves are mesoporous, (i.e. the substructure is not only asymmetric, but truly hierarchical).[3] This is in stark contrast to what has been described for PS-*b*-P4VP diblock copolymer derived UF membranes.[2] Therefore, we expect tortuous paths of solute molecules through these mesopores all the way through the entire membrane. As a result, in order to simplify the theoretical description, we used the hindered diffusion model and assumed a constant porosity throughout. For example, the measured diffusion coefficient, D(exp), of methyl orange

dye in UF membrane ISV99 in the open state at pH 7 (160 x 10^{-8} cm^2/s) is about a factor of three lower than the bulk solution value that is calculated using the Stokes-Einstein relationship, $D_w = k_bT/(6\pi \eta r_s) \sim 5.4 \times 10^{-6}$ cm^2/s (where k_b is Boltzmann's constant, T = 25°C, and η is the viscosity of water at 25°C, and the solute radius is estimated from Eqn. 6 as r_s = 0.45 nm). Based on the hydrodynamic theory for hindered diffusion of a solid, spherical solute through an array of cylindrical pores with comparable size as described by the Renkin equation (Eqn. 5), theoretical diffusion coefficients, $D(\lambda)$, were calculated for the different ISV terpolymer membranes as listed in Table 3.5. A hindered diffusion model was chosen to simplify solute diffusion through the complex pore structures of ISV membranes using the whole membrane thickness of l = 100 μm. Here we note that the assumption of continuity of the cylindrical nanopore structure of the separation layer across the total membrane thickness is not consistent with the actual membrane structure that shows a graded morphology with interconnected meso-, and macroporous regions (*vide infra*). Nevertheless, in the absence of a complete description of the membrane structure, the applied approximation was found to be helpful to interpret transport in terpolymer based UF membranes. Following this approach, the diffusion coefficients (for ISV119 membranes) were determined through Eqn. 3 (time-lag method) and Eqn. 4 for comparison. Additionally, theoretical permeability coefficients, $P(\lambda)$, were determined as a function of solute-to-pore size ratio and tortuosity **(**Eqn. 7**)**. In order to compare experimental and theoretical permeability coefficients, $P(\lambda)$ values were first calculated assuming a membrane thickness of l = 100 μm and without taking tortuosity into account (i.e. $\tau = 1$). The resulting values were within the same order of magnitude as P(exp), (compare columns 2 and 4 in Table 3.5).

As evidenced in earlier studies by cross sectional SEM images, neither separation layer nor substructure of ISV terpolymer membranes consist of vertical cylinder pores. For example, in the separation layer the cubic pore network is characterized by vertical and horizontal channels.[3,6-8,11] The solutes' pathway is therefore expected to be very tortuous as molecules can move vertically as well as horizontally through the selective layer. By equating $P(\text{exp})$ to $P(\lambda)$, calculated values of τ, used here as a fitting parameter, fall close to the typical tortuosity range of 1.5 – 2.5[27] for mesoporous membranes. These results suggest that the combined effects of hydrodynamic hindered diffusion and pore tortuosity can account for the observed small molar mass solute transport through ISV based UF membranes taking into account the entire membrane thickness (l = 100 μm).

For comparison $P(\lambda)$ values were also calculated assuming that only the selective top separation layer with l = 100 nm contributes to hindered diffusion. It is obvious from Table 3.5 that this does not provide satisfactory results as theoretical $P(\lambda, \tau = 1)$ values now are different by orders of magnitude from the experiments (compare $P(\lambda)$ in column 6 with $P(\text{exp})$ in column 2). Furthermore, matching experimental with theoretical results would require non-physical tortuosity values as also shown in Table 3.5 (column 7).

Table 3.5. Summary of diffusion and permeability coefficients from theoretical predictions and experimental data.

Membrane	***P*(exp)*** **(x10^{-5} cm/s)**	***D*(λ)** **(x10^{-6} cm^2/s)**	***P*(λ)** **(x10^{-5} cm/s)** **τ=1** ***l*=100 μm**	**τ^c** ***l*=100 μm**	***P*(λ)** **(x10^{-2} cm/s)** **τ=1** ***l*=100 nm**	**τ^c** ***l*=100 nm**	***D*(exp)** **(x10^{-6} cm^2/s)** **τ=1**
ISV43	1.1	3.7	1.4	1.3	1.4	1300	2.8[a]
ISV99	2.9	4.4	8.0	2.8	8.0	2800	1.6[a]
ISV119 (40% RH)	3.5	4.2	6.6	1.9	6.6	1900	2.2[a] (0.033[b]; t_{lag}=8.3 min)
ISV119 (75% RH)	1.5	4.5	8.3	5.5	8.3	5500	0.8[a] (0.008[b]; t_{lag}=33 min)

[*]As determined from Eqn. 4 *i.e., P*(exp)=slope/(*AC*)
[a]As determined from Eqn. 4, $D(\text{exp}) = P(\text{exp})\,(\tau l)/\varepsilon$ (assuming τ=1),
[b]As determined by the time-lag method (Eqn. 3),
[c]As determined by equating *P*(exp) to $P(\lambda, \tau)$.

Conclusions

In summary, ISV membranes derived from the SNIPS process were fabricated from ISV triblock terpolymers ranging in molar mass from 43 kg/mol to 119 kg/mol at varying levels of RH during the casting process. Investigations into the influence of RH on membrane surface structure revealed that ISV membranes exhibited optimal surface ordering and pore density when casted at mid range values around 40-45% RH. The observed structural changes correlated with differences in permeation rate of a model small molar mass solute through membranes casted at optimal and non-optimal RH, with higher diffusivity observed in the membrane characterized by a more ordered surface structure obtained at optimal RH.

Analysis into the relationship between triblock terpolymer molecular size and diffusion performance revealed that membranes fabricated from higher molar mass ISV terpolymers exhibited higher small molar mass solute diffusivity. Results could be rationalized by taking into account observed membrane pore size and pore density.

Moreover, combining predictions of a hydrodynamic theory assuming hindered diffusion of a solid, spherical solute through an array of cylindrical pores of comparable size with the effect of pore tortuosity, observed values of the small molar mass solute permeability coefficients could only be accounted for when the entire membrane thickness (l = 100 μm) rather than only the thickness of the top separation layer (l = 100 nm) was used in the calculations.

The ability to extend the use of SNIPS membranes away from regular separation applications and towards the use as well-controlled delivery vehicles rests on tuning membrane properties via BCP molecular design and architecture as well as on finding optimal membrane casting conditions. This study suggests that through tailoring of BCP molar mass and relative humidity during casting, the rate of release and diffusion of solutes through SNIPS membranes can be controlled for targeted performance.

Acknowledgments

The authors would like to acknowledge funding of this work by the FLIR Systems, Inc. and the Defense Threat Reduction Agency (DTRA) Contract No. HDTRA1-13-C0003. This work utilized the Cornell Center for Materials Research (CCMR) facilities supported by NSF MRSEC program (DMR-1120296). Y.G. acknowledges funding by the National Science Foundation (DMR-1409105).

REFERENCES

[1] R.M. Dorin, D. Salomon Marques, H. Sai, U. Vainio, W.A. Phillip, K.V. Peinemann, S.P. Nunes, U. Wiesner, Solution Small Angle X ray Scattering as a Screening and Predictive Tool in the Fabrication of Asymmetric Block Copolymer Membranes, ACS Macro Lett. 1 (2012) 614−617.

[2] K.V. Peinemann, V. Abetz, P.F.W. Simon, Asymmetric superstructure formed in a block copolymer via phase separation, Nat. Mater. 6 (2007) 992-996.

[3] W.A. Phillip, R.M. Dorin, J. Werner, E.M. Hoek, U. Wiesner, M. Elimelech, Tuning structure and properties of graded triblock terpolymer-based mesoporous and hybrid films, Nano Lett. 11 (2011) 2892-2900.

[4] R.A. Mulvenna, J.L. Weidman, B. Jing, J.A. Pople, Y. Zhu, B.W. Boudouris, W.A. Phillip, Tunable nanoporous membranes with chemically-tailored pore walls from triblock polymer templates, J. Membr. Sci. 470 (2014) 246-256.

[5] Q. Zhang, Y. Gu, Y.M. Li, P.A. Beaucage, T. Kao, U. Wiesner, Dynamically Responsive Multifunctional Asymmetric Triblock Terpolymer Membranes with Intrinsic Binding Sites for Covalent Molecule Attachment, Chem. Mater. 28 (2016) 3870–3876.

[6] Y.M. Li, D. Srinivasan, P. Vaidya, Y. Gu, U. Wiesner, Asymmetric Membranes from Two Chemically Distinct Triblock Terpolymers Blended during Standard Membrane Fabrication, Macromol. Rapid Commun. 37 (2016) 1689-1693.

[7] Q. Zhang, Y.M. Li, Y. Gu, R.M. Dorin, U. Wiesner, Tuning substructure and properties of supported asymmetric triblock terpolymer membranes, Polymer 107 (2016) 398-405.

[8] M.M. Pendergast, R.M. Dorin, W.A. Phillip, U. Wiesner, E.M.V. Hoek, Understanding the structure and performance of self-assembled triblock terpolymer membranes, J. Membr. Sci. 444 (2013) 461-468.

[9] S. Rangou, K. Buhr, V. Filiz, J.I. Clodt, B. Lademann, J. Hahn, A. Jung, V. Abetz, Self-organized isoporous membranes with tailored pore sizes, J. Membr. Sci. 451 (2014) 266-275.

[10] A. Jung, S. Rangou, C. Abetz, V. Filiz, V. Abetz, Structure Formation of Integral Asymmetric Composite Membranes of Polystyrene‐block‐Poly (2‐vinylpyridine) on a Nonwoven, Macromol. Mater. Eng. 297 (2012) 790-798.

[11] Y. Gu, U. Wiesner, Tailoring Pore Size of Graded Mesoporous Block Copolymer Membranes: Moving from Ultrafiltration toward Nanofiltration, Macromol. 48 (2015) 6153-6159.

[12] S.P. Nunes, R. Sougrat, B. Hooghan, D.H. Anjum, A.R. Behzad, L. Zhao, N. Pradeep, I. Pinnau, U. Vainio, K.V. Peinemann, Ultraporous films with uniform nanochannels by block copolymer micelles assembly, Macromol. 43 (2010) 8079-8085.

[13] V. Abetz, Isoporous block copolymer membranes, Macromol. Rapid Commun. 36 (2015) 10-22.

[14] C. Stegelmeier, V. Filiz, V. Abetz, J. Perlich, A. Fery, P. Ruckdeschel, S. Rosenfeldt, S. Förster, Topological paths and transient morphologies during formation of mesoporous block copolymer membranes, Macromol. 47 (2014) 5566-5577.

[15] L. Oss-Ronen, J. Schmidt, V. Abetz, A. Radulescu, Y. Cohen, Y. Talmon, Characterization of block copolymer self-assembly: from solution to nanoporous membranes, Macromol. 45 (2012) 9631-9642.

[16] D.S. Marques, R.M. Dorin, U. Wiesner, D.M. Smilgies, A.R. Behzad, U. Vainio, K.V. Peinemann, S.P. Nunes, Time-resolved GISAXS and cryo-microscopy characterization of block copolymer membrane formation, Polymer 55 (2014) 1327-1332.

[17] Y. Gu, R.M. Dorin, K.W. Tan, D.M. Smilgies, U. Wiesner, In Situ Study of Evaporation-Induced Surface Structure Evolution in Asymmetric Triblock Terpolymer Membranes, Macromol. 46 (2016) 4195-4201.

[18] B. Sutisna, G. Polymeropoulos, V. Musteata, K.V. Peinemann, A. Avgeropoulos, D.M. Smilgies, N. Hadjichristidis, S.P. Nunes, Design of block copolymer membranes using segregation strength trend lines, Mol. Syst. Des. Eng. 1 (2016) 278-289.

[19] S.Y. Yang, J.A. Yang, E.S. Kim, G. Jeon, E.J. Oh, K.Y. Choi, S.K. Hahn, J.K. Kim, Single-file diffusion of protein drugs through cylindrical nanochannels. ACS Nano, 4 (2010) 3817-3822.

[20] J. Crank, The Mathematics of Diffusion, Oxford University Press, Oxford, 1975.

[21] R.A. Siegel, E.L. Cussler, Reactive barrier membranes: some theoretical observations regarding the time lag and breakthrough curves. J. Membr. Sci. 229 (2004) 33-41.

[22] E.M. Renkin, Filtration, diffusion, and molecular sieving through porous cellulose membranes. J. Gen. Physiol, 38 (1954), 225-243.

[23] W.R. Bowen, A.W. Mohammad, Characterization and prediction of nanofiltration membrane performance—a general assessment. Chem. Eng. Res. Des., 76 (1998), 885-893.

[24] M. Mitsuishi, A. Datyner, Diffusion of methyl orange and its homologs in water and in micellar solution of dodecyltrimethylammonium bromide. Sen'i Gakkaishi, 36 (1980), T175-T178.

[25] R.M. Dorin, W.A. Phillip, H. Sai, J. Werner, M. Elimelech, U. Wiesner, Designing block copolymer architectures for targeted membrane performance. Polymer, 55 (2014) 347-353.

[26] K.H. Youm, S.W. Kim, Prediction of intrinsic pore properties of ultrafiltration membrane by solute rejection curves: effects of operating conditions on pore properties. Journal of chemical engineering of Japan, 24 (1991), 1-7.

[27] R.W. Baker, Membrane technology and applications, England, 2004.

CHAPTER 4

ASYMMETRIC MEMBRANES FROM TWO CHEMICALLY DISTINCT TRIBLOCK TERPOLYMERS BLENDED DURING STANDARD MEMBRANE FABRICATION

Abstract

Deviating from the traditional formation of block copolymer (BCP) derived isoporous membranes from one block copolymer chemistry, here asymmetric membranes with isoporous surface structure were derived from two chemically distinct block copolymers blended during standard membrane fabrication. As a first proof of principle, we report the fabrication of asymmetric membranes blended from two chemically distinct triblock terpolymers, poly(isoprene-*b*-styrene-*b*-(4-vinyl)pyridine) (ISV) and poly(isoprene-*b*-styrene-*b*-(dimethylamino)ethyl methacrylate) (ISA), differing in the pH-responsive hydrophilic segment. Using block copolymer self-assembly and non-solvent induced phase separation (SNIPS) process, pure and blended membranes were prepared by varying weight ratios of ISV to ISA. Pure and blended membranes exhibited a thin, selective layer of pores above a macroporous substructure. Observed permeabilities at varying pH values of blended membranes depended on relative triblock terpolymer composition. These results open a new direction for membrane fabrication through the use of mixtures of chemically distinct block copolymers enabling the tailoring of membrane surface chemistries and functionalities.

Adapted with permission from Y.M. Li, D. Srinivasan, P. Vaidya, Y. Gu, U. Wiesner, Asymmetric Membranes from Two Chemically Distinct Triblock Terpolymers Blended during Standard Membrane Fabrication, *Macromol. Rapid Commun.* **37**, 1689-1693 (2016).

Introduction

There has been growing interest in asymmetric ultrafiltration (UF) membranes derived from block copolymers since the first report by Peinemann *et al*.[1] resulting in isoporous membranes that combine a highly ordered surface structure with high permselectivity. The most widely studied polymer system fabricated to date with this block copolymer self-assembly and non-solvent induced phase separation (SNIPS) process[2] is the diblock copolymer, poly(styrene-*b*-(4-vinyl)pyridine) (PS-*b*-P4VP, SV). The phase inversion technique was successfully applied to other diblock copolymer systems including poly(styrene-*b*-(dimethylaminoethyl) methacrylate) (PS-*b*-PDMAEMA),[3] poly(styrene-*b*-ethylene oxide) (PS-*b*-PEO),[4] poly(styrene-*b*-methyl methacrylate) (PS-*b*-PMMA),[5] as well as triblock terpolymer systems like poly(isoprene-*b*-styrene-*b*-4-vinylpyridine) (PI-*b*-PS-*b*-P4VP, ISV),[6] poly(isoprene-*b*-styrene-*b*-*N,N*-dimethylacrylamide) (PI-*b*-PS-*b*-PDMA)[7] and poly(styrene-*b*-4-vinylpyridine-*b*-propylene sulfide) (PS-*b*-P4VP-*b*-PPS, SVPS).[8]

Employing a second component in the casting dope solution, various membrane properties were tailored. For example, the morphology of the top surface layer was tuned by the addition of small organic molecules[9] and metal ions which form metal-polymer complexes.[10] With the introduction of an additive that chemically interacts/swells one block of the block copolymer, pore sizes were tailored.[11] For example, an organic additive, glycerol, was added to the ISV system in order to tailor the pore size moving the range of filtration from UF to nanofiltration.[12] Pore sizes were also tailored in ISV terpolymer derived membranes by blending a homopolymer[6] or in SV copolymer derived membranes by blending of other SV block copolymers with varied molar mass and block

volume fractions.[13] Finally, organic-inorganic hybrid membranes have been reported from the SNIPS process by mixing in sol- or other inorganic nanoparticles into the block copolymer dough,[14] while carbon materials with asymmetric structure were derived from adding in resols[15] and subsequent heat processing at elevated temperatures.

To the best of our knowledge, however, to date no studies have been reported in which the SNIPS process was applied to the mixture of two or more chemically distinct block copolymers. This would be particularly interesting for mixtures in which the blocks that end up decorating the pore walls would be chemically distinct. In this case it would be possible to mix and match different chemistries and therefore different functionalities and properties to the pore walls during standard membrane fabrication. Previously, systems that desired e.g. a combination of chemistries and/or stimuli responsive performances in the pore walls were limited to an extra post-modification grafting step on the final membrane.[8,16] In contrast, here we demonstrate the facile approach for the fabrication of membranes that exhibit two chemistries in the pores as a consequence of incorporating two chemically distinct triblock terpolymers into the casting dope solution. In this way, the ability to dial in different chemistries and their associated functionalities to the pore surface is accomplished during the standard fabrication step, completely eliminating extra post-modification steps. Combining different chemistries into the pore wall may enable new and attractive capabilities in selectivity, e.g. in complex protein separations.

Methods

Polymer synthesis: The triblock terpolymers, poly(isoprene-*b*-styrene-*b*-(4-vinyl)pyridine) and poly(isoprene-*b*-styrene-*b*-(dimethylamino)ethyl methacrylate), were synthesized *via* a sequential anionic polymerization technique. Detailed descriptions can be found in the literature.[6,20,21] The molar mass of ISV and ISA in tetrahydrofuran (THF) as the solvent was determined by gel permeation chromatography (GPC) on a Waters Ambient-Temperature GPC equipped with a Waters 410 differential refractive index detector. The volume fraction of each domain was determined by a combination of GPC on individual blocks (PI) with ^{1}H solution nuclear magnetic resonance (^{1}H NMR) on a INOVA 400 MHz spectrometer with $CDCl_3$ as the solvent.

Membrane fabrication and characterization: Membranes were fabricated as described in the text. A hole punch was used to punch out sections of the membrane with an active area of 4.1 cm^2 for pH dependent permeability measurements.

SEM micrographs were acquired using a Tescan Mira3 field emission scanning electron miscrope (FE-SEM) equipped with an in lens detector. Prior to SEM imaging, samples were coated with Au-Pd for 6 s using a Denton Vacuum Desk II sputter coater. FFT image analysis was performed on surface SEM micrographs using ImageJ64 software with the Radial Profile Extended plugin (Philippe Carl).

Performance tests: For pH-stimulus responsive performance tests, pure and blended membranes were evaluated in a 10 mL dead end stirred ultrafiltration test cell (Amicon 8010, Millipore) with an applied pressure of N_2 gas at ~0.07 bar. The experimental details are described in the literature.[12] During the test, the volume of buffer solution permeated was <10 mL. Three data points under the same applied pressure were

averaged to estimate the permeability under different pH conditions. Sodium acetate-acetic acid solutions were prepared as buffers with pH less than 6. Imidazole-hydrochloric acid solutions were prepared as buffers ranging from pH 6 to 10. The buffers were tested with a pH meter before performance tests were conducted.

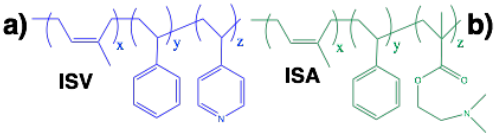

b)

Polymer	Molar Mass (kg/mol)	f_{PI}	f_{PS}	f	PDI
ISV	119	0.22	0.64	0.14	1.17
ISA	118	0.23	0.63	0.14	1.07

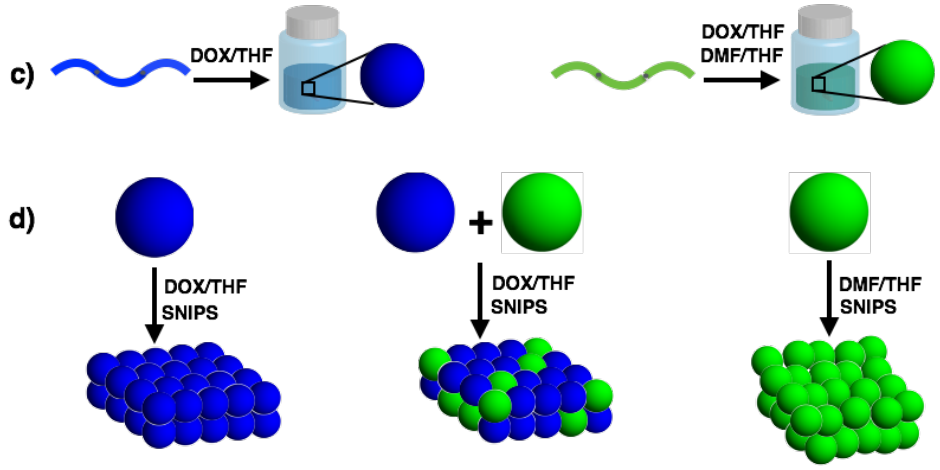

Figure 4.1. Pure and blended mesoporous membranes are derived from poly(isoprene-*b*-styrene-*b*-(4-vinyl)pyridine) (ISV) and poly(isoprene-*b*-styrene-*b*-(dimethylamino)ethyl methacrylate) (ISA) triblock terpolymers. a) Chemical structures of ISV and ISA. b) Table displaying molar mass, volume fractions (*f*), and polydispersity index (PDI) of the two terpolymers. c) Terpolymers and their respective solvent systems. d) Schematic of formation of pure and blended membranes casted by block copolymer self-assembly and non-solvent induced phase separation (SNIPS) process. For simplicity, ISV and ISA are indicated as blue and green spheres, respectively, to visualize the compositional variations within the membrane. The true distribution of the terpolymers in the membrane is currently unknown.

Results and Discussion

Triblock terpolymer characterization: For this study, two triblock terpolymers, poly(isoprene-*b*-styrene-*b*-(4-vinyl)pyridine) (ISV) and poly(isoprene-*b*-styrene-*b*-(dimethylamino)ethyl methacrylate) (ISA), of similar molar mass and volume fractions, were synthesized by sequential anionic polymerization. The molar mass of ISV and ISA was 119 and 118 kg mol^{-1}, respectively. ISV had volume fractions of 0.22, 0.64, and 0.14, for the polyisoprene (PI; ρ=0.913), polystyrene (PS; ρ=1.05), and poly-4-vinylpyridine (P4VP; ρ=1.15) blocks, respectively. Similarly, ISA had volume fractions of 0.23, 0.63, and 0.14, for the PI, PS, and poly(dimethylamino)ethyl methacrylate (PDMAEMA; ρ=1.18) blocks, respectively. Figure 4.1a,b shows the chemical structures of ISV and ISA together with a table summarizing the polymer characterization results.

Membrane preparation, fabrication, and characterization: Membranes were fabricated by a hybrid process of block copolymer self-assembly and non-solvent induced phase separation (SNIPS). The triblock terpolymers were dissolved in an appropriate solvent system. The solvent system was chosen similar to previous studies on ISV terpolymer derived asymmetric membranes.[6] In order to generate blended membranes, ISV and ISA were separately dissolved in the binary solvent system of 1,4-dioxane (DOX) and tetrahydrofuran (THF) in a 7:3 ratio (by weight) (7:3 DOX/THF). For pure membranes, ISV was dissolved in 7:3 DOX/THF while ISA was dissolved in dimethylformamide (DMF) and THF in a 7:3 ratio (by weight) (7:3 DMF/THF) as described in Figure 4.1c. A change of the solvent system for pure ISA membranes was necessary in order to fabricate mechanically stable and cohesive membranes enabling pH-stimulus responsive performance studies (see Figure B.1a).

All membranes were cast from dope solutions with a final polymer concentration of 15 wt%. The membrane casting solutions contained different ISV:ISA weight ratios: 1:0, 9:1, 7:3, 6:4, and 0:1. Majority ISA blended membranes could not be studied as the SNIPS process did not lead to mechanically stable structures (see Figure B.1b). For casting solutions containing both triblock terpolymers, final dope solutions were prepared by mixing ISV and ISA polymer solutions and allowed to stir at 200 rpm for ten minutes before casting.

The 15 wt% dope solutions were cast onto a glass substrate using an automated blade-casting machine. The thin films were evaporated for 100 seconds. This evaporation period creates a concentration gradient in the film normal direction driving the self-assembly of block copolymers near the top surface to produce the selective skin layer while the bottom structure remains disordered resulting in a sponge-like substructure providing mechanical stability upon plunging into the water precipitation bath.

In order to correlate the addition of ISA, relative to ISV, to the casting solution with membrane structure and performance, three ISV:ISA mixing ratios (by weight) were employed: 9:1, 7:3, and 6:4. Pure ISV and ISA membranes were fabricated to serve as references. A schematic of pure and blended membrane top surface structures is shown in Figure 4.1d where the different terpolymers are depicted as spheres of different color (blue: ISV; green: ISA) and for simplicity only two layers of terpolymer micelles are depicted. This schematic reflects the cubic BCP micelle morphology that is at the origin of the square pore lattice observed for ISV based BCP UF membranes.[6,17,18]

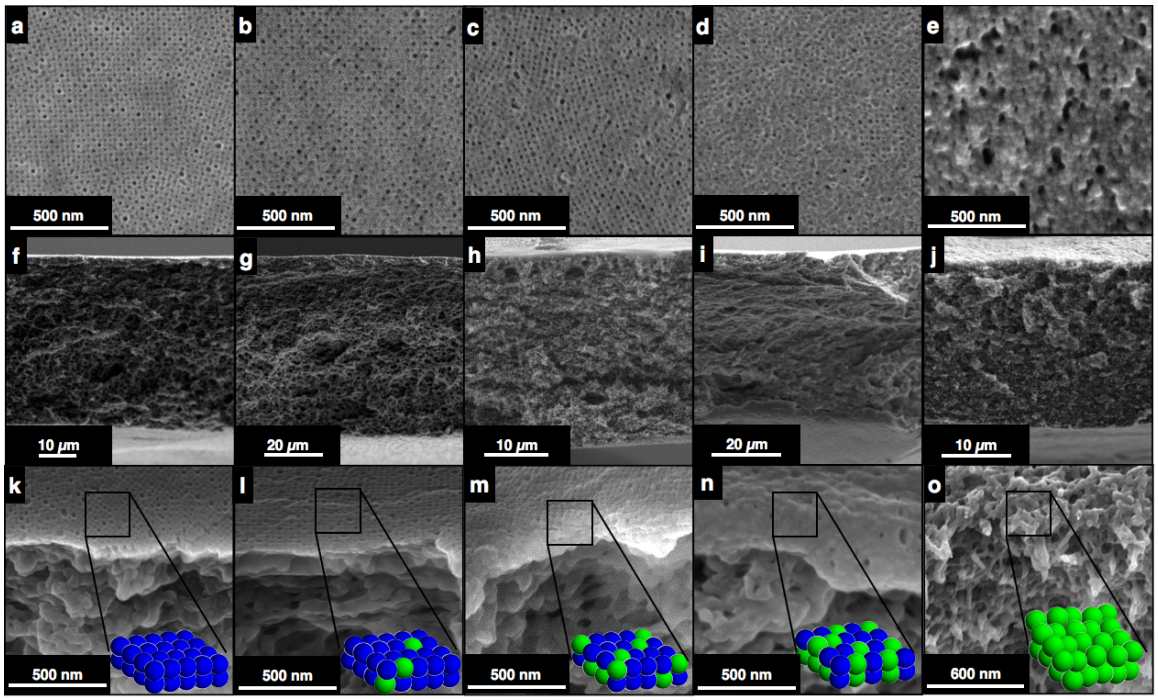

Figure 4.2. SEM characterization of surface structures (top row), cross sections (middle row), and areas close to the surface (45° tilted images) of (a,f,k) 15% ISV in 7:3 DOX/THF, (b,g,l) 15% 9:1 blend in 7:3 DOX/THF, (c,h,m) 15% 7:3 blend in 7:3 DOX/THF, (d,i,n) 15% 6:4 blend in 7:3 DOX/THF, and (e,j,o) 15% ISA in 7:3 DMF/THF derived membranes.

SEM micrographs of the resultant membranes' top surface (top row), cross section (middle row), and areas close to the top surface (45° tilted image, bottom row) are shown in Figure 4.2. All five membranes are composed of a porous top surface spanning the skin layer thickness (~200 nm) above a hierarchically porous, sponge-like substructure. The pure ISV membrane (Fig. 4.2a) exhibited a high density of uniform pores arranged in a 2-D square lattice typically associated with ISV membranes (see Figure B.2).[16] The surface structure reflects the underlying cubic block copolymer microphase separated lattice as demonstrated by Gu *et al.*[18] With the introduction of ISA (10% and 30%; Fig. 4.2b,c), the top surface structure remains ordered. Both blended membranes retain a high density of well-ordered and packed pores. For the 6:4 blend, a

marked loss of surface order is already detected in parts of the membrane surface consistent with a disordered surface structure for pure ISA membranes (Fig. 4.2d,e).

Membrane performance: In order to correlate composition with membrane performance, pH dependent permeabilities were measured for pure and blended membranes using a pressurized dead-end stirred cell (see Appendix C, Methods section). Normalized permeability results from the flow experiments are presented in Figure 4.3 (for absolute permeability values see Figure B.3). In a previous study it was shown that the permeability of ISV membranes is a strong function of pH due to pH dependent protonation and chain stretching of the P4VP brushes at the pore surface.[6] This is consistent with the pH-responsive permeability observed for the pure ISV membrane in Figure 4.3.

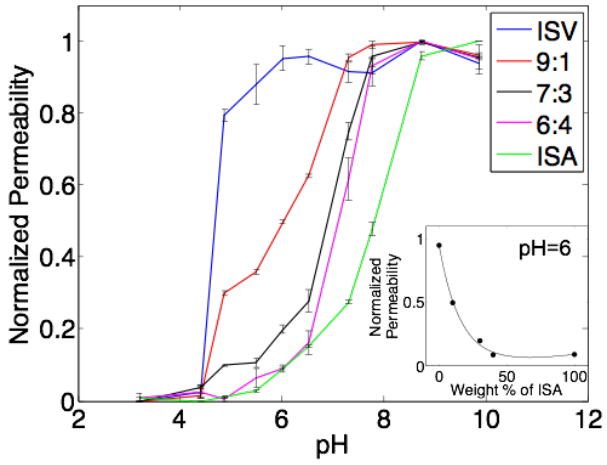

Figure 4.3. Permeability (normalized) for pure (ISV, ISA) and blended (9:1, 7:3, & 6:4 blends of ISV + ISA) membranes at various pH values. Indicated errors are standard deviations from three replicate measurements. Inset: Effect of composition on permeability at pH=6. The associated curve is used only as a guide for the eye.

Above the pK_a of 4.6 of P4VP,[6] the permeability is high due to the low degree of protonation resulting in the collapse of the P4VP chains. Around the pK_a of P4VP, the permeability strongly decreases due to the increased protonation of P4VP causing the

chains to extend towards the center of the pore and therefore, hindering transport through the membrane.[19] A similar behavior is observed in Figure 4.3 for ISA membranes where PDMAEMA chains reside at the pore walls. However, since PDMAEMA has a pK_a of 7.8,[3] the curve is shifted to higher pH values relative to behavior of ISV.

Blended membranes exhibit a mixed performance intermediate between that of pure ISV and ISA membranes. In particular, a pronounced shift to higher pH values of the pH dependent behavior is observed in membranes with increasing amounts of ISA. For example, the onset of permeability reduction occurs at a higher pH for 9:1, and at even higher pH for 7:3 and 6:4 blended membranes relative to pure ISV membrane. Details of the changes of the permeability curves relative to each other are also instructive. In all blended membranes, the majority polymer is ISV. This is consistent with the observation of decreasing low pH sections/steps in the curves that resemble ISV behavior as a function of increasing ISA weight fraction. In contrast, the high pH sections of the blended membrane permeability curves do not show pure ISA behavior but rather shift to lower pH values as a whole (vide supra). When normalized permeability for the blended membranes is plotted versus wt% ISA for a pH value around 6, i.e. midway between the pK_a values of ISV and ISA (see inset Figure 4.3), the sensitivity to composition becomes quite apparent. Finally, at pH 3, the full protonation of PDMAEMA and P4VP segments are achieved enabling the full extension of all charged chains resulting in minimum permeability. The same trends and behaviors were observed in an independent replicate of membrane formation and measurements for pure ISV and ISA and blended (9:1, 7:3, & 6:4 blends of ISV and ISA) membranes (see Figure B.4).

Conclusions

In summary, self-assembly and non-solvent induced phase separation process (SNIPS) was utilized to fabricate blended membranes comprised of two chemically distinct triblock terpolymers, ISV and ISA. The asymmetric blended membranes possess an ordered surface structure packed in a 2-D square pore lattice above a hierarchically porous sponge-like substructure. Their pH dependent behavior is based on the relative percentage of ISV to ISA, enabling the tailoring of transport properties and tunability in the gating mechanism.

The generation of blended membranes by simply "mixing and matching" two chemically distinct triblock terpolymers in the casting solution demonstrates a pathway to advanced asymmetric block copolymer derived UF membranes in which different pore surface chemistries and associated functionalities can be integrated into a single membrane via standard membrane fabrication, i.e. without requiring laborious post-fabrication modification steps. As the present proof of principle experiments have shown these mixed chemistries result in performance profiles different from those of membranes obtained from either of the two constituting block copolymers alone. The work poses a number of scientific questions for future studies concerning e.g. the limits of this blending approach in terms of allowable differences in molar mass and block fractions. It may also have interesting implications for separation applications. For example, blending two distinct chemistries into the membrane surface may provide affinities to proteins that are different to those of membranes obtained from either of the two constituting block copolymers alone, and therefore may lead to improved selectivity. And the blending may not be confined to only two block copolymers but may be extended to multiple (i.e. more

than two) chemically distinct block copolymers and block copolymers with different end functionalities,[8] enabling to tailor membrane properties in unprecedented ways.

Acknowledgements

This project was funded by Contract No. HDTRA1-13-C0003 from the Defense Threat Reduction Agency (DTRA). Y.G. was funded by the National Science Foundation (DMR-1409105). This work utilized the Cornell Center for Materials Research (CCMR) facilities supported by NSF MRSEC program (DMR-1120296).

APPENDIX B

Mechanical stability of membranes: Images of pure ISA in 7:3 DOX/THF (Figure B.1a) and 5:5 ISV/ISA blend in 7:3 DOX/THF (Figure B.1b) derived membranes contrasted to pure ISV in 7:3 DOX/THF (Figure B.1c) derived membrane reveal problems in obtaining homogeneous membranes with good mechanical stability. As a result, studies of majority ISA blended membranes in the solvent system 7:3 DOX/THF were not possible. Furthermore, based on these results, in order to obtain pure ISA based membranes the solvent system was changed from 7:3 DOX/THF to 7:3 DMF/THF. This provided membranes without holes while featuring a similar appearance to pure ISV membranes enabling examination of performance characteristics serving as a comparison for pure ISV and blended ISV/ISA membranes.

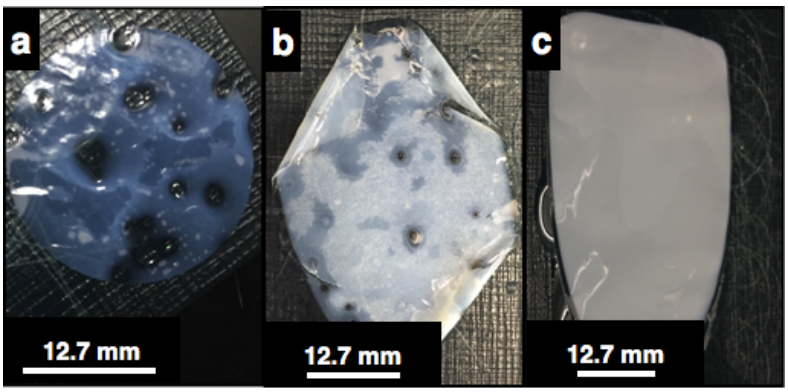

Figure B.1. Images of a) 15% ISA in 7:3 DOX/THF, b) 15% 5:5 blend in 7:3 DOX/THF, and c) 15% ISV in 7:3 DOX/THF derived membranes.

Image analysis: SEM micrographs of the top surfaces of the three most ordered membranes analyzed by ImageJ software to produce a two-dimensional fast Fourier transform (FFT) pattern. The radially integrated FFT patterns confirm pores packed in a 2-D square pore geometry for 9:1 and 7:3 blended membranes (Figure 4.2), similar to

pure ISV membranes. The calculated pore-to-pore distance is 40.4, 41.5, and 42.5 nm for pure ISV, and 9:1 and 7:3 blended membranes, respectively.

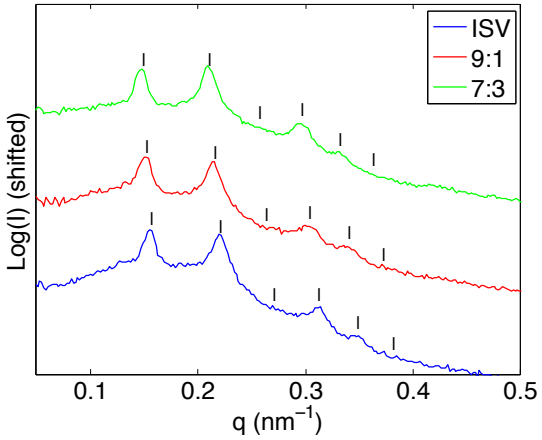

Figure B.2. Radially integrated FFT results of SEM images of the surface structure of different membranes indexed with a 2D square lattice (see ticks). ISV (bottom), 9:1 blend (middle), and 7:3 blend (top) yielding *d*-spacings of 40.4, 41.5, 42.5 nm, respectively.

Performance tests: pH dependent permeabilities were measured for pure ISV and ISA membranes, as well as for membranes blended from ISV and ISA (9:1, 7:3, and 6:4), at various pH values. Figure B.3 depicts the absolute permeabilities while the normalized data set is presented in Figure 4.3 of the main manuscript.

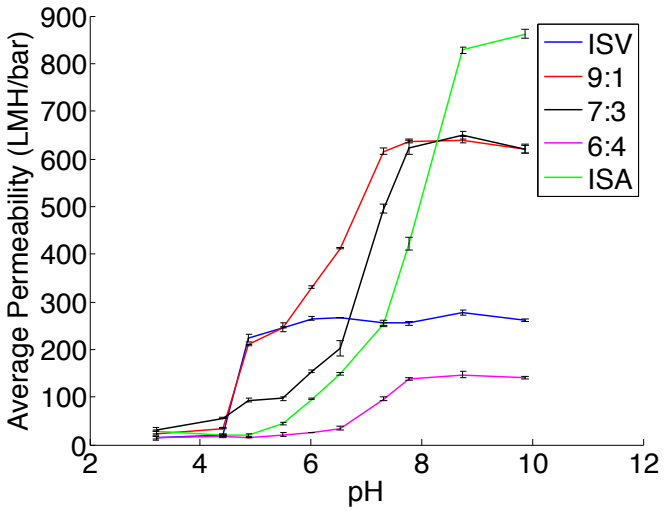

Figure B.3. Average absolute permeability for pure (ISV, ISA) and blended (9:1, 7:3, & 6:4 blends of ISV + ISA) membranes at various pH values. Indicated errors are standard deviations from three replicate measurements.

Replicate experiments were performed on a separately produced set of pure ISA and blended (9:1, 7:3, & 6:4 blends of ISV + ISA) membranes with the results shown in Figure B.4. The same behavior and trends are reproduced as for the data set shown in Figure 4.3 in the main text of the paper. Although there may be other parameters influencing absolute permeabilities, the fact that the relative trends were the same between two completely separate sets of membranes suggests that dope viscosity, which is expected to vary as a function of dope composition, could be the leading parameter responsible for the variation in absolute permeabilities.

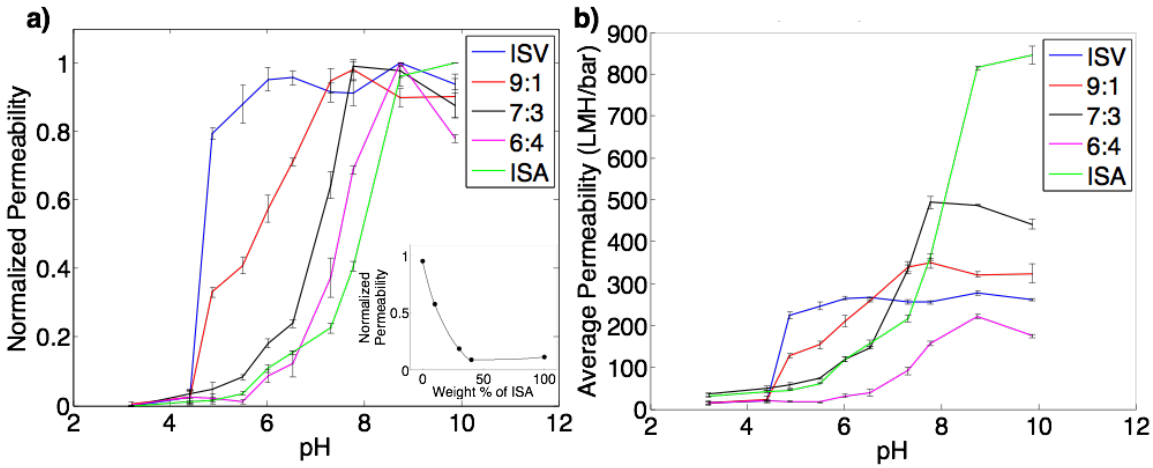

Figure B.4. Average a) normalized and b) absolute permeability values for pure (ISV, ISA; replicates) and blended (9:1, 7:3 & 6:4 blends of ISV + ISA; replicates) membranes at various pH values. Indicated errors are standard deviations from three replicate measurements. Inset: Effect of composition on permeability at pH=6. The curve through the data points is used as a guide for the eye.

REFERENCES

[1] K. V. Peinemann, V. Abetz, P. F. W. Simon, *Nat. Mater.* **2007**, *6* (12), 992-996.

[2] R. M. Dorin, D. S. Marques, H. Sai, U. Vainio, W. A. Phillip, K. V. Peinemann, S. P. Nunes, U. Wiesner, *ACS Macro Lett*. **2012**, *1* (5), 614-617.

[3] F. Schacher, T. Rudolph, F. Wieberger, M. Ulbricht, A. H. Muller, *ACS Appl. Mater. Interfaces* **2009**, *1* (7), 1492-1503.

[4] J. Hahn, V. Filiz, S. Rangou, J. Clodt, A. Jung, K. Buhr, C. Abetz, V. Abetz, *J. Polym. Sci. Part B Polym. Phys.* **2013**, *51* (4), 281-290.

[5] M. Karunakaran, R. Shevate, K. V. Peinemann, *RSC Adv.* **2016**, *6* (35), 29064-29071.

[6] W. A. Phillip, R. M. Dorin, J. Werner, E. M. Hoek, U. Wiesner, M. Elimelech, *Nano Lett*. **2011**, *11* (7), 2892-2900.

[7] J. L. Weidman, R. A. Mulvenna, B. W. Boudouris, W. A. Phillip, (2016). *J. Am. Chem. Soc.* **2016**, *138* (22), 7030-7039.

[8] Q. Zhang, Y. Gu, YM Li, P. A. Beaucage, T. Kao, U. Wiesner, *Chem. Mater*. **2016**, *28* (11), 3870-3876.

[9] P. Madhavan, K. V. Peinemann, S. P. Nunes, *ACS Appl. Mater. Interfaces* **2013**, *5* (15), 7152-7159.

[10] S. P. Nunes, A. R. Behzad, B. Hooghan, R. Sougrat, M. Karunakaran, N. Pradeep, U. Vainio, K. V. Peinemann, *ACS Nano* **2011**, *5* (5), 3516-3522.

[11] H. Yu, X. Qiu, N. Moreno, Z. Ma, V. M. Calo, S. P. Nunes, K. V. Peinemann, *Angew. Chem. Int. Ed.* **2015,** *54* (47), 13937-13941.

[12] Y. Gu, U. Wiesner, *Macromolecules*, **2015,** *48*(17), 6153-6159.

[13] M. Radjabian, V. Abetz, *Adv. Mater*. **2015**, *27* (2), 352-355.

[14] Y. Gu, R. M. Dorin, U. Wiesner, *Nano Lett.* **2013**, *13* (11), 5323-5328.

[15] S. A. Hesse, J. G. Werner, U. Wiesner, *ACS Macro Lett*. **2015**, *4* (5), 477-482.

[16] J. I. Clodt, V. Filiz, S. Rangou, K. Buhr, C. Abetz, D. Höche, J. Hahn, A. Jung, V. Abetz, *Adv. Funct. Mater*. **2013**, *23* (6), 731-738.

[17] R. M. Dorin, W. A. Phillip, H. Sai, J. Werner, M. Elimelech, U. Wiesner, *Polymer* **2014**, *55* (1), 347-353.

[18] Y. Gu, R. M. Dorin, K. W. Tan, D. M. Smilgies, U. Wiesner, *Macromolecules* **2016,** *49* (11), 4195-4201.

[19] S. Qu, T. Dilenschneider, W. A. Phillip, *ACS Appl. Mater. Interfaces* **2015**, *7* (35), 19746-19754.

[20] S. Creutz, P. Teyssié, R. Jérôme, *Macromolecules* **1997**, *30* (1), 6-9.

[21] Z. Li, K. Hur, H. Sai, H.; T. Higuchi, A. Takahara, H. Jinnai, S. M. Gruner, U. Wiesner, *Nat. Commun.* **2014**, *5*.

CHAPTER 5

PH-RESPONSIVE ISOPOROUS ASYMMETRIC MEMBRANES WITH ANTI-FOULING PROPERTIES DERIVED FROM A MIX AND MATCH APPROACH

Abstract

Two chemically distinct triblock terpolymers, poly(isoprene-*b*-styrene-*b*-4-vinyl pyridine) (ISV) and poly(isoprene-*b*-styrene-*b*-ethylene oxide) (ISO), were blended in the dope solution for the fabrication of isoporous asymmetric ultrafiltration membranes using block copolymer self-assembly and non-solvent induced phase separation (SNIPS). The ratio of ISV to ISO in the blended solutions was varied by weight from 1:0, 9:1, 7:3, to 5:5. Pure ISV derived and blended membranes exhibited an isoporous skin layer atop a macroporous substructure. Blended membranes retained their pH-responsive permeability behavior characteristic for pure ISV membranes. Protein adsorption decreased with increasing amounts of ISO. Blended membranes therefore exhibited properties characteristic for the constituent terpolymers blended in the polymer dope that could be tailored via a simple "mix and match" approach during the standard membrane fabrication process. Results suggest the use of straight-forward polymer blending concepts to molecularly engineer pore surface chemical characteristics. The work opens pathways to advanced isoporous asymmetric ultrafiltration membranes for a number of applications requiring a combination of properties not easily accessible from the use of single component polymer dopes. At the same time it raises fundamental questions about

the exact mechanism of mixed membrane formation, the nature of compositional heterogeneities along the surface of individual pore walls, as well as the limitations of this approach.

P. Vaidya, Y.M. Li, Y. Gu, U. Wiesner, To be submitted for publication.

Introduction

First introduced by Peinemann *et al*. a decade ago,[1] membranes prepared using block copolymer self-assembly and non-solvent induced phase separation process, now referred to as SNIPS,[2] have become increasingly desirable candidates for water purification, protein separation, or virus filtration applications. These integral-asymmetric membranes, which exhibit an ordered isoporous top surface layer and a macroporous underlying substructure, are able to deliver higher permeability and superior selectivity when compared to traditional ultrafiltration (UF) membranes.[3] Moreover, the facile SNIPS approach offers a high degree of structural control over both the mesoporous skin layer and the underlying graded substructure. For example, pore size of the selective top layer of SNIPS membranes has been tailored by simply changing block copolymer molar mass,[4,5] using organic additives,[6] or forming binary blends from the same block copolymer varying in composition,[7] effectively employing established soft condensed matter physics principles to molecularly engineer ultrafiltration membrane properties. In another study, the cross-sectional morphology of membranes was tuned by varying parameters such as polymer solution concentration, evaporation time, and temperature of the non-solvent bath.[8] The most extensively studied polymer system is the diblock copolymer poly(styrene-*b*-4-vinylpyridine).[9-13] However, other diblock copolymers such as poly(styrene-*b*-2-vinylpyridine)[14] and poly(styrene-*b*-4-vinylpyridine-N-oxide)[15] have been previously explored. In order to improve the mechanical properties of the resulting membranes, particularly at lower molar mass (*e.g.* below 100 kg/mol),[16] the SNIPS process has also been extended to a variety of triblock terpolymer systems such as poly(isoprene-*b*-styrene-*b*-4-vinyl pyridine) (ISV),[16] poly(isoprene-*b*-styrene-*b*-*N*,*N*-

dimethylacrylamide),[17] and poly(styrene-*b*-4-vinylpyridine-*b*-propylene sulfide).[18]

A major problem encountered in filtration processes is membrane fouling. Previous studies have suggested a high tendency of protein adsorption onto the surface of SV or ISV membranes which have 4-vinylpyridine chains decorating the pore walls.[19,20] The resulting biofouling may lead to a variety of undesirable consequences such as reduction in surface porosity and effective pore size from pore blockage and formation of a biofilm on the surface.[21] These could translate into poor permselectivity and the need to frequently clean or replace membranes greatly limiting their use for protein separation and biopharmaceutical applications. Thus, there is a pressing need to design systems that incorporate anti-fouling properties while retaining the high performance capabilities of SNIPS membranes.

Poly(ethylene oxide) (PEO) has been widely used to reduce the fouling behavior of membranes which is attributed to the hydrophilic nature of PEO. Moreover, the water solubility and inherent biocompatibility of PEO makes it highly attractive for biomedical applications. Various strategies such as grafting[22,23] and incorporation as additives[24,25] have been used to introduce PEO into membranes. Alternatively, there have been recent efforts to fabricate SNIPS membranes from block copolymers containing a PEO block such as in poly(styrene-*b*-ethylene oxide).[26,27] In a separate study an ABC triblock terpolymer system, poly(styrene-*b*-2-vinylpyridine-*b*-ethylene oxide), was used to fabricate pH-responsive self-assembled asymmetric membranes that showed improved hydrophilicity.[28]

The application of the SNIPS process to block copolymers with new block compositions is very challenging as it involves optimizing a multitude of parameters to

determine appropriate preparation conditions for successful membrane formation. As an example, in our hands it has been difficult to prepare poly(isoprene-*b*-styrene-*b*-ethylene oxide) (ISO) based membranes via SNIPS that display an ordered isoporous top surface structure and exhibit excellent membrane performance combined with antifouling wall surface properties. Here, we thought that one way to mitigate this problem may be to employ a recently devised "mix and match" approach in which multiple chemically distinct block copolymers are mixed in the polymer dope in order to tailor the surface chemical properties of the pore wall surfaces.[29] Rather than working with an O block containing block copolymer only, the idea was to mix such a block copolymer with one of the standard block copolymers known to provide excellent structure control using SNIPS and to determine whether this mixed membrane formation approach provides improved anti-fouling properties while maintaining desirable structure control.

To that end in this study we demonstrate the ability to blend ISV and ISO triblock terpolymers at varying compositions in the dope used for SNIPS based membrane fabrication resulting in blended ultrafiltration membranes with pH-responsiveness and tunable protein adsorption behavior. This blending approach in combination with SNIPS process promises to be an effective tool to fabricate highly engineered asymmetric ultrafiltration membranes with unique chemical pore surface properties.

Experimental

Polymer synthesis and characterization: The triblock terpolymers poly(isoprene-*b*-styrene-*b*-4-vinylpyridine) (ISV) and poly(isoprene-*b*-styrene-*b*-ethyleneoxide) (ISO) used in this study were prepared using sequential anionic

polymerization technique as described previously.[16,30] The synthesized ISV and ISO had similar number average molar mass (M_n) and volume fractions of the different polymer blocks (f), which were determined using a combination of gel permeation chromatography (GPC) and ^{1}H NMR. A summary of triblock terpolymer characterization results is shown for both terpolymers in Table 5.1.

Table 5.1. Summary of triblock terpolymer characteristics.

Terpolymer	M_n **(kg/mol)**	f_{PI}	f_{PS}	f	**PDI**
ISV	164	0.25	0.65	0.10	1.17
ISO	154	0.24	0.67	0.09	1.07

*Number average molar mass (M_n), volume fraction (f), and polydispersity index (PDI) of the triblock terpolymers used in this study.

Membrane fabrication and characterization: Isoporous asymmetric ultrafiltration membranes were fabricated by blending two triblock terpolymers during the SNIPS process following a procedure described previously.[29] A schematic depicting the blending process employed is shown in Figure 5.1. A ternary solvent mixture of 1,4-dioxane (DOX), tetrahydrofuran (THF), and acetonitrile (MeCN) (~67/28/5 wt%) was used as the solvent system for both ISV and ISO triblock terpolymers as well as the mixed terpolymer systems. The casting solutions were prepared by separately dissolving 11% ISV and 18% ISO in this solvent system at 300 rpm overnight. The individual casting solutions were then mixed and stirred together at 300 rpm for 10 minutes to form blended casting solutions with ISV:ISO weight ratios of 9:1, 7:3, and 5:5. A pure ISV membrane was prepared as a reference for comparison.

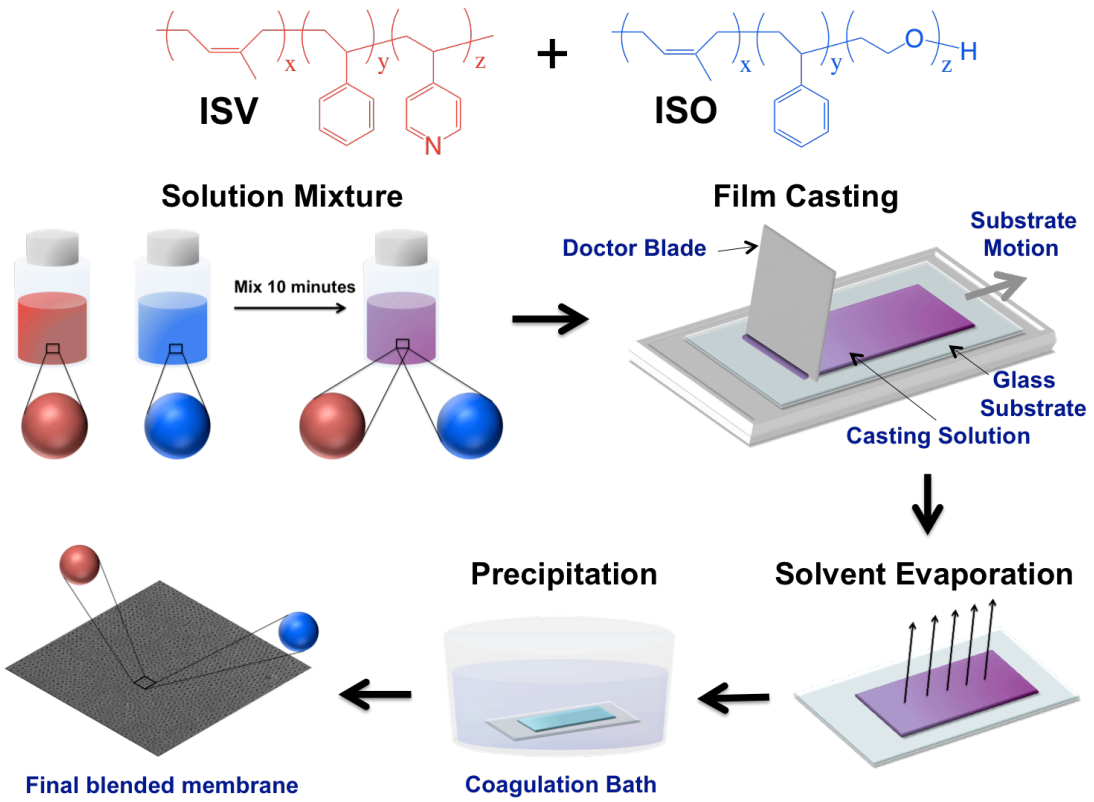

Figure 5.1. The chemical structures of ISV and ISO and a schematic depicting the procedure used for blending ISV and ISO triblock terpolymers to form a blended membrane. Individual casting solutions of ISV and ISO were prepared in a solvent system of DOX/THF/MeCN (~67/28/5 wt%) and stirred overnight. The solutions were then mixed together for 10 minutes to form the blended casting dopes. Solutions were casted into a polymer film by using a doctor blade set at a predetermined gate height. The solvents were then allowed to partially evaporate, driving the block copolymer self-assembly process. Finally, films were plunged into a coagulation bath to obtain the blended SNIPS membranes.

The dope solution was pipetted onto a glass substrate and a thin film was casted using an automated blade-casting machine permitting substrate motion with the gate height set between 203 μm and 229 μm. The solvents were allowed to partially evaporate from the thin films for 120 seconds before precipitation in a coagulation bath of 18.2 MΩ deionized water. The solvent evaporation step is critical to drive the self-assembly of the triblock terpolymers and is responsible for the thin selective mesoporous skin layer formation atop the macroporous substructure of the resultant asymmetric membrane. The final membranes were detached from the glass substrate by razor blade and stored in deionized water until tested.

Scanning electron microscopy (SEM) micrographs were obtained using a Tescan Mira3 field emission scanning electron microscope (FE-SEM) at an acceleration voltage of 5 kV and a working distance of 3-5 mm. The membrane samples were dried and sputter coated with gold-palladium using a Denton Vacuum Desk II for 8 seconds prior to imaging.

SEM micrographs were analyzed using Mathematica and Image J software to determine pore size, pore density, and porosity of the membrane top surfaces. Average values reported were calculated from analysis of two SEM images for each sample.

Membrane performance tests

pH-responsive Permeability Tests. Membranes with an active area of 4.1 cm^2 were punched out and pH-responsive permeability tests were performed using a dead-end stirred cell (Amicon 8010, Millipore, Co.) connected to a nitrogen gas source. To prevent damage of the membrane from the stirred cell, the membranes were placed on a 0.2 μm nylon support (Sterlitech) during testing. pH buffers of sodium acetate and acetic acid

were used for pH values in the range of 3-6, while pH buffers of imidazole and hydrochloric acid were used for the 7-8 pH range. The pH values of the buffer solutions were measured with a pH probe prior to permeability tests. Three measurements were conducted for each sample at varying trans membrane pressures of 1, 2, and 3 psi and the average values were reported.

Contact angle measurements using the sessile drop technique. The hydrophilicity of the membranes was characterized by the contact-angle measuring instrument Advanced Goniometer Model 500 equipped with DROPimage Advanced software (ramé-hart). Contact angle measurements for all samples of the contact angle between water and membrane surfaces were performed with 10 μL deionized water droplets at three randomly selected regions of the dry samples. For each sample, an average of three such readings at t=0 was determined and reported.

Protein Adsorption Tests. The hydrophilicity of the membranes was characterized by the contact-angle measuring instrument Advanced Goniometer Model 500 equipped with DROPimage Advanced software (ramé-hart). Contact angle measurements for all samples of the contact angle between water and membrane surfaces were performed with 10 μL deionized water droplets at three randomly selected regions of the dry samples. For each sample, an average of three such readings at t=0 was determined and reported.

$$\text{Adsorbed Protein} = \frac{m_0-(m_s+m_w)}{A} \quad (1)$$

where m_0 is the mass of protein in soak solution prior to the test, m_s is the mass of protein in soak solution after the test, m_w is the mass of reversibly attached protein in wash solution, and A is the membrane area. For each protein, three repeats were performed per sample and average values reported in μg/cm^2.

Results and Discussion

Membrane structure characterization: Scanning electron microscopy (SEM) images of top surface, bottom surface, and cross-section of the parent ISV and three blended ISV:ISO (9:1, 7:3, and 5:5) membranes are shown in the top, middle, and bottom rows of Figure 5.2, respectively. Magnified views of a selected region of the bottom surface are shown in the insets of each micrograph of the middle row. SEM images of pure ISV, and 9:1 and 7:3 blended membranes display an ordered square lattice pore arrangement in the top surface layer, as confirmed by two-dimensional fast Fourier Transform (FFT) analysis (see Figure C.1). The top surface SEM images (Figure 5.2 first row) depict increasing disorder when moving from the pure ISV based membrane to the blended membranes. The contrast is particularly clear between pure ISV, 9:1 and 7:3 blends, and 5:5 blended membrane. This observation is consistent with the finding that pure ISO membranes did not exhibit ordered top surfaces under similar SNIPS conditions used in this study (see Figure 5.2). Except for the membrane fabricated from the 5:5 blend, which overall exhibited less well defined structural membrane features, all other membranes studied showed open bottom surfaces (Figure 5.2 second row and inset) and finger-like cross-sections (Figure 5.2 third row).

The top surface SEM images of the membranes were analyzed using Mathematica and Image J software to determine composition dependent surface pore size distributions and calculate average values of pore size, pore density, and porosity which are listed in Table 5.2 (see Figure C.3 for more details). As the amount of ISO in the blends increases, a widening of the pore size distribution is observed. All membranes analyzed show similar values of average pore size and the same order of magnitude for pore density. A

net decrease of average porosity was observed when moving from pure ISV to blended membranes.

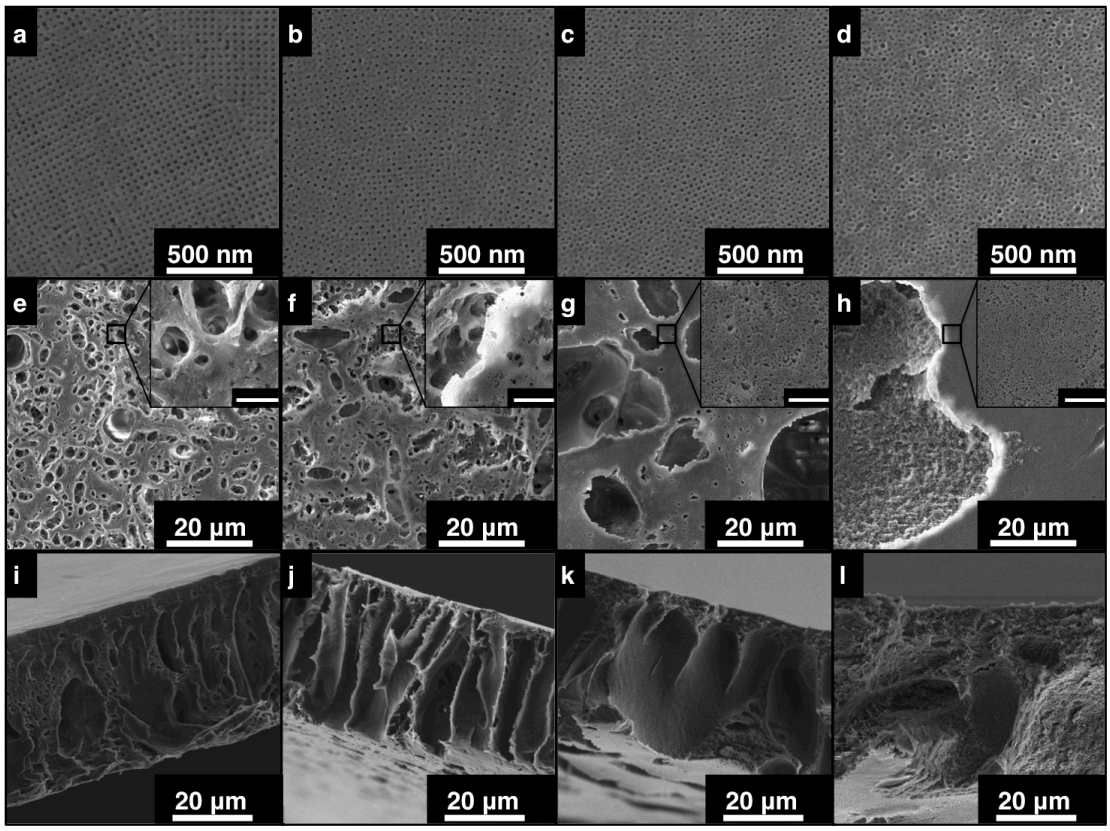

Figure 5.2. SEM micrographs of pure and blended SNIPS membranes. Top surfaces (top row), bottom surfaces and higher magnification images of selected regions (middle row and insets, respectively), and cross-sectional images (bottom row) of asymmetric membranes fabricated using (a,e,i) ISV, (b,f,j) 9:1 ISV:ISO blend, (c,g,k) 7:3 ISV:ISO blend, and (d,h,l) 5:5 ISV:ISO blend. Each polymer solution (11% ISV and 18% ISO) was first prepared separately in solvent system DOX/THF/MeCN (~67/28/5 wt%). For blended membranes, ISO and ISO polymer solutions were mixed at appropriate amounts for 10 minutes at 300 rpm before casting. Polymer films were evaporated for 120 seconds prior to plunging in the coagulation bath. Scale bars for inset images (middle row) are 2 µm.

Table 5.2. Average values for pore size, pore density, and porosity of top surfaces of pure and blended membranes.

System	Average Pore Size (nm)	Average Pore Density (pores m^{-2})	Average Porosity (%)
ISV	21.0 ± 0.1	5.1×10^{14}	18
9:1 Blend	19.1 ± 0.8	7.3×10^{14}	10
7:3 Blend	21.6 ± 0.4	7.4×10^{14}	15
5:5 Blend	23.8 ± 0.1	2.5×10^{14}	8

Pore size and pore density were calculated using Mathematica and surface porosity was calculated using ImageJ.

Membrane Performance Testing: Hydraulic permeability was tested of pure and blended membranes as a function of the feed solution's pH. A pressurized dead-end stirred cell was used with 10 mL of buffer feed solutions at varying pH values (Experimental section). For each data point, three values at pressure drops of 1, 2, and 3 psi were measured. The average values of permeability as a function of varying pH are reported in Figure 5.3.

In this work, the permeability of ~1800 LMH/bar at pH values 5 and above for pure ISV is consistent with results for other ISV terpolymers studied before and is due to the collapsed structure of P4VP brushes lining the membrane pores.[16,29] At pH values lower than the pK_a of P4VP (pK_a = 4.6), the hydraulic permeability drastically drops. This is due to increasing protonation of P4VP brushes, which as a result of coulombic repulsion extend outward towards the center of the pore thereby reducing the effective pore size.[16,32,33] The flow of feed solution through the membrane pores is thus restricted and leads to a reduced average permeability. For the 9:1 and 7:3 ISV:ISO blended

membranes, this membrane pH-responsiveness is preserved, albeit at overall permeability values decreasing with increasing amount of ISO in the blend. For the 5:5 blended membrane, permeability values are already low at high pH (around ~100 LMH/bar) and therefore exhibit only a slight further decrease with decreasing pH. The pH-responsive flux was re-measured for an independent set of pure and blended membranes (see Figure C.4) indicating excellent reproducibility. Results suggest that in the blends the ISV blocks remain at the pore surface thereby continuing to enable pH dependent membrane responsiveness. Furthermore, the reduction in membrane permeability with decreasing feed pH, irrespective of composition, suggests that there are no major defects in these membranes. Finally, the observations that (i) as the amount of ISO in the blends increases, overall permeability decreases, and (ii) from top surface image analysis (Table 5.2) there is no clear trend in the top surface pore size or pore density as a function of blend composition, suggest that the decrease in permeability is due to composition dependent variations in membrane structure directly below the top surface layer.

Protein Adsorption Resistance Testing*:* The susceptibility of membranes that have P4VP lining the pore walls to protein fouling has been described before.[19,20] Several studies aimed to reduce protein adsorption to block copolymer membranes by leveraging the anti-fouling behavior of PEO due to its hydrophilicity.[15-19,21-28] In this study, successful incorporation of the triblock terpolymer, ISO, blended into the dope for SNIPS membrane formation and the location of the O block on the surface of the pore walls was tested by static contact angle measurements using the sessile drop technique as well as through its characteristic property of reducing protein adsorption. As described in Appendix D, static contact angle measurements did not show any clear trend as a

function of membrane composition (Figure C.5), most likely due to the small portion of the overall top surface area covered by P4VP and PEO blocks relative to hydrophobic material (PS and PI blocks) and pore void (see schematic in Figure C.6). We therefore moved to protein adsorption measurements.

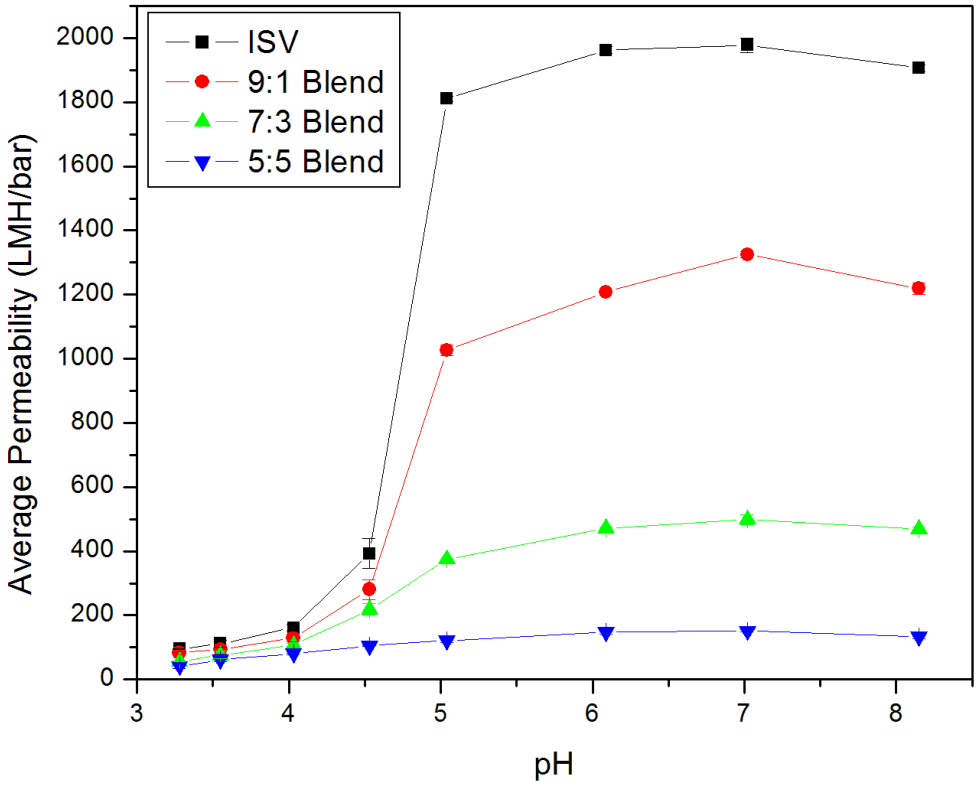

Figure 5.3. Average permeability of pure ISV and blended (9:1, 7:3, 5:5) ISV:ISO membranes as a function of varying pH of feed solution. Indicated errors are standard deviations from three replicate measurements performed at 1, 2, and 3 psi transmembrane pressure drop and are often smaller than the size of the data points.

To measure the resistance to protein adsorption of pure and blended membranes, 3 mL of a 1 g/L solution containing one of two model proteins, bovine serum albumin (BSA) or γ-globulin (IgG), were used to foul the membranes. For each membrane sample, three repeats were performed and the average value reported in μg/cm^2. From Figure 5.4, for both BSA and IgG the amount of protein adsorbed decreases as the

amount of ISO in the blends increases. For both proteins tested, about a threefold decrease in protein adsorption was observed between pure ISV and the 5:5 ISV:ISO blend. This can be rationalized by increasing amounts of the hydrophilic PEO block decorating the pore walls of the blended membranes.[21,22] As more ISO is added, the hydrophilic character of the membrane surface increases making the membrane more resistant to protein adsorption. Through simple compositional control of the polymer dope used to fabricate these blended membranes, while maintaining their pH responsiveness we were therefore able to demonstrate the ability to tune adsorption properties of the membrane pore surfaces. This suggests that the facile "mix and match" approach to the SNIPS process may become a powerful tool to tailor surface chemical properties of these isoporous asymmetric UF membranes.

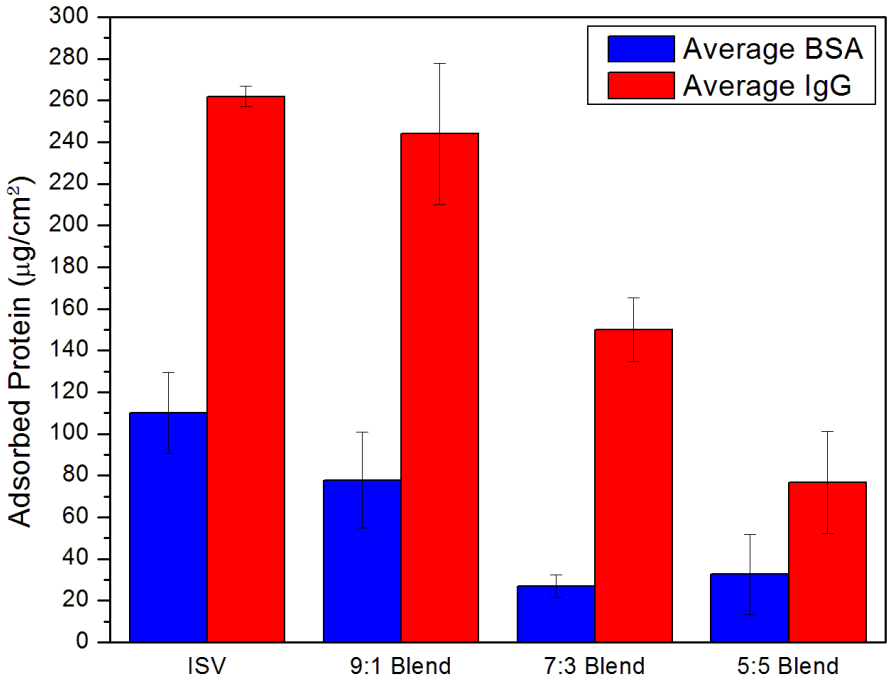

Figure 5.4. Comparison of BSA (bovine serum albumin) and IgG (γ-globulin) model protein adsorption on pure ISV and blended ISV:ISO membranes.

Conclusions

In this study, we applied the "mix and match" approach to the SNIPS process by blending two chemically distinct triblock terpolymers, ISV and ISO, into the polymer dope used for isoporous asymmetric ultrafiltration membrane fabrication. The resulting blended membranes exhibited a combination of properties unique to their respective terpolymer constituents, *i.e.* pH-responsiveness from the V block in ISV and anti-fouling properties characteristic for the O block in ISO. Furthermore, the weight ratio of parent ISV and ISO in the blended polymer dope could be used to tailor these properties in the final membranes. These results suggest that the amounts of V and O blocks ending up on the membrane pore surface can be tailored by simply controlling the relative amounts of the respective terpolymers in the polymer dope, providing a powerful example of how simple blending concepts can be used to molecularly engineering membrane surface properties.

This study provided insights into the potential, but also the limitations of the "mix and match" approach. For example, while the 5:5 ISV:ISO blended membrane showed superior resistance to protein adsorption, it showed only limited pH-responsive behavior and a comparatively low overall permeability level. Furthermore, compositions with even higher amounts of ISO in the blended dope did not provide useful membranes at all (data not shown), consistent with results from pure ISO dopes.

The ability to fabricate block copolymer derived asymmetric membranes using SNIPS that exhibit ordered top surface pore arrangements leading to maximum pore density, open substructures, high values of permselectivity and stimuli-responsive behavior has provided new directions for the improvement of advanced UF membranes

relative to existing technologies. The ability of adding anti-fouling characteristics to these aforementioned properties through a facile "mix and match" approach further enhances the suitability of this approach to generate advanced UF membranes for various applications including protein separation important *e.g.* for the biopharmaceuticals industry. In a wider context, the "mix and match" approach poses interesting scientific questions regarding the exact mechanism of the mixed membrane nanostructure formation starting from the blended dopes, the exact local compositional variations of the surface chemistry within a single pore, and the limits of this approach to control membrane pore surface chemical composition and characteristics. Gaining insights into these fundamental aspects may help to expand the achievable property profiles of this advanced class of porous materials.

Acknowledgements

The authors would like to acknowledge funding of this project by Contract No. HDTRA1-13-C0003 from the Defense Threat Reduction Agency (DTRA). Y.G. was funded by the National Science Foundation (DMR-1409105). This work utilized the facilities provided by the Cornell Center for Materials Research (CCMR) supported by NSF MRSEC program (DMR-1719875) and the Cornell Nanobiotechnology Center (NBTC). The authors thank Q. Zhang and F. Matsuoka from the Wiesner group for help in the block copolymer synthesis.

APPENDIX C

Membrane top surface analyses (FFT): The top surface SEM images of the membranes analyzed using ImageJ were used to calculate two-dimensional Fast Fourier transforms (FFTs). Similar to the pure ISV membrane, FFTs of the 9:1 and 7:3 blended membranes were consistent with a 2D square lattice pore arrangement (see ticks in Figure C.1). Resulting pore-to-pore distances (*d*) for the membranes are indicated in the figure.

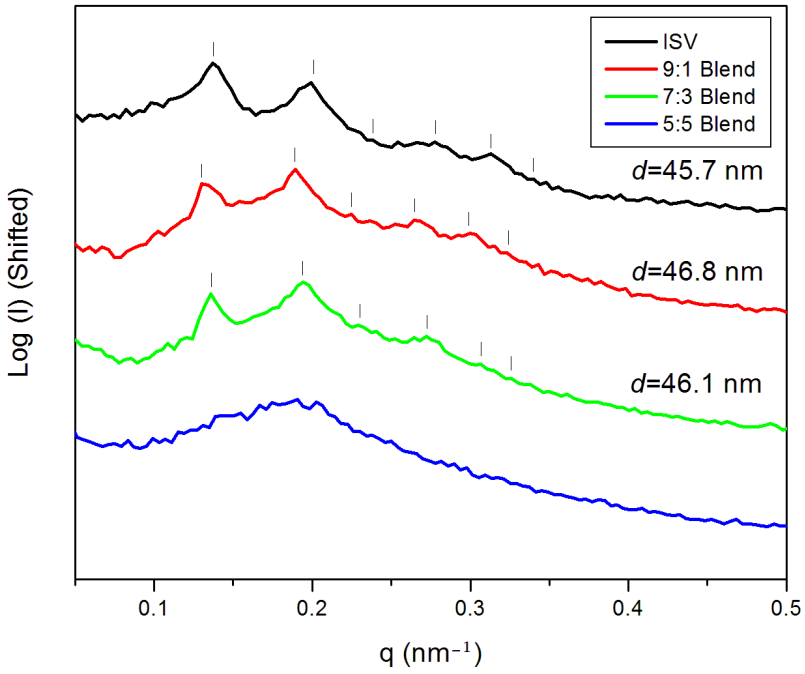

Figure C.1. The radially integrated FFT analysis of SEM images of the top surfaces of parent (ISV) and blended membranes investigated in this study, indexed (where appropriate) with a 2D square lattice (see ticks) and corresponding pore-to-pore distances, *d*.

SEM micrographs of pure ISO membrane: The SEM images of a pure SNIPS derived ISO membrane is shown in Figure C.2. The top surface SEM image suggests a lack of pore order. As shown in Figure 5.2 of the main text, an increase in the amount of ISO added to the blend led to more disorder in the top surfaces as revealed by SEM

imaging. This result is consistent with the disordered top surface observed here for the pure ISO membrane.

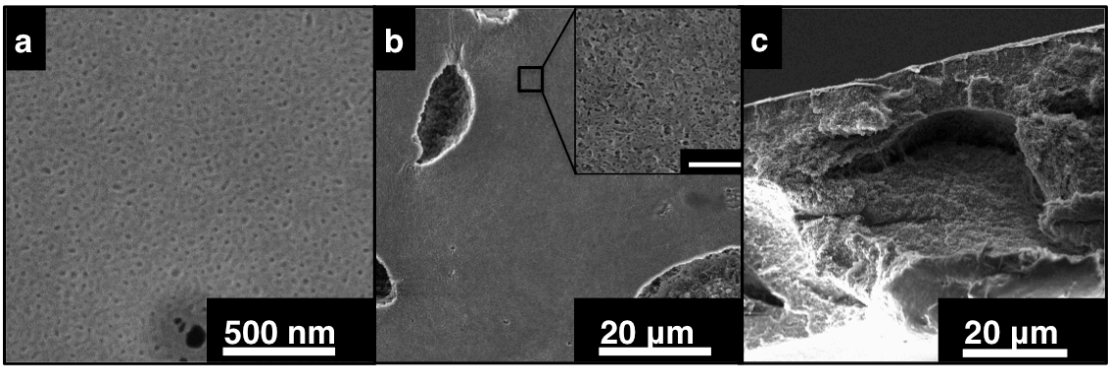

Figure C.2. SEM images of a pure ISO derived SNIPS membrane. (a) Top surface, (b) bottom, and (c) cross-section of a membrane derived from18% ISO dissolved in a solvent system of DOX/THF/MeCN (~67/28/5 wt%) and evaporated for 80 seconds prior to plunging into a DI water coagulation bath. The scale bar for the image in the inset in (b), which is a magnified view of a selected region of the bottom surface, is 2 µm.

Membrane top surface analysis (pore size distribution): Pore size distributions were determined using ImageJ software and log-normal fits of the resulting histograms were obtained using MATLAB. The histograms for the pore size distribution of the individual blended membranes and the corresponding log-normal fit curves are shown in Figure C.3(a-d). A comparative analysis of all the log-normal fits obtained for the various blends is represented in Figure C.3(e). As the amount of ISO in the blends increases, a widening of the pore size distribution is observed.

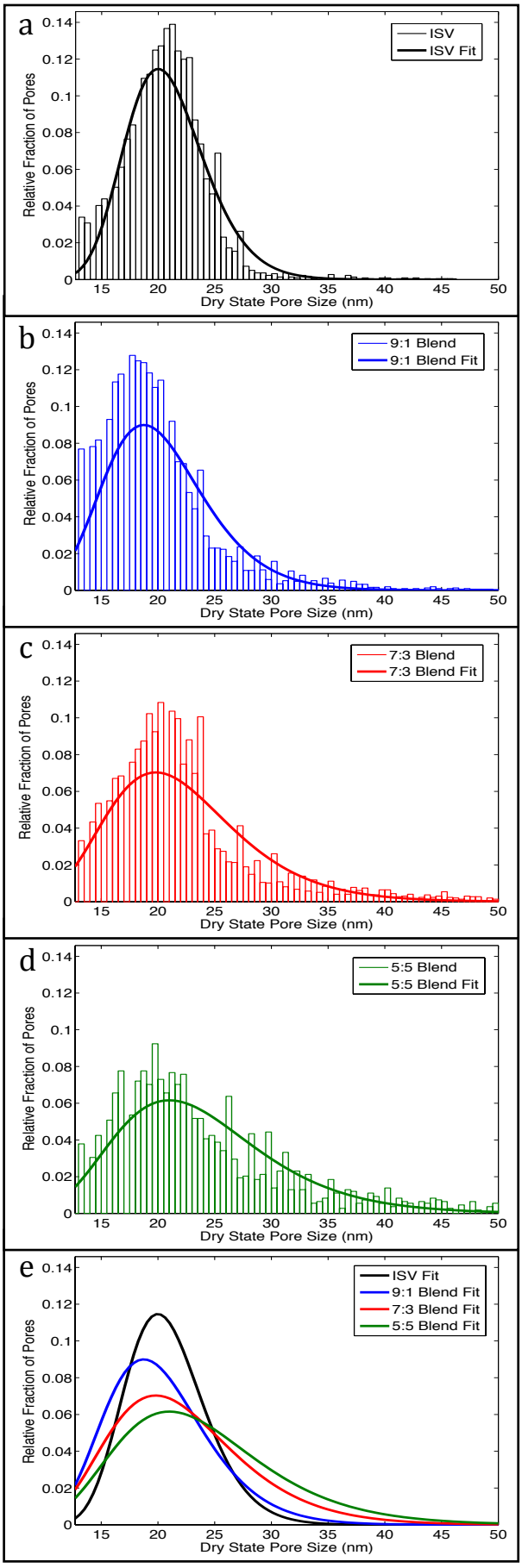
a
ISV
ISV Fit
Relative Fraction of Pores
Dry State Pore Size (nm)
b
9:1 Blend
9:1 Blend Fit
Relative Fraction of Pores
Dry State Pore Size (nm)
c
7:3 Blend
7:3 Blend Fit
Relative Fraction of Pores
Dry State Pore Size (nm)
d
5:5 Blend
5:5 Blend Fit
Relative Fraction of Pores
Dry State Pore Size (nm)
e
ISV Fit
9:1 Blend Fit
7:3 Blend Fit
5:5 Blend Fit
Relative Fraction of Pores
Dry State Pore Size (nm)

Figure C.3. Pore size distributions of parent (ISV) and blended membrane top surface layers (as indicated) obtained from SEM image analysis. The top surface SEM images were analyzed by ImageJ to calculate pore size distributions that were subsequently fit using a log-normal distribution.

Membrane performance testing: A separate set of parent ISV and blended membranes (9:1, 7:3, and 5:5 blends of ISV:ISO) were analyzed in terms of pH-dependent flux properties. For each feed solution, three replicate measurements were performed at 1, 2, and 3 psi trans-membrane pressure and an average value of permeability was calculated as shown in Figure C.4. The analysis yielded consistent results with the first set of membranes shown in Figure 5.3 of the main text.

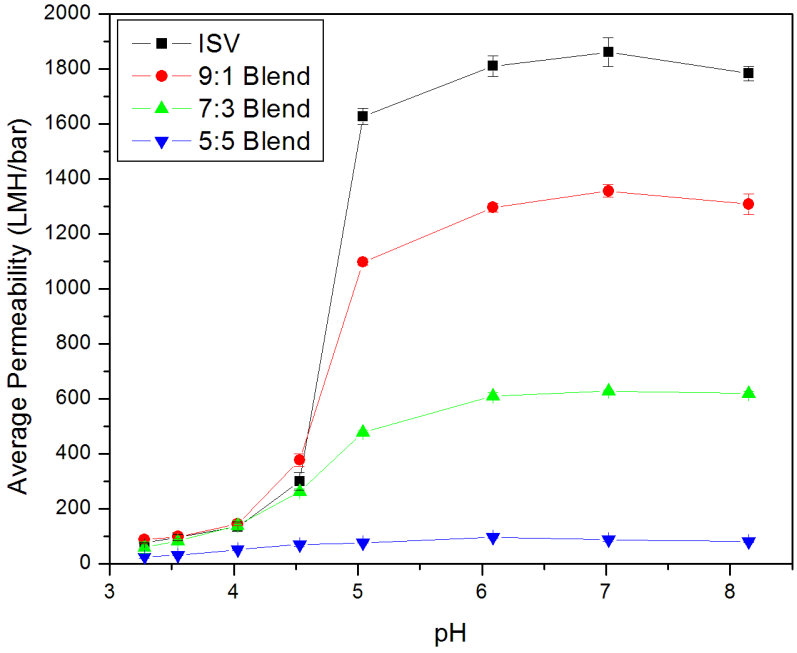

Figure C.4. pH-dependent permeability testing performed on a second set of parent ISV and blended ISV:ISO SNIPS derived membranes. Three replicate tests at 1, 2, and 3 psi pressure drops were performed for every feed buffer solution. Error bars indicate standard deviations obtained from these replicate measurements and are often smaller than the size of the data points.

Contact angle testing: To determine the hydrophilicity of the membranes, water contact angle testing was performed using the sessile drop technique. A ramé-hart Model 500 Advanced Goniometer equipped with DROPimage Advanced software was employed for the analyses. Measurements were performed at randomly selected regions of the membrane samples with 10 μL deionized water droplets. For each sample, an average of three such readings at t=0 was determined and reported in Figure C.5. No clear trend in the static contact angles was observed as a function of composition of the membranes.

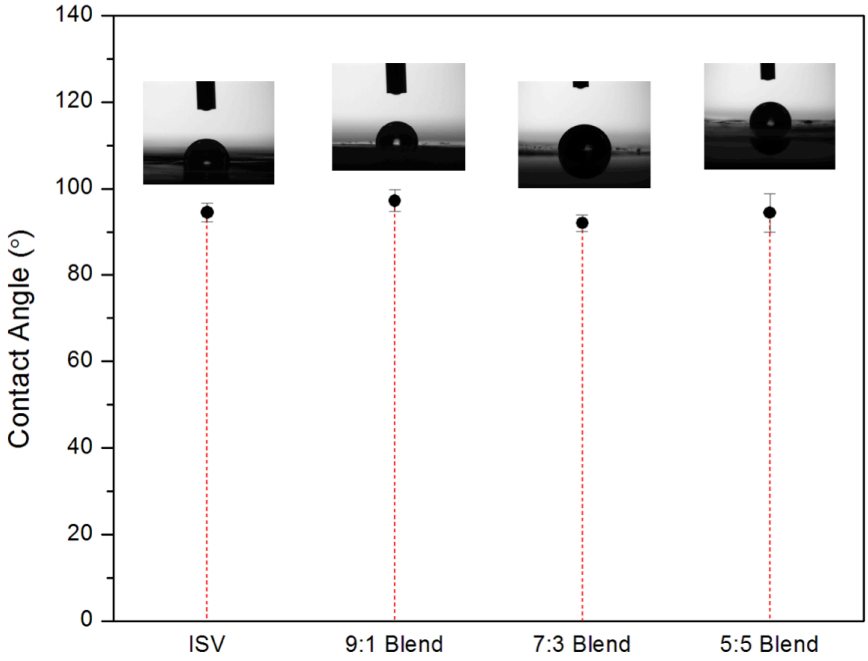

Figure C.5. Contact angle measurements performed on the parent (ISV) and ISV:ISO blended membranes. A 10 μL water droplet was used for each measurement and an average of the values measured at three randomly selected portions of the sample was reported.

A schematic depicting the top surface composition of the membranes is shown in Figure C.6. The majority of the membrane top surface is expected to be made up of either the hydrophobic matrix of poly(isoprene) and poly(styrene) or of the pore void (green

and black regions in Figure C.6). Only a very small portion of the top surface is expected to be covered by the poly(4-vinyl-pyridine) or poly(ethylene oxide) blocks to form the pore walls depicted in the schematic as blue areas. The influence of the changing hydrophilicity of the pore wall on the contact angle is therefore expected to be relatively small. This may explain why contact angle measurements were so insensitive to the change in the pore wall composition. In contrast, protein adsorption tests described in the main text (see Figure 5.4) were quite sensitive to the changing hydrophilicity of the pore walls as a function of blend composition.

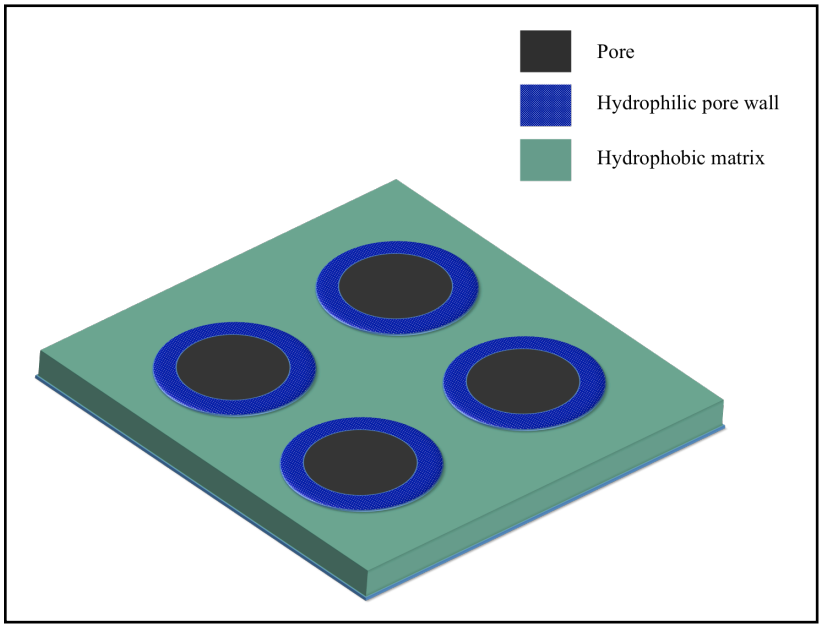

Figure C.6. A schematic representing the top surface of a SNIPS derived membrane. The pore walls made up of the hydrophilic components of the triblock terpolymers used to fabricate the membranes have a much lower surface area as compared to the combined area of the hydrophobic matrix made of poly(isoprene) and poly(styrene) and the pore void.

REFERENCES

[1] K.V. Peinemann, V. Abetz, P.F.W Simon, Asymmetric superstructure formed in a block copolymer via phase separation. *Nat. Mater.* 6 (2007**)** 992–996.

[2] R.M. Dorin, D.S. Marques, H. Sai, U. Vainio, W.A. Phillip, K.V. Peinemann, S.P. Nunes, U. Wiesner, Solution Small-Angle X-ray Scattering as a Screening and Predictive Tool in the Fabrication of Asymmetric Block Copolymer Membranes. *ACS Macro Lett.* 1 (2012) 614–617.

[3] M.M Pendergast, R.M. Dorin, W.A. Phillip, U. Wiesner, E.M. Hoek, Understanding the structure and performance of self-assembled triblock terpolymer membranes. *J. Membr. Sci.* 444 (2013) 461–468.

[4] R.M. Dorin, W.A. Phillip, H. Sai, J. Werner, M. Elimelech, U. Wiesner, Designing block copolymer architectures for targeted membrane performance. *Polymer* 55 (2014) 347–353.

[5] S. Rangou, K. Buhr, V. Filiz, J.I. Clodt, B. Lademann, J. Hahn, A. Jung, V. Abetz, Self-organized isoporous membranes with tailored pore sizes. *J. Membr. Sci.* 451 (2014) 266–275.

[6] Y. Gu, U. Wiesner, Tailoring pore size of graded mesoporous block copolymer membranes: moving from ultrafiltration toward nanofiltration. *Macromolecules* 48 (2015) 6153–6159.

[7] M. Radjabian, V. Abetz, Tailored pore sizes in integral asymmetric membranes formed by blends of block copolymers. *Adv. Mater.* 27 (2014) 352–355.

[8] Q. Zhang, Y.M. Li, Y. Gu, R.M. Dorin, U. Wiesner, Tuning substructure and properties of supported asymmetric triblock terpolymer membranes. *Polymer* 107 (2016) 398–405.

[9] S.P. Nunes, R. Sougrat, B. Hooghan, D.H. Anjum, A.R. Behzad, L. Zhao, N. Pradeep, I. Pinnau, U. Vainio, K.V. Peinemann, Ultraporous films with uniform nanochannels by block copolymer micelles assembly. *Macromolecules* 43 (2010) 8079–8085.

[10] S.P. Nunes, M. Karunakaran, N. Pradeep, A.R. Behzad, B. Hooghan, R.Sougrat, H. He, K.V. Peinemann, From micelle supramolecular assemblies in selective solvents to isoporous membranes. *Langmuir* 27 (2011) 10184–10190.

[11] J.I. Clodt, S. Rangou, A. Schröder, K. Buhr, J. Hahn, A. Jung, V. Filiz, V. Abetz, Carbohydrates as additives for the formation of isoporous PS-b-P4VP diblock copolymer membranes. *Macromol. Rapid Commun.* 34 (2012) 190–194.

[12] D.S. Marques, R.M. Dorin, U. Wiesner, D.M. Smilgies, A.R. Behzad, U. Vainio, K.V. Peinemann, S.P. Nunes, Time-resolved GISAXS and cryo-microscopy characterization of block copolymer membrane formation. *Polymer* 55 (2014) 1327–1332.

[13] M. Radjabian, C. Abetz, B. Fischer, A. Meyer, V. Abetz, Influence of solvent on the Structure of an Amphiphilic Block Copolymer in Solution and in Formation of an Integral Asymmetric Membrane. *ACS Appl. Mater. Inter.* 9 (2017) 31224-31234.

[14] A. Jung, S. Rangou, C. Abetz, V. Filiz, V. Abetz, Structure Formation of Integral Asymmetric Composite Membranes of Polystyrene-block-Poly (2-vinylpyridine) on a Nonwoven. *Macromol. Mater. Eng.* 297 (2012) 790–798.

[15] R. Shevate, M. Karunakaran, M. Kumar, K.V. Peinemann, Polyanionic pH-responsive polystyrene-b-poly (4-vinyl pyridine-N-oxide) isoporous membranes. *J. Membr. Sci.* 501 (2016) 161–168.

[16] W.A. Phillip, R.M. Dorin, J. Werner, E.M.V. Hoek, U. Wiesner, M. Elimelech, Tuning structure and properties of graded triblock terpolymer-based mesoporous and hybrid films. *Nano Lett.* 11 (2011) 2892–2900.

[17] R.A. Mulvenna, J.L. Weidman, B. Jing, J.A. Pople, Y. Zhu, B.W. Boudouris, W.A. Phillip, Tunable nanoporous membranes with chemically-tailored pore walls from triblock polymer templates. *J. Membr. Sci.* 470 (2014) 246–256.

[18] Q. Zhang, Y. Gu, Y.M. Li, P.A. Beaucage, T. Kao, U. Wiesner, U. Dynamically responsive multifunctional asymmetric triblock terpolymer membranes with intrinsic binding sites for covalent molecule attachment. *Chem. Mater.* 28 (2016) 3870–3876.

[19] J. Hahn, J.I. Clodt, V. Filiz, V. Abetz, Protein separation performance of self-assembled block copolymer membranes. *RSC Adv.* 4 (2014) 10252.

[20] J.L. Poole, S. Donahue, D. Wilson, Y.M. Li, Q. Zhang, Y. Gu, R. Ferebee, Z. Lu, R.M. Dorin, L.F. Hancock, L. Takiff, I.F. Hakem, M.R. Bockstaller, U. Wiesner, J. Walker, Biocatalytic stimuli-responsive asymmetric triblock terpolymer membranes for localized permeability gating. *Macromol. Rap. Commun.* 38 (2017) 1700364

[21] D. Rana, R. Matsuura, Surface modifications for antifouling membranes. *Chem. Rev.* 110 (2010) 2448–2471.

[22] J. Park, M. Acar, A. Akthakul, W. Kuhlman, A. Mayes, Polysulfone-graft-poly (ethylene glycol) graft copolymers for surface modification of polysulfone membranes. *Biomaterials* 27 (2006) 856–865.

[23] B. Dong, H. Jiang, S. Manolache, A.C.L. Wong, F.S. Denes, Plasma-mediated grafting of poly (ethylene glycol) on polyamide and polyester surfaces and evaluation of antifouling ability of modified substrates. *Langmuir* 23 (2007) 7306–7313.

[24] A. Asatekin, S. Kang, M. Elimelech, A.M. Mayes, Anti-fouling ultrafiltration membranes containing polyacrylonitrile-graft-poly (ethylene oxide) comb copolymer additives. *J. Membr. Sci.* 298 (2007) 136–146.

[25] Y.Q. Wang, T. Wang, Y.L. Su, F.B. Peng, H. Wu, Z.Y. Jiang, Remarkable reduction of irreversible fouling and improvement of the permeation properties of poly (ether sulfone) ultrafiltration membranes by blending with pluronic F127. *Langmuir* 21 (2005) 11856–11862.

[26] J. Hahn, V. Filiz, S. Rangou, J. Clodt, A. Jung, K. Buhr, C. Abetz, V. Abetz, V. Structure formation of integral‐asymmetric membranes of polystyrene‐block‐Poly (ethylene oxide). *J. Polym. Sci., Part B: Polym. Phys.* 51 (2012) 281–290.

[27] M. Karunakaran, S.P. Nunes, X. Qiu, H. Yu, K.V. Peinemann, Isoporous PS-b-PEO ultrafiltration membranes via self-assembly and water-induced phase separation. *J. Membr. Sci.* 453 (2014) 471–477.

[28] A. Jung, V. Filiz, S. Rangou, K. Buhr, P. Merten, J. Hahn, J. Clodt, C. Abetz, V. Abetz, Formation of integral asymmetric membranes of AB diblock and ABC

triblock copolymers by phase inversion. *Macromol. Rapid Commun.* 34 (2013) 610–615.

[29] Y.M. Li, D. Srinivasan, P. Vaidya, Y. Gu, U. Wiesner, Asymmetric Membranes from Two Chemically Distinct Triblock Terpolymers Blended during Standard Membrane Fabrication. *Macromol. Rapid Commun.* 37 (2016) 1689–1693.

[30] S.W. Robbins, H. Sai, F.J. Disalvo, S.M. Gruner, U. Wiesner, Monolithic Gyroidal Mesoporous Mixed Titanium–Niobium Nitrides. *ACS Nano* 8 (2014) 8217–8223.

[31] M.M. Bradford, A rapid and sensitive method for the quantitation of microgram quantities of protein utilizing the principle of protein-dye binding. *Anal. Biochem.* 72 (1976) 248–254.

[32] J.I. Clodt, V. Filiz, S. Rangou, K. Buhr, C. Abetz, D. Höche, J. Hahn, A. Jung, V. Abetz, Double Stimuli-Responsive Isoporous Membranes via Post-Modification of pH-Sensitive Self-Assembled Diblock Copolymer Membranes. *Adv. Funct. Mater.* 23 (2012) 731–738.

[33] S.P. Nunes, A.R. Behzad, B. Hooghan, R. Sougrat, M. Karunakaran, N. Pradeep, U. Vainio, K.V. Peinemann, Switchable pH-responsive polymeric membranes prepared via block copolymer micelle assembly. *ACS Nano* 5 (2011) 3516–3522.

CHAPTER 6

CONCLUSIONS

This thesis demonstrates that a deeper understanding in structure-property relationships of block copolymer SNIPS membranes is pivotal to enhancing membrane performance and expanding their use as advanced ultrafiltration technologies. It also illustrates the enormous academic as well as technological promise that this new class of materials holds for a number of applications, reaching far beyond separation technologies.

Chapter 2 evaluated the effect of different casting parameters on membrane substructure. The results show that with increasing dope concentration and evaporation time, the membrane substructure changes from a finger-like to a sponge-like morphology while retaining the ordered top surface pore structure. Additionally, by varying solvent composition (dioxane to tetrahydrofuran), the membrane substructure was tuned from a more finger-like to a 50/50 finger- and sponge-like to a sponge-like morphology. The results are consistent with morphologies derived from the phase inversion process applied to homopolymers and can therefore be rationalized by similar demixing arguments. Furthermore, membranes with different substructure were cast onto nylon supports to enhance mechanical stability. As expected, resulting membranes with finger-like morphologies have higher permeabilities as compared to membranes with sponge-like morphologies.

In chapter 3, the effect of relative humidity, an environmental casting parameter often overlooked, on membrane surface structure was investigated. Results show that there is an optimal relative humidity (~40%) for obtaining membranes characterized by a

high density of square packed surface pores with a narrow size distribution. Moreover, the rate of permeation of a small molar mass solute through these membranes was highest for membranes cast at optimal relative humidity and could be further tuned by fabricating membranes from triblock terpolymers with varying molar mass. These dynamically responsive membranes act as chemical valves allowing a small molar mass dye to permeate under basic conditions whereas it is retained under acidic conditions due to the pH dependent protonation of the P4VP block and resulting pore closure.

Through these studies, we have gained several handles for tuning membrane surface structure and substructure. There have been studies on the 3D reconstruction of membrane structure in order to use mathematical models to evaluate porosity and average pore size.[1] However, the ability to control membrane performance based on the design of macromolecules which in turn determines membrane structure is something the field is still striving towards. Future work on block copolymer SNIPS membranes should focus on building a mathematical model to provide the experimenter with casting parameters in order to fabricate membranes with specific, designed membrane performance charateristics. With this predictive technology, customized membranes could be achieved. As a start, the Wiesner group has begun 3D reconstructing membranes for use in conjunction with a mathematical model provided by Prof. Yeghiazarian at the University of Cincinnati.

A different route for generating designer membranes is through membrane composition. Chapter 4 demonstrated, as proof of principle, the fabrication of asymmetric SNIPS membranes by a “mix and match” approach using two chemically distinct triblock terpolymers in the dope during the standard membrane formation process. Membranes

were composed of the two triblock terpolymers, poly(isoprene-*b*-styrene-*b*-4-vinylpyridine) (ISV) and poly(isoprene-*b*-styrene-*b*-(dimethylamino)ethylmethacrylate) (ISA), in varying ratios. Since these two ABC terpolymers have polyamine end C blocks with different pk_a values, resulting in differences in pH dependent membrane permeabilities, distinct features in the pH dependent permeability of the mixed membranes unequivocally allowed to correlate membrane performance to pore surface composition as a function of dope composition (relative percentage of ISV to ISA).

Chapter 5 expanded the "mix and match" approach to a second membrane system: ISV and poly(isoprene-*b*-styrene-*b*-ethylene oxide) (ISO). This work demonstrated the formation of blended membranes with a combination of distinct properties, here pH-dependent permeability and anti-fouling pore surface behavior, associated with the constituting terpolymers, i.e. with ISV and ISO, respectively, and not easily accessible from a single block copolymer alone. The results also elucidated that there are limits on the influence of each triblock terpolymer on membrane structure and performance. For example, casting at conditions optimal for ISV, ISV dominated blended membranes retained an ordered top surface structure and showed pH-dependent permeability characteristic of pure ISV membranes. These properties become less pronounced with increasing amounts of ISO. But by incorporating ISO into the membrane system, resistance to protein adsorption can be introduced and moreover, tuned by varying its amount.

The ability to fabricate blended membranes by a simple "mix and match" approach enables incorporation of distinctly different properties into a single membrane. In particular, by varying the blocks of the block copolymers that end up on the membrane

pore surface, e.g. C and D blocks in mixtures of ABC and ABD triblock terpolymers as described above, this opens a pathway to precisely tune the pore surface chemical characteristics of the resulting ultrafiltration membranes thereby generating an entirely novel paradigm in the molecular engineering of membrane properties. This work therefore added to the push towards customized membranes as next generation ultrafiltration technologies. Future work should focus on probing the formation mechanism involved in the "mix and match" approach including, but not limited to, the dope solution structure and the compositional variations in the resultant membranes. The "mix and match" approach can also be extended to more than just two block copolymers thereby increasing the possibilities to fine tune membrane properties in general, and pore surface chemical characteristics in particular.

Future work on block copolymer SNIPS membranes could focus on synthesizing new and exciting block copolymers as building blocks for dynamically responsive material systems. Block copolymers could be selected for their response to various external stimuli or their catalytic abilities enabling membranes with these inherent abilities without post modification steps. As an alternate route, ISV membranes have been infiltrated with enzymes to create biocatalyic membranes.[2] For dynamically responsive material systems, the leverage of nanotechnology for enhancing membrane performance could have enormous implications for many different industries such as the biopharmaceutical and food industry.

Finally, since P4VP decorated membrane pores act as chemical valves, these membranes could be explored for applications beyond separations. One such application is as a drug delivery system (e.g. as dermal patches) which may enable single file

diffusion for controlled drug delivery. Additionally, alternative preparation techniques could be investigated to enable these thin films as dynamically responsive coatings.

REFERENCES

[1] Sundaramoorthi, G., Hadwiger, M., Ben-Romdhane, M., Behzad, A. R., Madhavan, P., & Nunes, S. P. (2016). 3d membrane imaging and porosity visualization. *Industrial & Engineering Chemistry Research*, *55*(12), 3689-3695.

[2] Poole, J.L., Donahue, S., Wilson, D., Li, Y.M., Zhang, Q., Gu, Y., Ferebee, R., Lu, Z., Dorin, R.M., Hancock, L.F. and Takiff, L., 2017. Biocatalytic Stimuli‐Responsive Asymmetric Triblock Terpolymer Membranes for Localized Permeability Gating. *Macromolecular rapid communications*, *38*(19).